Calhoun: The NPS Institutional Archive
DSpace Repository

Theses and Dissertations 1. Thesis and Dissertation Collection, all items

1975

Heat budget parameterization for the FNWC primitive equation model using data for 16 January 1974.

Spaeth, Warren Theodore

Monterey, California. Naval Postgraduate School

http://hdl.handle.net/10945/20885

Downloaded from NPS Archive: Calhoun

Calhoun is the Naval Postgraduate School's public access digital repository for research materials and institutional publications created by the NPS community. Calhoun is named for Professor of Mathematics Guy K. Calhoun, NPS's first appointed -- and published -- scholarly author.

Dudley Knox Library / Naval Postgraduate School
411 Dyer Road / 1 University Circle
Monterey, California USA 93943

http://www.nps.edu/library

HEAT BUDGET PARAMETERIZATION FOR THE FNWC PRIMITIVE EQUATION MODEL USING DATA FOR 16 JANUARY 1974

Warren Theodore Spaeth

LIBRARY
[illegible] SCHOOL
[illegible]

DUDLEY KNOX LIBRARY
NAVAL POSTGRADUATE SCHOOL
MONTEREY, CALIFORNIA 939[illegible]5002

NAVAL POSTGRADUATE SCHOOL
Monterey, California

THESIS

HEAT BUDGET PARAMETERIZATION FOR THE FNWC PRIMITIVE EQUATION MODEL USING DATA FOR 16 JANUARY 1974

by

Warren Theodore Spaeth, Jr.

March 1975

Thesis Advisor: F. L. Martin

Approved for public release; distribution unlimited.

T167569

REPORT DOCUMENTATION PAGE

READ INSTRUCTIONS
BEFORE COMPLETING FORM

1. REPORT NUMBER	2. GOVT ACCESSION NO.	3. RECIPIENT'S CATALOG NUMBER

4. TITLE (and Subtitle)
Heat Budget Parameterization for the FNWC Primitive Equation Model Using Data for 16 January 1974

5. TYPE OF REPORT & PERIOD COVERED
Master's Thesis;
March 1975

6. PERFORMING ORG. REPORT NUMBER

7. AUTHOR(s)
Warren Theodore Spaeth, Jr.

8. CONTRACT OR GRANT NUMBER(s)

9. PERFORMING ORGANIZATION NAME AND ADDRESS
Naval Postgraduate School
Monterey, California 93940

10. PROGRAM ELEMENT, PROJECT, TASK AREA & WORK UNIT NUMBERS

11. CONTROLLING OFFICE NAME AND ADDRESS
Naval Postgraduate School
Monterey, California 93940

12. REPORT DATE
March 1975

13. NUMBER OF PAGES
152

14. MONITORING AGENCY NAME & ADDRESS(if different from Controlling Office)

15. SECURITY CLASS. (of this report)
Unclassified

15a. DECLASSIFICATION/DOWNGRADING SCHEDULE

16. DISTRIBUTION STATEMENT (of this Report)

Approved for public release; distribution unlimited.

17. DISTRIBUTION STATEMENT (of the abstract entered in Block 20, if different from Report)

18. SUPPLEMENTARY NOTES

19. KEY WORDS (Continue on reverse side if necessary and identify by block number)

Tropospheric Heat Balance Model
Radiation Budget
Cloud Parameterization

20. ABSTRACT (Continue on reverse side if necessary and identify by block number)

The radiational model employed here computes the planetary albedo and the solar absorption by atmospheric layers and by earth's surface for the primitive equation model of FNWC. Large-scale cloud parameterization in several layers enters into these computations. The solar computations are made on a gridpoint basis employing the water-vapor mass over each gridpoint. Longwave cooling effects over the same layers and

(20. ABSTRACT Continued)

at the earth's surface are calculated using emissivity formulas after Sasamori, and are also dependent upon the cloud-parameterizations.

Two forms of the cloud-parameterizations were tested using FNWC gridpoint oceanic data for 16 January 1974. The objective was to determine the parameterization which better verified the radiational balance as a function of latitude at the tropopause, as compared with the January satellite climatology. Separate heat-budget checks of the tropospheric columns and of the oceanic-water mass were tested for consistency with January climatology. The smaller cloud-parameterization values gave the best verification.

Heat Budget Parameterization for the FNWC Primitive Equation Model Using Data for 16 January 1974

by

Warren Theodore Spaeth, Jr.
Lieutenant, United States Navy
B.S., United States Naval Academy, 1968

Submitted in partial fulfillment of the
requirements for the degree of

MASTER OF SCIENCE IN METEOROLOGY

from the

NAVAL POSTGRADUATE SCHOOL
March 1975

Thesis
S4648
c.1

ABSTRACT

The radiational model employed here computes the planetary albedo and the solar absorption by atmospheric layers and by earth's surface for the primitive equation model of FNWC. Large-scale cloud parameterization in several layers enters into these computations. The solar computations are made on a gridpoint basis employing the water-vapor mass over each gridpoint. Longwave cooling effects over the same layers and at the earth's surface are calculated using emissivity formulas after Sasamori, and are also dependent upon the cloud-parameterizations.

Two forms of the cloud-parameterizations were tested using FNWC gridpoint oceanic data for 16 January 1974. The objective was to determine the parameterization which better verified the radiational balance as a function of latitude at the tropopause, as compared with the January satellite climatology. Separate heat-budget checks of the tropospheric columns and of the oceanic-water mass were tested for consistency with January climatology. The smaller cloud-parameterization values gave the best verification.

TABLE OF CONTENTS

I. INTRODUCTION ---------------------------------- 19

II. DATA PREPARATION ----------------------------- 23

- A. INTERPOLATIVE PROCESSING TO k-LEVELS IN RADIATIVE SOUNDINGS ---------------------------- 28
  - 1. Temperatures ------------------------------ 28
  - 2. Humidities at k-Levels ------------------- 29
  - 3. Humidity Extrapolation to $P \leq 300$ mb ---- 30
  - 4. Pressure-Scaled Absorber Masses ---------- 31
- B. CLOUD PARAMETERIZATION ----------------------- 34
- C. WINDSPEED USED IN TURBULENT HEAT TRANSFERS --- 36

III. TERRESTRIAL RADIATION ----------------------- 39

- A. THEORETICAL AND EMPIRICAL BASIS -------------- 39
- B. NET FLUX $F_{10}*$ ---------------------------- 40
  - 1. Net Flux With Clear Skies, $F_{10}*(0, 0)$ ---- 45
  - 2. Net Flux With Overcast Clouds in Both Layers, $F_{10}*(1, 1)$ ---------------------- 45
  - 3. Net Flux With Overcast Clouds in Upper Layer Only, $F_{10}*(1, 0)$ ------------------- 46
  - 4. Net Flux With Overcast in Lower Layer Only, $F_{10}*(0, 1)$ ------------------------- 46
  - 5. The Composite $F_{10}*(CL(1)\ CL(2))$ Equation - 46
- C. NET FLUX F_6* ------------------------------ 48
  - 1. The Composite F_6* Equation --------------- 48
  - 2. Net Flux With Clear Skies $F_6*(0, 0)$ ------ 48
  - 3. Net Flux With Overcast Clouds in Both Layers $F_6*(1, 1)$ ------------------------- 49
  - 4. Net Flux With Overcast Clouds in Upper Layer Only $F_6*(1, 0)$ --------------------- 49
  - 5. Net Flux With Overcast Clouds in Lower Layer Only $F_6*(0, 1)$ --------------------- 49

D. NET FLUX F_2*-- 49

E. APPLICATION TO HEAT BALANCE COMPUTATIONS----- 50

F. STATISTICAL RESULTS AND COMPARISONS---------- 51

G. COMPARISONS WITH CLIMATOLOGICAL RESULTS OF F_2-- 54

H. COMPARISONS WITH CLIMATOLOGICAL RESULTS OF F_{10}*--- 58

IV. SOLAR RADIATION-- 60

A. PARTITION OF SOLAR INSOLATION---------------- 60

B. DISPOSITION OF F(S) INSOLATION--------------- 62

1. Clear-Sky Case---------------------------- 63

2. Cloudy-Sky Cases-------------------------- 63

3. Composite F(S) Insolation--------------- 64

C. DISPOSITION OF F(A) INSOLATION--------------- 65

1. The Clear-Sky Case (0, 0)---------------- 65

2. Cloudy Cases------------------------------ 66

3. Composite F(A) Layer-Absorptions and Surface-Absorbed Insolation-------------- 72

4. Absorptivity (ABA) by Layers------------- 72

D. ALBEDO (ALB) OF THE EARTH-TROPOSPHERE SYSTEM-- 73

E. COMPOSITE ABSORPTIVITY (ABG) BY THE EARTH-SURFACE; COMPOSITE ATMOSPHERIC TRANSMISSIVITY (ATRAN)----------------------- 74

1. Absorptivity (ABG) of Earth-------------- 74

2. Transmissivity (ATRAN) of the Troposphere------------------------------------ 74

3. Computational Check---------------------- 75

F. STATISTICAL ANALYSIS------------------------- 75

1. Clear Sky Cases--------------------------- 75

2. Relationships Between Albedo, Atmospheric, Absorptivity, Atmospheric Transmissivity, and Ground Insolation in the Cloudy and Clear Sky Cases----------------------------- 77

3. Some Conclusions ---------- 80

G. ALBEDO COMPARISONS WITH PUBLISHED RESULTS -- 80

V. SENSIBLE AND LATENT HEAT TRANSPORT AT THE SEA-AIR INTERFACE ---------- 84

A. GENERAL ---------- 84

B. SENSIBLE HEAT TRANSPORT ---------- 84

C. EVAPORATIVE HEAT TRANSPORT ---------- 89

D. TURBULENT HEAT TRANSPORTS OVER AN ICE-COVERED OCEAN ---------- 91

E. LARGE SCALE TURBULENT HEAT FLUX ACROSS THE AIR-SEA INTERFACE ---------- 93

VI. MERIDIONAL CROSS-SECTIONAL DEPICTION OF THE HEAT BUDGET SYSTEM COMPUTATIONS ---------- 95

A. GENERAL ---------- 95

B. EXPLANATION OF TERMS IN FIGURE 12 ---------- 98

1. Cross-Section at Level k = 2 ---------- 98

2. Cross-Section in Layer (2, 6) ---------- 100

3. Cross-Section in Layer (6, 10) ---------- 100

4. Cross-Section at Air-Sea Interface (k = 10) ---------- 101

VII. ZONALLY-AVERAGED RADIATIONAL BALANCE OF THE OCEAN-ATMOSPHERE SYSTEM ---------- 111

A. GENERAL ---------- 111

B. EARTH-ATMOSPHERE SYSTEM RADIATIONAL BALANCE RESULTS ---------- 117

C. EXPLANATION OF THE MEAN ZONAL RADIATIVE-BUDGET DISTRIBUTIONS ---------- 121

VIII. ZONALLY-AVERAGED TROPOSPHERIC AND OCEANIC HEAT BUDGETS FOR 16 JANUARY 1974 ---------- 124

A. THE TROPOSPHERIC HEAT BUDGET OVER ICE-FREE OCEANS ---------- 124

B. THE ZONALLY-AVERAGED HEAT BUDGET OF THE ICE-FREE OCEAN ---------- 128

C. OCEAN-TROPOSPHERIC HEAT-BUDGETS FOR ICE-COVERED OCEANS---------------------------------- 131

1. Computation of $(E + H_\Gamma)$ Over Ice-Covered Oceans---------------------------- 131

2. Budgetary Equations in Both Media With Ice-Covered Ocean---------------------- 133

IX. CONCLUSION-- 134

APPENDIX A: EMISSIVITY ε_{wc} FORMULAS AS A FUNCTION OF WATER VAPOR AND CO_2 ABSORBER MASSES ALONG THE PATH OF INTEGRATION------------- 136

APPENDIX B: FORMULAS USED IN DEPICTING THE DISPOSITION OF INCOMING SOLAR (F(A)) FROM LEVEL k = 2 TO THE EARTH'S SURFACE-------------- 140

COMPUTER PROGRAM-- 144

LIST OF REFERENCES-------------------------------------- 148

INITIAL DISTRIBUTION LIST------------------------------ 152

LIST OF TABLES

Table

I. a. Example of a Typical FNWC Sounding for Gridpoint (1, 1)---------------------------- 26

b. Example of the Corresponding Radiative Sounding with Temperature and Mixing Ratio Listed at k-levels and also Water Vapor and CO_2 Absorber Masses, Cloud Amounts, CL(1) and CL(2) Where Applicable in the Example Sounding-- 27

II. Example Listing of Gridpoint Values of the Terrestrial Radiation Fluxes Computed at Gridpoint (1, 1)---------------------------------- 44

III. a. Comparison of Net Flux to Space, F_2, as Found by this Study for Both the 2/3-CL Case and the full-CL Case, and by Raschke *et al.* (1973) using NIMBUS III Heat Budget Studies. Composite CL Amounts for Both Cases are Also Included--------------------- 55

b. Comparison of Net Flux at the Surface, F_{10}*, as Found by this Study for Both the 2/3-CL Case and the full-CL Case and the Annual Mean F_{10}* Derived from Budyko (1956)------------ 57

IV. Comparison of Planetary Albedo as Found by this Study for Both the 2/3-CL Case and the full-CL Case and by Raschke *et al.* (1973) Based Upon NIMBUS III Measurements. Also Included are the

Globally-Weighted Mean Values and the composite Cloud Amounts for Both Cloud Cases--------------- 82

V. Comparisons of the Zonally-Averaged Components (R, R_s, R_a) of the Radiational Balance of the Earth-Atmosphere System as Found by this Study and R_s as Reported by Raschke *et al.* (1973) From NIMBUS III Measurements, and, R and R_a, as Reported by Berliand (1956)------------------- 120

VI. Comparisons of the Zonally-Averaged Components, R_a, ($E + H_\Gamma$), ($Q_{va} + S_a$) of the Tropospheric Heat Budget as Found by this Study and the Same Values as Derived after Berliand (1956)---------- 125

VII. Comparisons of the Zonally-Averaged Components, R, ($E + H_\Gamma$), ($Q_{vo} + S$) of the Surface Heat Budget as Found by this Study and the Same Values as Derived after Berliand (1956)-------------------- 129

VIII. Surface Heat-Transports Over Ice at 170°W-------- 132

LIST OF FIGURES

Figure

1. FNWC Polar Stereographic Grid Meridians (lines 1, 2, 3, and 4) selected for study------ 20

2. Five-Layer Radiative Sounding Used in this Study ------------------------------------ 25

3. Section of FNWC Polar Stereographic Grid Illustrating the Method of Obtaining Contour Gradients in the Vicinity of a Gridpoint-------- 38

4. Terrestrial Net Flux $F_{10}*$
   a. Clear Sky Case------------------------------ 41
   b. Two Overcast Layers------------------------ 41
   c. High Level Overcast------------------------ 41
   d. Low Level Overcast------------------------- 41

5. Terrestrial Net Flux F_6*
   a. Clear Sky Case------------------------------ 42
   b. Two Overcast Layers------------------------ 42
   c. High Level Overcast------------------------ 42
   d. Low Level Overcast------------------------- 42

6. Terrestrial Net Flux F_2*
   a. Clear Sky Case------------------------------ 43
   b. Two Overcast Layers------------------------ 43
   c. High Level Overcast------------------------ 43
   d. Low Level Overcast------------------------- 43

7. Schematic Representation of F(A) Insolation Disposition in the Case of Two Overcast Layers-- 68

8. Schematic Representation at F(A) Insolation Disposition with an Upper Overcast Layer Only--- 69

9. Schematic Representation at F(A) Insolation Disposition with a Lower Overcast Layer Only---- 70

Figure

10. Schematic Representation of the Distribution of Convergence of Sensible Heat
    a. After Kaitala (1974) ---------- 87
    b. This Study ---------- 87
11. Schematic Representation of the Distribution of Convergence of Latent Heat
    a. After Kaitala (1974) ---------- 90
    b. This Study ---------- 90
12. Key to Meridional Cross-Sections for Figs. 13,..., 16 ---------- 96
13. 125°W Londitudinal Cross-Section. Two-thirds Cloud Model
    a. Tropical Section ---------- 102
    b. Higher Latitude Section ---------- 103
14. 170°W Longitudinal Cross-Section. Two-thirds Cloud Model
    a. Tropical Section ---------- 104
    b. Higher Latitude Section ---------- 105
15. 145°E Longitudinal Cross-Section. Two-thirds Cloud Model
    a. Tropical Section ---------- 106
    b. Higher Latitude Section ---------- 107
16. 35°W Longitudinal Cross-Section. Two-thirds Cloud Model
    a. Tropical Section ---------- 108
    b. Higher Latitude Section ---------- 109
17. Key to Zonally-Averaged Radiational Cross-Section for Figs. 18 (a, b) and 19 (a, b) ---------- 112
18. Zonally-Averaged Radiational Cross Section for the two-thirds Cloud Model Case
    a. Tropical Latitude Section ---------- 113

Figure

b. Mid to High Latitude Section---------------- 114

19. Zonally-Averaged Radiational Cross-Section for the Full Cloud Model Case

a. Tropical Latitude Section------------------- 115

b. Mid to High Latitude Section---------------- 116

20. Radiational Balance at the Tropopause (R_s), in the Atmospheric Column Between k = 2 and k = 10 (R_a), and at the Ocean Surface (R) of Both the two-thirds Cloud Case and the Full Cloud Case for 16 January 1974------------------------------- 118

21. Tropospheric Heat Budget Disposition of Both the two-thirds Cloud Case Model and the Full Cloud Case Model for 16 January 1974------------ 126

22. Surface Heat Budget Disposition of Both the two-thirds Cloud Case Model and the Full Cloud Case Model for 16 January 1974------------------ 130

A-1. Depiction of $\tilde{\varepsilon}_{wc}$ and $F_{wc}\downarrow$ on the Yamato Radiation Chart-------------------------------------- 138

LIST OF SYMBOLS AND ABBREVIATIONS

A(m,n) - solar insolation absorbed in the layer (m,n)

$\bar{a}(m,n)$ - Manabe-Möller absorptivity function

a* - turbulent transfer coefficient

ABA - absorptivity of the troposphere

ABG - fractional absorptivity of solar insolation by earth's surface

ALB - earth-atmospheric system albedo

ATRAN - transmissivity of the troposphere

B_k - Stefan-Boltzmann blackbody flux at T_k

BALB - 24-hour averaged radiational balance at earth's surface

BALk_1k_2 - 24-hour averaged radiational balance for layer (k_1,k_2)

BALT - 24-hour averaged radiational balance at tropopause

BBB - ice conduction coefficient

C - carbon dioxide layer absorber mass

cal. cm.$^{-2}$ min^{-1} - calories per centimeter squared per minute

CL - total opaque cloud cover

CL(I) - fractional cloud amount for layer:
I = 1 in 600 to 400 mb;
I = 2 in 900 to 800 mb

CL'(I) - two-thirds of cloud amount CL(I)

E - East longitude; evaporation

e_x - vapor pressure at top of constant flux layer

F(A) - solar insolation subject to water vapor absorption only

FADJ - total incoming insolation at top of atmosphere

Fk_1k_2	- net infrared flux divergence between level k_1 and k_2 .
F_k^*	- net infrared flux at level k
FNWC	- Fleet Numerical Weather Central
F(S)	- solar insolation subject to Rayleigh scattering only
g	- gravity
h	- hour angle
H	- height of homogeneous atmosphere; 24-hour averaged hour angle
H_Γ	- sensible heat transport
HICE	- heat conduction into ice
I	- abscissa grid location
IA10(m,n)	- solar insolation absorbed at surface with cloud condition (m,n)
IS10(m,n)	- solar insolation at surface subject to Rayleigh scatter with cloud condition (m,n)
J	- ordinate grid location
k	- pressure level used in this study equal to 10σ
K*	- eddy turbulent transfer coefficient
L	- latent heat of vaporization
$\ell y\ \mathrm{min}^{-1}$	- langleys per minute
M	- water-vapor mass path length
N	- North latitude
P	- pressure
P_k	- pressure in millibars (mb) at level k
q_k	- mixing ratio at level k
q_{s_k}	- saturated mixing ratio at level k
QAVE	- 24-hour averaged insolation at the tropopause

r	- Bowen ratio
R	- correlation coefficient; net radiation balance at the surface
R_a	- mean radiative cooling rate in troposphere
R_d	- universal gas constant
REF	- total insolation reflected back to space
REFA	- F(A) insolation reflected back to space
REFS	- F(S) insolation reflected back to space
R.H.	- relative humidity
R_s	- mean radiative energy gain (loss) rate at ocean-troposphere system
S	- South latitude; effective solar constant; heat storage at surface
S_a	- heat storage term for the troposphere
T_k	- temperature at level k
T_o	- freezing point of sea water
TRAN	- total insolation incident at the earth's surface
T_x	- temperature at the top of constant flux layer
U	- water-vapor layer absorber mass
V_g	- geostrophic windspeed
V_s	- surface windspeed
W	- West latitude
W(m,n)	- cloud fractional weight for cloud condition (m,n)
Z	- Zenith angle
Z_k	- height at level k
$\alpha(G)$	- surface albedo
$\alpha(R)$	- Rayleigh clear sky albedo
γ_c	- critical lapse rate

δ - solar declination angle

ε_{wc} - emissivity due to water and carbon dioxide absorber mass at indicated layer

θ_k - potential temperature at level k

Λ - longitude

π - surface pressure; pi = 3.1416

ρ - density

σ - sigma pressure level used by FNWC, normalized to surface pressure

ϕ - latitude

ACKNOWLEDGEMENT

The author wishes to express his appreciation to his wife, Cheryl, for her patience and support as well as for her typing of the rough draft of this thesis.

Appreciation is also expressed to Professor F. L. Martin, the author's thesis advisor, for his tireless guidance and support, in addition to his helpful advice and suggestions.

Further recognition is also due for the efforts of Mr. Russell D. Schwanz for programming assistance.

I. INTRODUCTION

This thesis represents a continuing study of a radiative heating parameterization for use in appropriate σ-layers of the Fleet Numerical Weather Central (FNWC) numerical prediction system. The immediate goal of this thesis is to analyze the heat balance of the earth-ocean system utilizing FNWC gridded data-fields at constant pressure levels for 16 January 1974. These gridpoint data were selected along four meridians, three in the Pacific and one in the Atlantic Ocean. Most of the gridpoints were located in the Northern Hemisphere (Fig. 1).

The most important influence on the radiational dispositions (short and long-wave) of this study was the specification of amounts of clouds in two specific layers. The initial specification of the fractional amounts CL(1) and CL(2) are based on large-scale formulations developed by Smagorinsky [1960] and first used in a similar study based upon 16 October 1973 data by Warner [1974].

The governing equations of the radiational transfers of the model have been devised by Martin [1972, 1974], who modified the streams of radiation, both solar and terrestrial, to respond to the presence of clouds in specified amounts in the two layers. The radiational model developed by Martin and utilized here has similarities to those in use in UCLA and NCAR General Circulation models, but with special adaptation to the σ-levels of interest to FNWC.

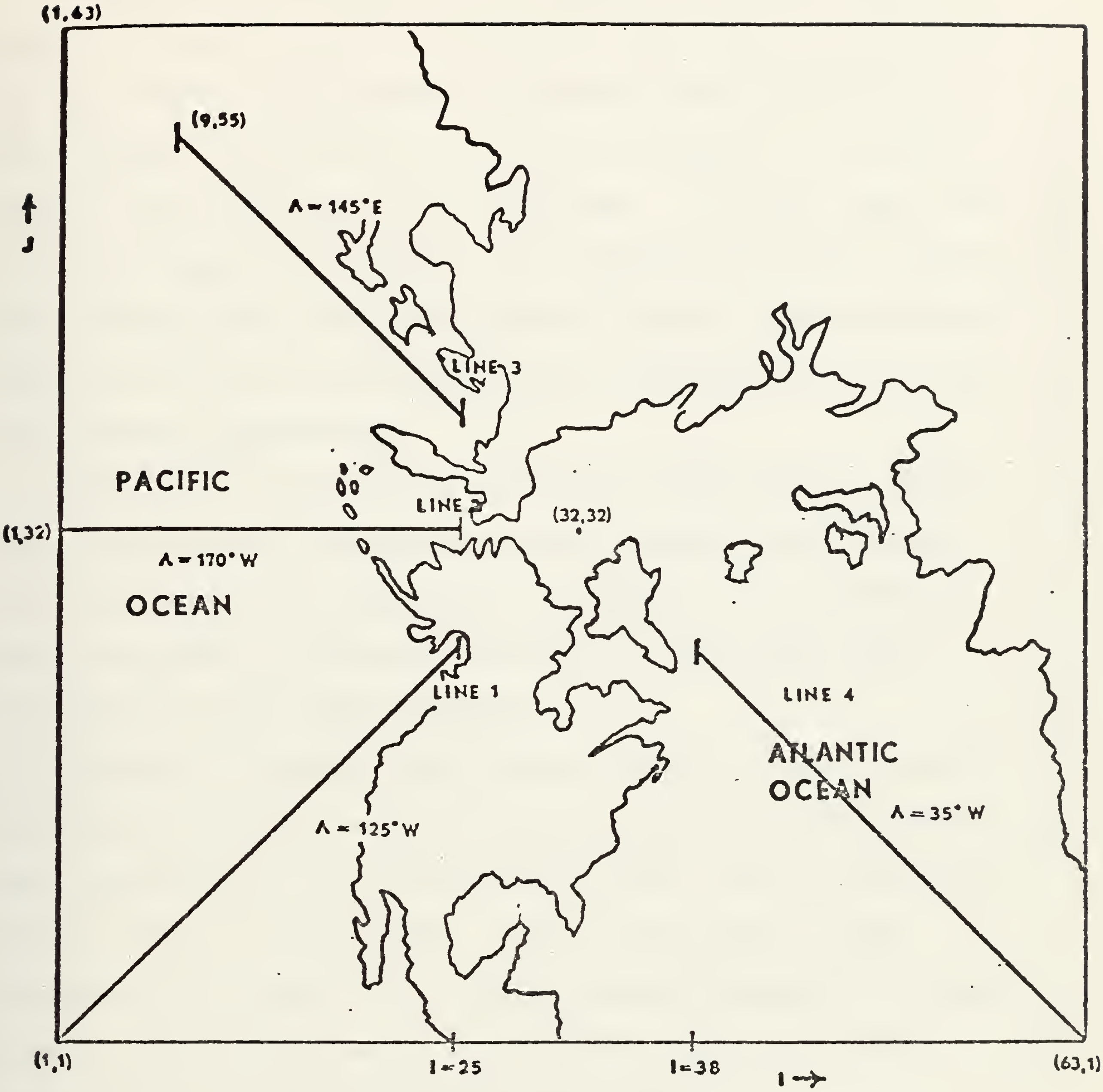

Figure 1. FNWC polar stereographic grid and meridians (lines 1, 2, 3, and 4) selected for study. The longitudes Λ are shown for each meridian as well as the extent considered of each meridian.

Warner found that his global albedo estimates were too high as compared with the satellite climatology of Raschke *et al.* [1973], thus leading to underestimates of the radiative balance both at the top of the atmosphere and at the surface for the data of his experiment. In this study, the original Smagorinsky [1960] cloud-specifications CL_1 and CL_2 were computed for use in the model; however, reduced cloud-amounts (2/3-CL) in each layer were also included for radiative budget comparisons.

The comparative results afforded by the "2/3-CL" model gave reasonably close agreement as a function of latitude with the radiative climatology of Raschke *et al.* [1973], for the NIMBUS III period 21 January - 3 February 1970, examined by these experimenters.

In order to analyze the effects of the "2/3-CL" versus the "full-CL" model used by Warner, oceanic and tropospheric-heat balances were also computed for both sets of cloud conditions for 16 January 1974. It was necessary in this connection to augment the purely radiative model by a turbulent boundary-layer model for sensible and latent heat transports as adapted from Kaitala [1974].

In the 2/3-CL case, the zonally averaged results for the components of the ocean-tropospheric system gave realistic results when compared to climatology for this mid-winter period.

The possible error-source of using one set of computational data to be representative of mid-January climatology is recognized. Nevertheless, the heat-package results computed

with the 2/3-CL cloud model were encouraging when examined against climatology. The major effect noted by the reduction in cloud cover was the reduction in global albedo in both low- and mid-latitudes thus contributing to greater surface net heating rates. This latter result is in general accord with recent observations of Von der Haar and Hanson [1969], Von der Haar and Oort [1973], as well as with Raschke *et al.* [1973]. However, the specification of layered amounts of clouds in the tropics still seems to give somewhat excessive global albedos. It is felt that the geometry of solar radiation streams impinging upon cumulus subgrid cells in the tropics must be reexamined so as to divert a greater percentage of solar radiation downward, as compared with corresponding cloud-layering reflective effects in middle and high latitudes.

II. DATA PREPARATION

Temperature and humidity data utilized in this study were taken from gridpoint soundings along four meridians of the FNWC 63-by-63 gridmesh. The data gridpoints along these meridians (Fig. 1) were chosen so as to ensure conditions representative of oceanic locations for computations of the radiational and other heat budget items. The reasons for choosing oceanic locations for such computations were threefold: (1) the maritime-area heating-rate computations are likely to be relatively stable timewise over the data-day (16 January 1974); (2) the constant $\sigma = P/\pi$ surfaces of the FNWC primitive equation system are close to being constant pressure levels; and (3) values of the heat-budget items computed here may be compared with corresponding climatology during mid-winter. Corresponding values over land areas appear to be less amenable to comparison.

Along the four oceanic meridians used, a total of 67 gridpoint soundings were selected from I = 1 to I = 25 on lines 1, 2, and 3 (over the Pacific Ocean), and 26 soundings from I = 63 to I = 38 along the Atlantic meridian, line 4 (cf., Fig. 1). The device of selecting gridpoint soundings chosen from the indicated meridians of the FNWC polar stereographic map, made it unnecessary to resort to spatial interpolation between original data gridpoints along the meridians.

The gridpoint soundings from the data lines just mentioned were taken from the original FNWC 63-by-63 gridpoint analyses

of temperature at the surface and of T(P) and q(p) at nine other standard pressure levels up to and including 100 millibars (Table I (a)). Those soundings were then modeled into a radiative sounding model compatible in the vertical with FNWC primitive equation prediction levels (Fig. 2).

The Pacific Ocean gridpoint data cases were taken from the 0000GMT, 16 January, 1974 FNWC analyses, while the Atlantic Ocean data cases were taken from the 1200GMT, 16 January 1974 analyses. The reason for the choice of the 0000GMT time-analysis was to correspond to a set of "soundings" as close as possible to local solar noon over the mid-Pacific, whereas those of 1200GMT approximate a near-noon conditions over the Atlantic meridian.

At each gridpoint selected, the original data listed the five moisture values given dewpoint depressions for the analysis levels from 925 mb to 400 mb. Since the standard instrument level vapor pressure (e_{air}) was missing from the original FNWC analysis at all gridpoints, e_{air} was approximated using the FNWC field of e_x, a computed value of vapor pressure at about 20 meters above MSL in the turbulent boundary layer. The FNWC values of T_x and e_x over the ocean had been made available using an operational planetary boundary layer model detailed by Kaitala [1974].

In Sections V and VI it was necessary to recompute values of e_x (and of T_x) by application of the FNWC planetary boundary layer model to data reported in the gridpoint soundings. It was found that FNWC values of e_x as initially reported were accurate enough to be representative of the near-surface

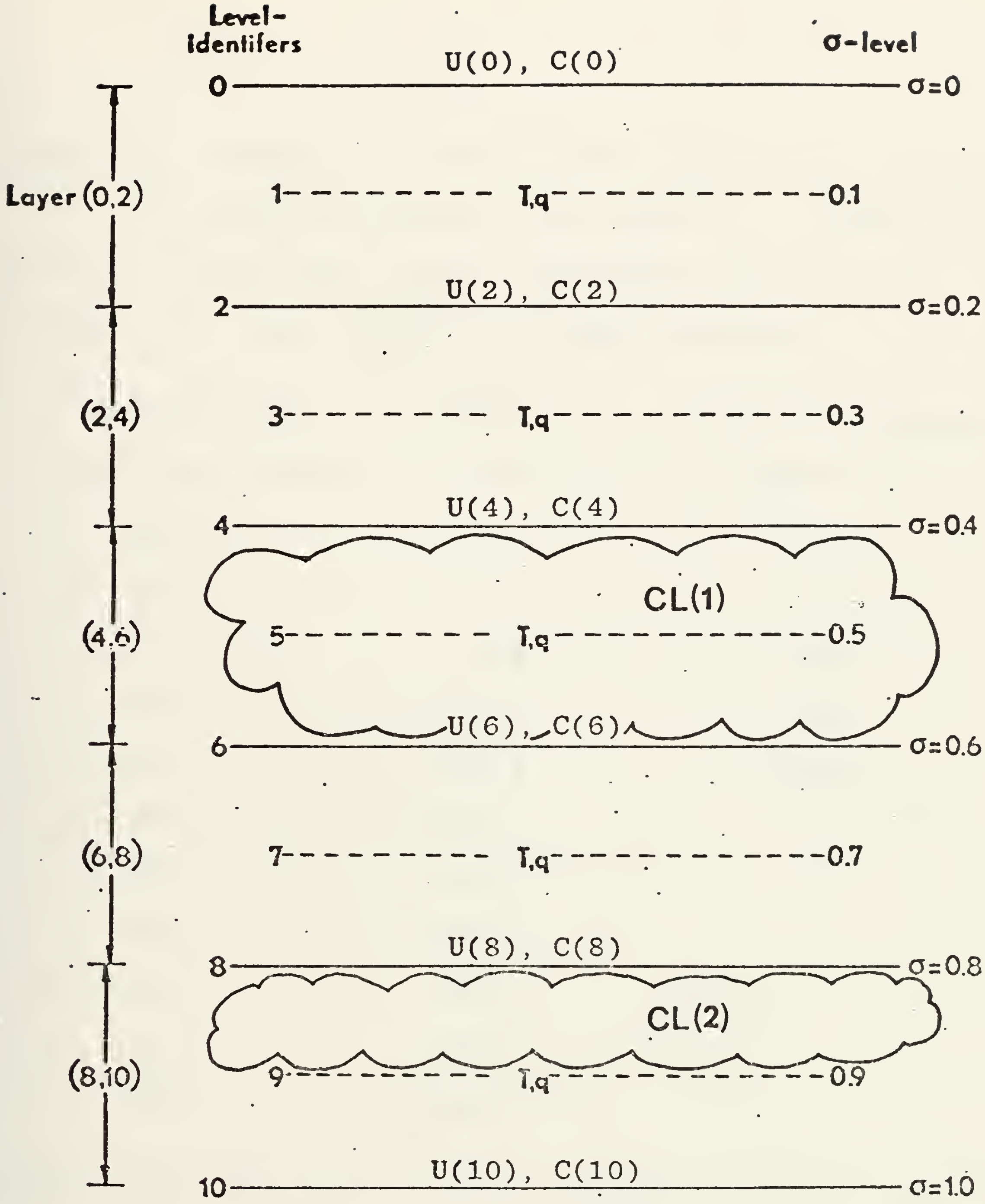

Figure 2. Five-layer radiative sounding used in this study. Levels are identified by their values on the k-scale, while layers are identified by their level boundary indices in parentheses, e.g. (8,10). Pressure-scaled water vapor and CO_2 mass increments U and C, respectively, are integrated with respect to the surface and introduced at even levels while the mixing ratio, q, is formulated at odd levels. The temperature, T, is expressed for all levels. Amounts of clouds CL(1) and CL(2) in the layers shown have been parameterized for consideration of their radiative effects.

Table I(a). Example of typical FNWC sounding for gridpoint (1,1). The humidity parameters between 925,...,400mb are dew-point depressions, and at the surface and top of the constant flux layer (9999*) are vapor pressures.

Pressure (mb)	T(°C)	Humidity Parameters
surface, 1000mb	25.8	e_x=24.9 mb
925	18.7	1.5°C
850	14.9	1.6°C
700	5.9	4.4°C
500	-10.7	4.9°C
400	-22.4	2.0°C
300	-37.3	
250	-46.2	
200	-56.2	
150	-67.4	
100	-80.7	
9999*	T_x=22.9	

*Code 9999 indicates data taken from the top of the constant-flux level (CFL) of the FNWC initial data program.

Table I(b). Example of the corresponding radiative sounding with mixing ratio listed at odd k-levels (Fig. 2). Additionally, water vapor and CO_2 absorber masses, cloud amounts, CL(1) and CL(2) where applicable in the radiative sounding.

Pressure (mb)	T(°K)	Mixing Ratio g/kg	Absorber Masses		Cloud Amounts CL(1),CL(2)
			Water Vapor (gm/cm^2)	CO_2 (cm/cm^2)	
1000	25.8	15.49			
900	17.1	12.76			
800	12.1		2.392	45.53	CL(2) 1.000
700	5.9	6.12			
600	- 1.3		3.349	83.53	CL(1) .650
500	-10.7	2.31			
400	-22.4	1.37	3.633	113.35	
300	-37.3	.54			
200	-56.2		3.679	134.00	
100	-80.7	.02	3.680	138.67	
0	-80.7	.00	3.680	143.35	

humidity values, e_{air}, even though the computations for e_x made in Sections V and VI employed other parameter-values for these computations.

In addition to the parameters listed in Table I(a, b), surface geostrophic windspeeds were also calculated. In the procedure for calculation of the windspeeds at the gridpoints, use was made of the 100 mb FNWC analysis to determine the contour heights as D-values. At certain locations, climatic geostrophic windspeeds were used (Atkinson, 1970). A more complete explanation of the use of the geostrophic windspeed calculations and its use in connection with the planetary boundary layer sensible and latent heat transports is found in Section V, and the windspeed values are listed in that section.

To perform the radiative calculations indicated in Table I (b), data-processing methods were applied to convert both the temperature and mixing-ratio data at k-levels to obtain the cloud amounts, CL (1) and CL (2) at certain required k-level boundaries (Fig. 2). It should be observed that all soundings in this study start at sea level with the approximation of surface pressure $\pi \doteq 1000$ mb. Thus the k-levels correspond approximately to the FNWC σ-levels and are taken as P = 1000., 900., 800., ..., 200., 100., 0.0 respectively.

A. INTERPOLATIVE PROCESSING TO k-LEVELS IN RADIATIVE SOUNDINGS

1. Temperatures

At each mandatory level of Table I(a) between the 1000.,..., 100 mb, gridpoint temperatures were listed. An

assumption was made that at the top of the atmosphere, the temperature was isothermal from 100 mb to p = 0.0 mb. The listed FNWC sea-surface temperature was taken as T_{10}. At the remaining k-levels, air temperatures were derived from either the corresponding FNWC listed temperature or where necessary by interpolation from listed values of the original FNWC data. The interpolation scheme used was that of the three-point Lagrangian formula in the vertical.

$$\begin{aligned} T_k = T_o & \; ((P_k-P_1)(P_k-P_2))/((P_o-P_1)(P_o-P_1)) \\ & + T_1 \; ((P_k-P_o)(P_k-P_2))/((P_1-P_o)(P_1-P_2)) \qquad (2\text{-}1) \\ & + T_2 \; ((P_k-P_o)(P_k-P_1))/((P_2-P_o)(P_2-P_1)). \end{aligned}$$

It is noted that in Equation 2-1, k is the required pressure level needed for the T_k interpolation. The level P_o lies above P_k and the pressure levels P_1, and P_2 lie below level k. The temperatures T_o, T_1, and T_2 are at the same levels as P_o, P_1 and P_2 respectively.

2. Humidities At k-Levels

Moisture parameters from the original gridpoint soundings (Table I (a)) were converted into mixing ratios at each of the original sounding levels (Table I (a)). Then utilizing Equation 2-2 the near-surface vapor pressure (taken as e_x) was employed to calculate the mixing ratio at k = 10 as follows:

$$q_{1000} \doteq 621.97 \; (e_{air}/1000) \qquad (2\text{-}2)$$

where $e_{air} \doteq e_x$ is in mb and q_{1000} is in gm(kgm)$^{-1}$. The

remaining mixing ratios were calculated from the original FNWC dewpoint depression data levels (Table I (a)) using Equation 2-3 (after Fleagle and Businger, 1963):

$$q(P) = \frac{621.97 \exp (A-B/T)}{P} \exp \left[\frac{-B(T-T_D)}{T\ T_D} \right] \qquad (2\text{-}3)$$

where $q(P)$ = mixing ratio at pressure level P and

A = 21.656

B = 5418.0°K

T = temperature (deg. K) at level P

T_D = dewpoint (deg. K) at level P

$T-T_D$ = dewpoint depression at level P.

The computed q-values were subsequently interpolated to k-levels using the procedure indicated in Equation 2-1. An example of the interpolated q-values is shown for the case of the radiative sounding at point (1, 1) (Table I (b)).

3. Humidity Extrapolation to $p \leq 300$ mb

Due to the fact that most radiosonde humidity data for $p \leq 300$ mb is either unreliable or not available, a power-law extrapolation formula (Equation 2-4) similar to one used by Smith [1966], was employed to obtain q-values at k = 3, 2, and 1:

$$\frac{q(P)}{q_5} = \left(\frac{P}{500} \right)^{\lambda} \qquad (2\text{-}4)$$

where $q(P)$ = mixing ratio at level k in g Kg^{-1}

q_5 = mixing ratio at level P = 500 mb in g Kg^{-1}

P = pressure at level k in mb.

Equation 2-4 was solved for the best-fit parameter λ, relating the variables $y \equiv \log(q(P)/q_5)$ and $x \equiv \log(P/500)$. Six q-values from the original sounding including P = 1000, 925,

850, 700, 500, and 400 mb from Table I (a) are used in the best fit solution (e.g., Crow *et al.*, 1960):

$$\lambda = \frac{\sum_{i=1}^{i=6} y_i x_i}{\sum_{i=1}^{i=6} x_i^2} \, . \qquad (2\text{-}5)$$

After the determination of λ from Equation 2-5, extrapolation of q-values from P = 400 to P = 300, 200, and 100 mb, was performed utilizing Equation 2-4.

The procedure of the previous paragraph was carried out at each gridpoint. As a test of the usefulness of the λ-profile technique in determining q-values above 300 mb, a correlation coefficient was statistically computed for each λ-profile. The correlation coefficient computed was between y and x and had the form:

$$R_{y/x} \equiv \lambda \sqrt{\frac{\sum_{i=1}^{i=6} x_i^2}{\sum_{i=1}^{i=6} y_i^2}} \qquad (2\text{-}6)$$

As was found in the studies of Jenks [1974] and Warner [1974], the correlation coefficient was found generally to lie in the range of .95 to .99. Such high correlations indicate that the λ-profile technique for determining upper atmosphere q-values has realistic estimation value for the vertical-scale involved.

4. Pressure-Scaled Absorber Masses

By using the mixing-ratio values computed at the five odd k-levels, the layer pressure-scaled water vapor absorber masses denoted by ΔU (Fig. 1) were calculated for

each layer centered at the five odd k-levels. The general equation for computing the pressure-scaled water vapor mass was:

$$U(k-1,k+1) = \frac{q_k \Delta P}{g} \left[\frac{P_k}{1013.25} \right]^{.72} \qquad (2\text{-}7)$$

where the pressure ratio raised to the exponent 0.72 has been employed (after Möller and Raschke, 1964). k is the odd-level centered in each vertical layer concerned and $\Delta P = 200$ mb was used for each of the five layers. The procedure was followed for each layer (8, 10), (6, 8), (4, 6), (2, 4), and (0, 2).

The algorithm for computing the integrated water vapor mass above the earth's surface was then developed as follows:

$$\begin{aligned} U(10) &= 0.0 \\ U(8) &= U(10) + U(8, 10) \\ U(6) &= U(8) + U(6, 8) \\ U(4) &= U(6) + U(4, 6) \qquad (2\text{-}8) \\ U(2) &= U(4) + U(2, 4) \\ U(1) &= U(2) + 0.5U(0, 2) \\ U(0) &= U(2) + U(0, 2). \end{aligned}$$

In the computation of the carbon-dioxide scaled absorber mass, a computational routine similar to the one used for water vapor was employed. Because it is customary to state the CO_2 absorber masses in terms of the N. T. P. volume of the gas in cms over a cm^2 of the earth's surface, the CO_2 absorber mass (ΔC) centered on an odd k-level becomes

$$\Delta C_k \equiv C(k-1,k+1) = 3.14 \times 10^{-4} \left(\frac{\Delta P}{g\rho_s} \right) \left(\frac{P_k}{1013.25} \right)^{0.72}. \tag{2-9}$$

Here k is the odd-level indicator, 3.14×10^{-4} is the constant mixing ratio of CO_2 by volume, while $\Delta P/g\rho_s$ is the N. T. P. thickness of any layer of pressure-increment $\Delta P = 200$ mb. ρ_s is the constant density in a homogeneous atmosphere of depth H, in which

$$T_{(Surf)} = 273.16 \text{ deg. K and } P_s = 1013.25 \text{ mb.}$$

Finally, Equation 2-9 is shown to be represented in the form

$$C(k-1,k+1) = 3.14 \times 10^{-4} (H) \left(\frac{\Delta P}{1013.25} \right) \left(\frac{P_k}{1013.25} \right)^{.72}$$

$$H = \frac{RT_s}{g} = 7.9954 \times 10^5 \text{ cm.} \tag{2-10}$$

Equation 2-10 was then utilized for each odd level k = 9, 7, 5, 3, 1.

As was done in the water-vapor case, an algorithm similar to Equation 2-8 is developed to find the integrated carbon dioxide mass above the earth's surface:

$$\begin{aligned} C(10) &= 0.0 \\ C(8) &= C(10) + C(8, 10) \\ C(6) &= C(8) + C(6, 8) \\ C(4) &= C(6) + C(4, 6) \\ C(2) &= C(4) + C(2, 4) \\ C(1) &= C(2) + 0.5C(0, 2) \\ C(0) &= C(2) + C(0, 2). \end{aligned} \tag{2-11}$$

B. CLOUD PARAMETERIZATION

The relative humidities and thus the saturation vapor pressure at levels k = 5 and k = 9 are used in the calculations of the fractional cloud cover amounts in layers (4, 6) and (8, 9). The saturation vapor pressures at each level were computed using the following equations (cf., Equation 2-3):

$$q_s(5) = \frac{621.97 \exp\left[A - \frac{B}{T_5} \right]}{500} \qquad (2\text{-}12\ (a))$$

$$q_s(9) = \frac{621.97 \exp\left[A - \frac{B}{T_9} \right]}{900} \qquad (2\text{-}12\ (b))$$

where A = 21.656 and B = 5418.0 deg. K.

The relative humidities were then calculated from:

$$R.H.(5) = \frac{q(5)}{q_s(5)} \qquad (2\text{-}13\ (a))$$

$$R.H.(9) = \frac{q(9)}{q_s(9)} \ . \qquad (2\text{-}13\ (b))$$

Using these relative humidity values, the fractional cloud amounts for each layer were parameterized employing equations similar to Smagorinsky [1960]:

$$CL(1) = 2.0\ (RH(5)) - 0.7 \qquad (2\text{-}14\ (a))$$

$$CL(2) = 3.33\ (RH(9)) - 2.0. \qquad (2\text{-}14\ (b))$$

Equations 2-14 have been employed in the radiative studies of Jenks [1974] for a spring day in 1973 and by Warner [1974] for a case in mid-October, 1973. In the current study, Equations 2-14 are tested in a winter sample of FNWC data for 16 January 1974.

Smagorinsky's parameterization of CL(1) and CL(2) permits cloudiness fractions of 1.30 and 1.333 respectively with RH = 1.0. Values of CL of this magnitude were allowed originally by Smagorinsky to suggest the type of supersaturation which accompanies precipitation. However, in all of the radiative models in use (that of FNWC, UCLA, NCAR, etc.), it was considered correct procedure to limit $CL \leq 1.0$ in both layers. In the radiative calculations of this study an arbitrary reduction by one third of that computed by the Smagorinsky formulations (2-14) was made so that neither fractional cloud-cover could exceed unity. For radiative calculations, the degree of supersaturation in clouds was considered not of importance.

Thus CL(1) and CL(2) computed by (2-14a, b) are replaced respectively by their comparison cloud-covers, CL(1)' and CL(2)', defined by

$$\begin{aligned} CL(1)' &= 2/3\ CL(1) \\ CL(2)' &= 2/3\ CL(2) \end{aligned} \qquad (2\text{-}15)$$

computed at each gridpoint. The objective for testing the reduced cloud-covers (2-15) was to determine the relative sense of the displacement of the radiative balance of the earth atmosphere system. Such radiative tests were especially crucial since evidence from Warner's [1974] tests made with unmodified (CL(1), CL(2)) indicated that the planetary albedo was larger than observations from NIMBUS III (Raschke, *et al.* 1973). The one-third reduction in the Smagorinsky calculated amounts used in this study is an initial effort to tune cloud amounts to give radiational results in closer agreement with

the latest satellite results such as are found in Raschke *et al.* [1973]. Also, the fractional cloud amounts were considered functions of large-scale effects only. Small scale convective activity, seasonal conditions (other than the soundings themselves), and latitudinal effects were not considered in specifying this reduction factor. The purpose of the reduced cloud-parameterization modification was for estimating radiational effects only.

C. WINDSPEED USED IN TURBULENT HEAT TRANSFERS

For all gridpoints located between 5°N and 5°S, gradient windspeeds were taken from the climatological data for the month of January (Atkinson, 1970). Gradient isotach values were utilized at the tropical gridpoints noted due to the small Coriolis parameter f in Equation (2-16)(below) in the latitudes between 5°N and 5°S.

At all other gridpoints, Equation (2-16) was utilized to compute geostrophic windspeed given by

$$|V_g| = \frac{g}{f} \frac{|\Delta z|}{2(\frac{d}{m})} \qquad (2\text{-}16)$$

here $g = 9.80665 \mathrm{m\ sec}^{-2}$

m = map factor $= \frac{1.86603}{1 + \mathrm{Sin}\phi}$

ϕ = latitude

$d = 381. \times 10^3 \mathrm{m}$ = nominal FNWC grid-dimension

$$f = \left(\frac{4\pi}{86,400} \right) \mathrm{Sin}\phi \qquad (2\text{-}17)$$

$$|\Delta z| = \sqrt{(z_4 - z_2)^2 + (z_3 - z_1)^2} \; . \qquad (2\text{-}18)$$

In (2-16) and (2-18), Δz is the contour-difference centered in general on the gridpoint. At the map edge gridpoints of meridians 1, 2, 3, 4 it was possible to compute only a forward differenced version of Equation 2-18 (cf., Fig. 3). Thus at edge-points "0", Equation 2-19 was used (below). Note, the grid distance d/m in Equation 2-19 is one-half of that used in Equation (2-16).

$$|V_g| = \frac{g}{f} \frac{|\Delta z|}{(d/m)} \tag{2-19}$$

with

$$\Delta z = \sqrt{(z_4 - z_0)^2 + (z_3 - z_0)^2} \; . \tag{2-20}$$

All geostrophic windspeeds were then converted to surface windspeeds using the following empiricism due to Langlois and Kwok, [1969].

$$V_s = .8 \; |V_g| + 2.2 \tag{2-21}$$

where V_s = surface windspeed (mps)

V_g = 1000 mb geostrophic windspeed.

Note that in the interval 5 to 10 degrees of latitude in either hemisphere, the value of the Coriolis parameter was arbitrarily set at $f = .25 \times 10^{-4} \mathrm{sec}^{-1}$, following Kaitala [1974], while for $|\phi| \geq 10°$, the actual value of f for this particular latitude was used.

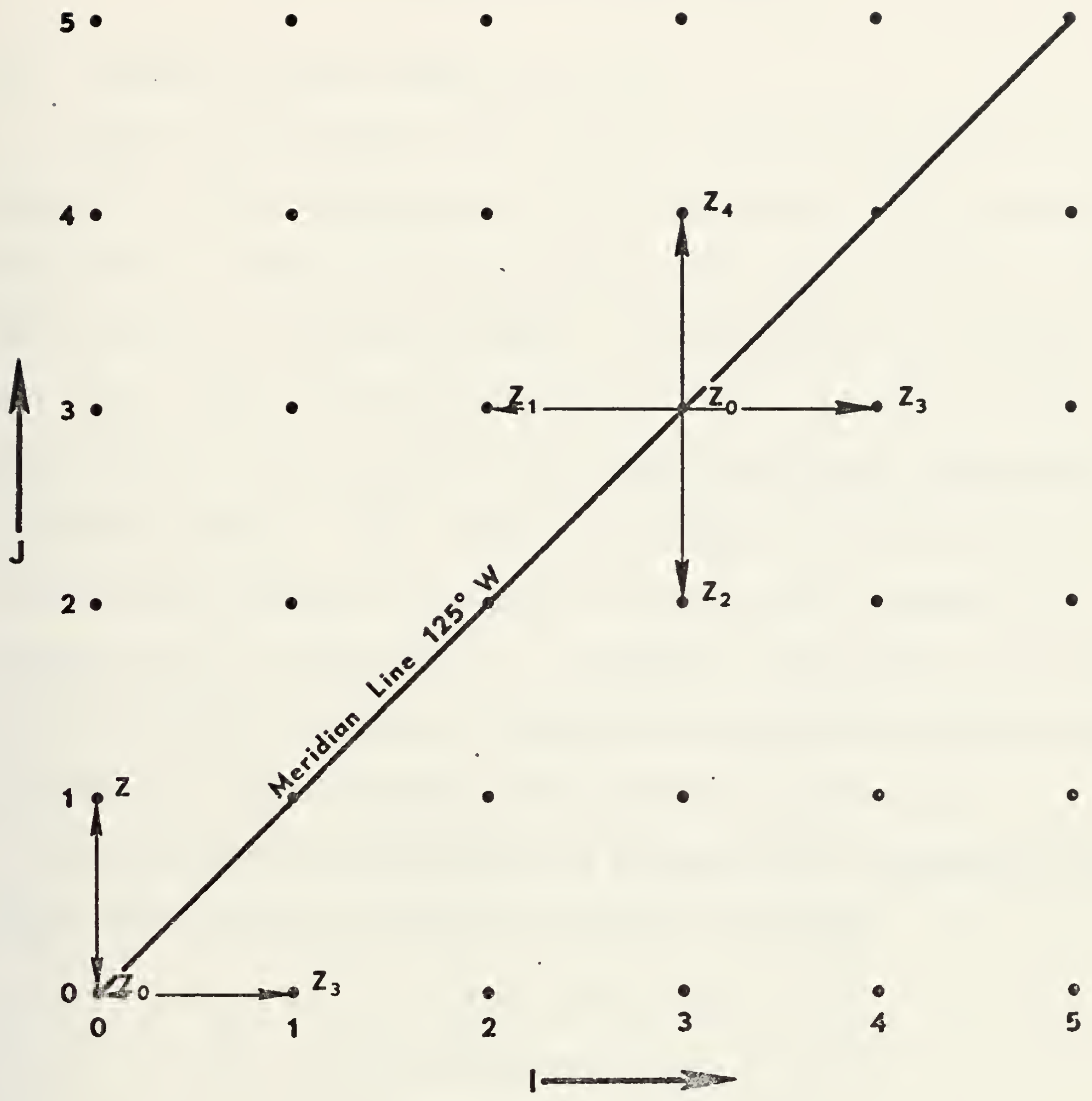

Figure 3. Section of FNWC polar stereographic meridian illustrating the method of obtaining contour gradients in the vicinity of a gridpoint. The values of contour-heights correspond to the 1000 mb D-values in the neighborhood of the gridpoint.

III. TERRESTRIAL RADIATION

A. THEORETICAL AND EMPIRICAL BASIS

Empirical formulas for computing emissivities for terrestrial flux calculations in the atmosphere were developed by Sasamori [1968] in association with the operation of the NCAR General Circulation Model. These empirical formulas for water vapor and CO_2 emissivities were matched to the theoretical values used in the Radiation Chart developed by Yamamoto [1952]. This chart was proved by Jenks [1974] to be accurate enough to simulate the empirical methods of Sasmori and is used here as a schematic guide for the integration of the radiative transfers through the various layers in the radiative soundings described in Section II.

For use in the FNWC heating package, the essential long-wave flux formulas required are the following:

$F_{10}*$ = net IR flux at earth, k = 10

F_6* = net IR flux at level, k = 6

F_2* = net IR flux at level, k = 2

F610 = net IR flux divergence in the layer (6, 10)

F26 = net IR flux divergence in the layer (2, 6).

In order to get the IR flux-divergences (i.e., cooling rates) in the layers (6, 10) and (2, 6), the differences $F_6* - F_{10}*$ and $F_2* - F_6*$ must be computed. The detailed scheme for making such computations for various combinations of cloud cover CL(1), CL(2) is similar to that used by Warner [1974] and is explained in the following subsections B, C, D,

and E along with the diagrams Figures (4a,b,c,d), (5a,b,c,d) and (6a,b,c,d). A complete listing of net IR fluxes and cloud amounts was computed at each gridpoint. An example of this listing is shown for "full-cloud" amounts, Equation 2-14, in Table II. One must further have a physically sound representation of the emissivity ε_{wc} as a function of both water-vapor and CO_2 absorber masses along the sounding, that is, along the path of integration in order to make IR net-flux calculations. For further explanation of the emissivity formulas (after Sasamori 1968) used in the quadrature scheme, refer to Appendix A.

B. NET FLUX F_{10}*

As depicted in Table I (b), radiative soundings have been computed as the combination of parameters U(k, 10), C(k, 10), T_k, for each required level k. Also, listed at each gridpoint are the cloud-cover parameters CL(1) and CL(2) computed from (2-14). The grid area may then be thought of being composed of areal fractions (or weights) W(0, 0), W(1, 1), W(1, 0), and W(0, 1) which are defined by Equations 3-1,......,3-4 as follows:

(a) totally clear skies, case (0, 0)

$$W(0,\ 0) = (1-CL(1))(1-CL(2)) \qquad (3\text{-}1)$$

(b) overcast in both layers, case (1, 1)

$$W(1,\ 1) = (CL(1))(CL(2)) \qquad (3\text{-}2)$$

(c) overcast in upper layer only, (case 1, 0)

$$W(1,\ 0) = (CL(1))(1-CL(2)) \qquad (3\text{-}3)$$

(d) overcast in lower layer only, (case 0, 1)

$$W(0,\ 1) = (1-CL(1))(CL(2)). \qquad (3\text{-}4)$$

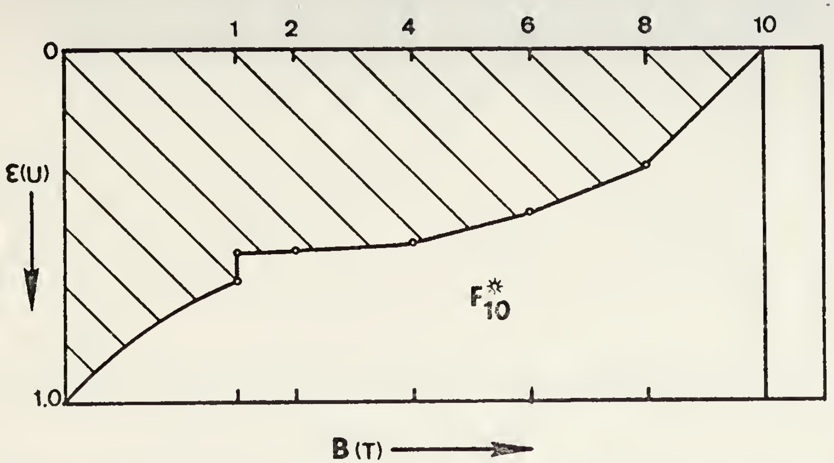

Figure 4(a). Terrestrial net flux F_{10}* with clear skies (case (0,0)). Unhatched area depicts F_{10}*.

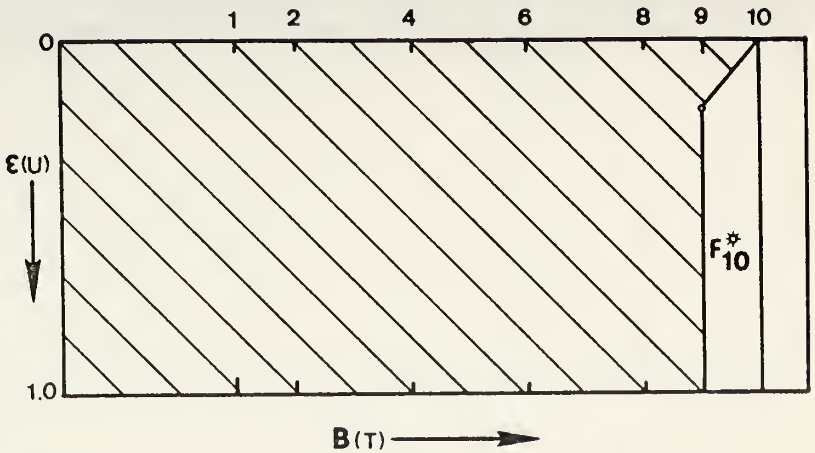

Figure 4(b). Terrestrial net flux F_{10}* with both high and low clouds present, (case (1,1)). Unhatched area depicts F_{10}*.

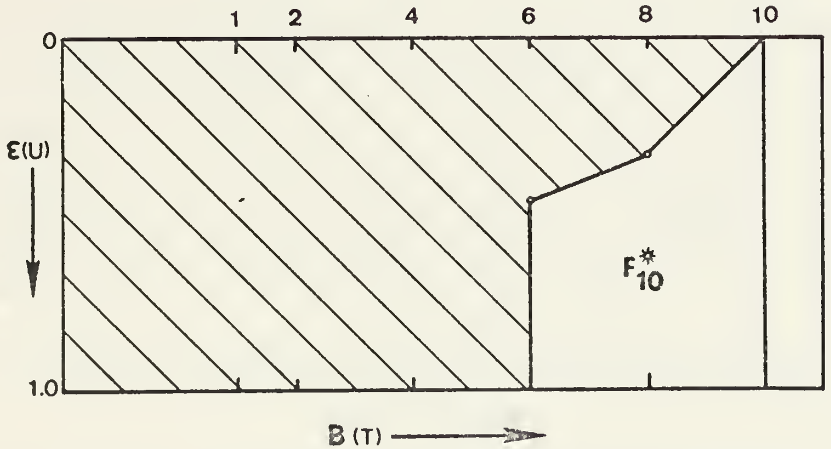

Figure 4(c). Terrestrial net flux F_{10}* with high clouds only, (case (1,0)). Unhatched area depicts F_{10}*.

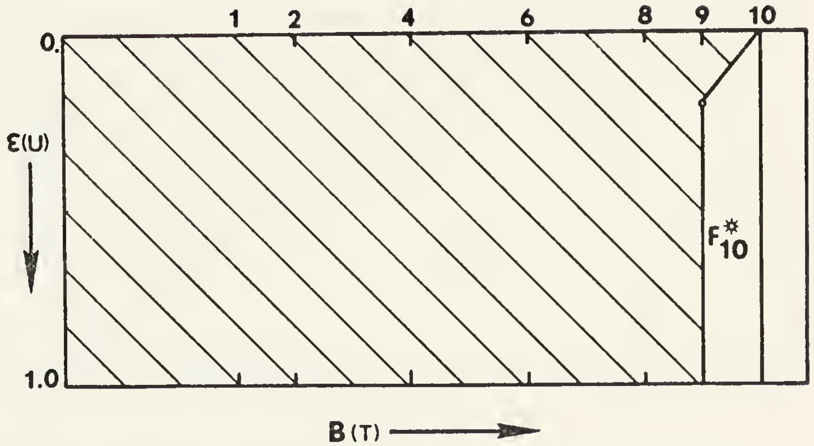

Figure 4(d). Terrestrial net flux F_{10}* with low clouds only, (case (0,1)). Unhatched area depicts F_{10}*.

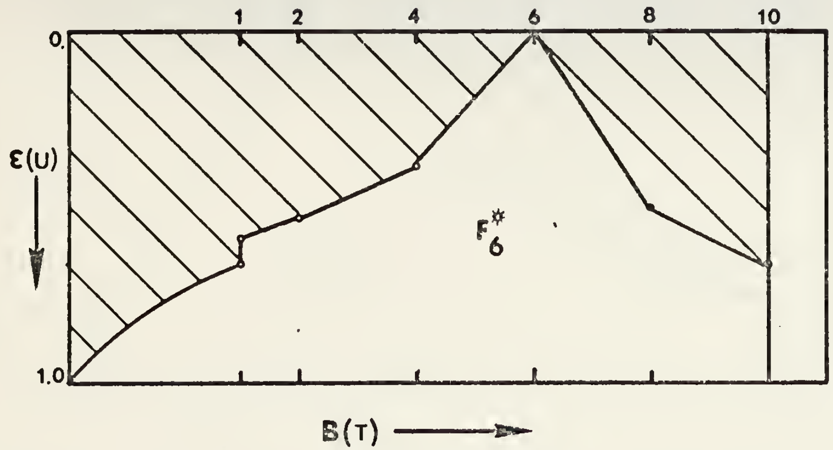

Figure 5(a). Terrestrial net flux F_6* with clear skies (case (0,0)). Unhatched area depicts F_6*.

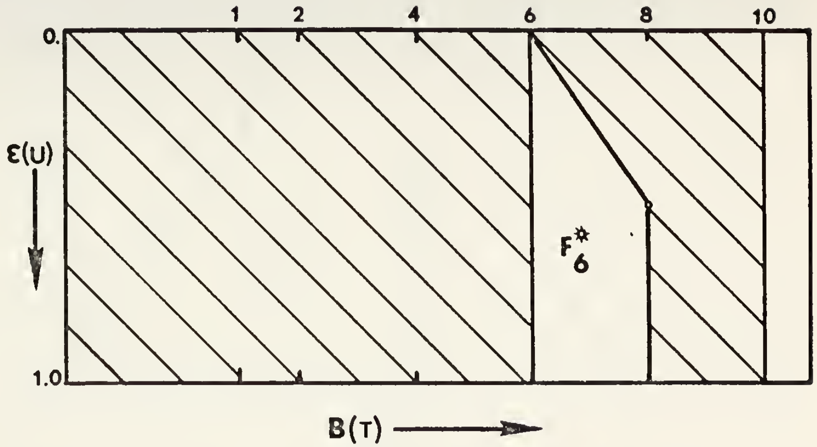

Figure 5(b). Terrestrial net flux F_6* with both high and low clouds (case (1,1)). Unhatched area depicts F_6*.

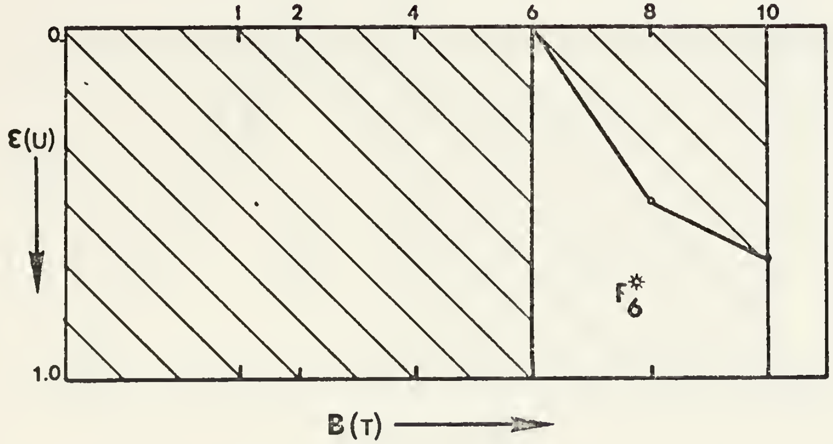

Figure 5(c). Terrestrial net flux F_6* with high clouds only (case (1,0)). Unhatched area depicts F_6*.

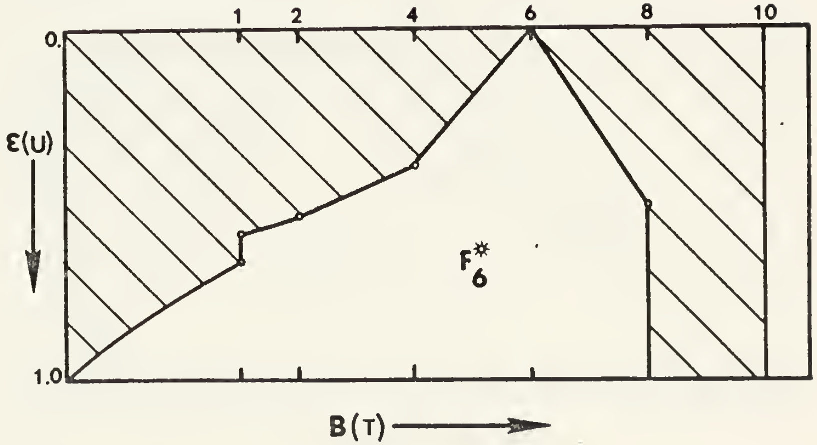

Figure 5(d). Terrestrial net flux F_6* with low level clouds (case (0,1)). Unhatched area depicts F_6*.

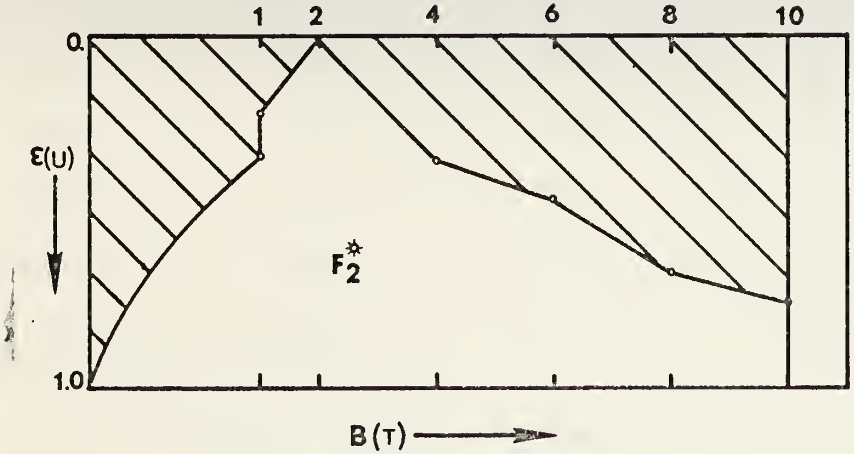

Figure 6(a). Terrestrial net flux F_2* with clear skies (case (0,0)). Unhatched area depicts F_2*.

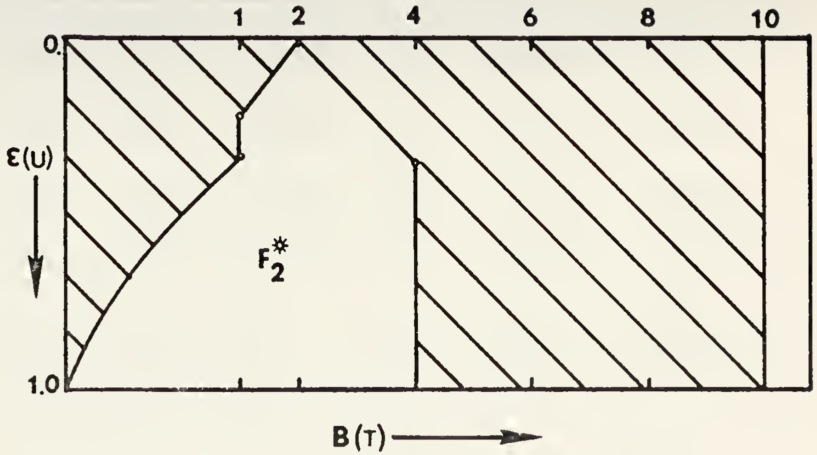

Figure 6(b). Terrestrial net flux F_2* with both high and low clouds (case (1,1)). Unhatched area depicts F_2*.

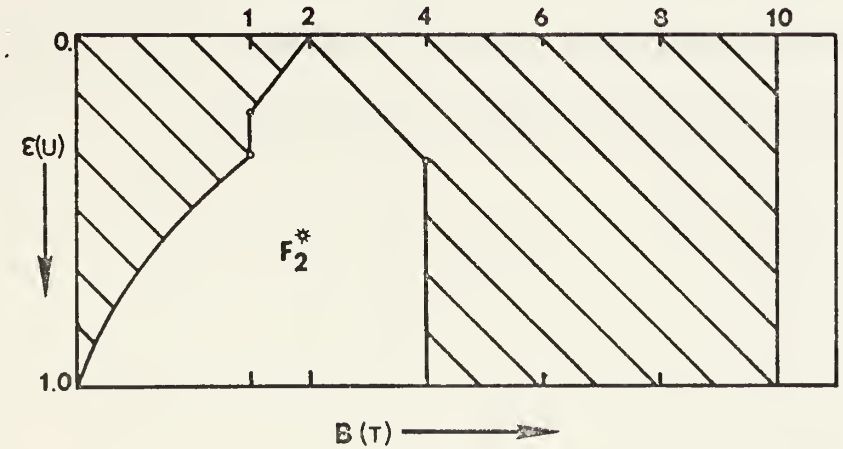

Figure 6(c). Terrestrial net flux with high level clouds only (case (1,0)). Unhatched area depicts F_2*.

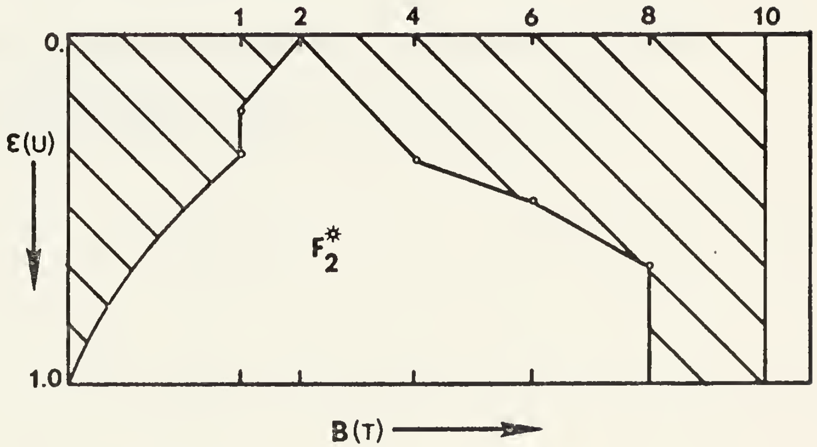

Figure 6(d). Terrestrial net flux with low level clouds only (case (0,1)). Unhatched area depicts F_2*.

CL(1) = 0.0 CL(2) = 0.0 WT = 0.0 F_{10}^* = .1639 F_6^* = .2701 F_2^* = .3575 ly/min.

CL(1) = 1.0 CL(2) = 0.0 WT = 0.0 F_{10}^* = .0910 F_6^* = .0910 F_2^* = .2407 ly/min.

CL(1) = 0.0 CL(2) = 1.0 WT = .3496 F_{10}^* = .0471 F_6^* = .2407 F_2^* = .3301 ly/min.

CL(1) = 1.0 CL(2) = 1.0 WT = .6504 F_{10}^* = .0471 F_6^* = .0616 F_2^* = .2407 ly/min.

COMPOSITE TOTALS F_{10}^* = .05 F_6^* = .12 F_2^* = .27 ly/min.

CL(1) = .65042 CL(2) = 1.000

Table II. A sample listing of gridpoint values of the terrestrial radiation fluxes computed at gridpoint (1,1) using the equations detailed in Sec. III.

By multiplying the appropriate weighting factors by the respective net flux computations $F_{10}*(0, 0),\ldots,$ $F_{10}*(0, 1)$ the composite net fluxes at level k = 10 for the combined cloud (CL(1), CL(2)) coverage over the grid area are then obtained. Such composite net flux values have the following form using level k = 10 as an example:

$$F_{10}* = W(0, 0)F_{10}*(0, 0) + W(1, 1)F_{10}*(1, 1) + W(1, 0)F_{10}*(1, 0) + W(0, 1)F_{10}*(0, 1). \qquad (3\text{-}5)$$

1. Net Flux with Clear Skies, $F_{10}*(0, 0)$

In Fig. 4 (a) the hatched area represents downward flux F10↓ at k = 10 or in integral form:

$$F_{wc}\downarrow = \int_{B=0}^{B_{10}} \varepsilon_{wc}\, dB\ , \quad B_k = \sigma T_k^4$$

B_k is the Stephen-Boltzman blackbody flux at T_k. ε_{wc} is the combined water-vapor and CO_2 emissivity along the sounding, and is related to absorber-masses as detailed in Appendix A. The unhatched area therefore depicts the net flux at k = 10 with clear skies given in the equation

$$F_{10}*(0, 0) = \int_{B=0}^{B_{10}} (1 - \varepsilon_{wc})dB,\ B_{10} = St*T_{10}^4. \qquad (3\text{-}6)$$

2. Net Flux with Overcast Clouds in Both Layers, $F_{10}*(1,1)$

Figure 4 (b) illustrates this case. By using the trapezoidal summation techniques, F10↓ at k = 10 is depicted once again by the hatched area representative of the case of an overcast with base at k = 9. The unhatched area depicts the integral

$$F_{10}*(1,\ 1) = \int_{B=0}^{B_{10}} (1 - \varepsilon_{wc})dB \qquad (3\text{-}7)$$

with overcast clouds at both upper and lower levels (Fig. 4 (b)).

3. Net Flux with Overcast Clouds in Upper Layer Only, $F_{10}*(1,\ 0)$

Here in Fig. 4 (c), the hatched area depicts the total F10↓ emitted down from the cloud base at k = 6, plus an increment in the upper right corner of Fig. 4 (c), which represents the contribution to F↓ from the water vapor and CO_2 in the atmospheric layer from k = 6 to k = 10. The unhatched area depicts the integral

$$F_{10}*(1,\ 0) = \int_{B=0}^{B_{10}} (1 - \varepsilon_{wc})dB. \qquad (3\text{-}8)$$

4. Net Flux with Overcast in Lower Layer Only $F_{10}*(0,\ 1)$

This case is the same as depicted for case $F_{10}*(1,\ 1)$ in Fig. 4 (d) and is explained in Section III.(B).2. $\tilde{\varepsilon}_{wc}$ is the temperature-dependent emissivity for the completion of the integration from level k = 1 to the origin (B = 0, ε = 1.0) of the Yamamoto Radiation Chart, applied for $T \leq 210$ deg. K. ε_{wc} is the temperature-independent emissivity applied where $T \geq 210$ deg. K in the level from k = 1 to k = 10. For the specific formulations of $\tilde{\varepsilon}_{wc}$ and ε_{wc} after Sasamori [1968] see Appendix A.

5. The Composite $F_{10}*$ (CL(1) CL(2)) Equation

The principle involved in compositing net fluxes has already been expressed by Equation 3-5. The following equation can be thought of as the general form of the quadrature

scheme used to evaluate the integrals for computing F_{10}^* for any combination of (CL(1), CL(2)). It is also used in computing the integral for the composite cloud-cover case F_{10}^*, corresponding to (3-5):

$$\begin{aligned} F_{10}^*(CL_1,CL_2) = {} & [1-CL(2)]\{(B_{10}-B_6)-.5[\varepsilon_{wc}(8,10)(B_{10}-B_8) \\ & + (\varepsilon_{wc}(8,10)+\varepsilon_{wc}(6,10))(B_8-B_6)]\} \\ & + (1-CL(2))(1-CL(1))\{B_6-.5[(\varepsilon_{wc}(6,10) \\ & + \varepsilon_{wc}(4,10))(B_6-B_4)+(\varepsilon_{wc}(4,10) \\ & + \varepsilon_{wc}(2,10))(B_4-B_2)+(\varepsilon_{wc}(2,10) \\ & + \varepsilon_{wc}(1,0))(B_2-B_1)+\tilde{\varepsilon}_{wc}((0,10),T_1)*B_1]\} \\ & + CL(2)\{(B_{10}-B_9)[1-.5\varepsilon_{wc}(9,10)]\}. \end{aligned} \tag{3-9}$$

By setting CL(1) = CL(2) = 0.0, Equation 3-9 reduces to the form needed in calculating $F_{10}^*(0, 0)$. Similarly, one can obtain the equation for computing $F_{10}^*(1, 1)$ as depicted on the chart in Fig. 4 (b) by setting CL(1) = CL(2) = 1.0. Finally, the other two subcases $F_{10}^*(1, 0)$ and $F_{10}^*(0, 1)$) can be formulated by setting CL(1) = 1.0, CL(2) = 0.0, and CL(1) = 0.0, CL(2) = 1.0, respectively in Equation 3-9. Similar procedures were followed for computing net IR flux at levels k = 6 and k = 2, as described in the Subsections C and D (Figs. 5 (a), (b), (c), (d) and 6 (a), (b), (c), (d), respectively.

C. NET FLUX F_6^*

1. The Composite F_6^* Equation

The following expression, which represents the F_6^* composite net flux, may be thought of as the weighted sum of the unhatched areas of Figs. 5 (a), (b), (c), and (d), with the appropriate weight factors W(0, 0), W(1, 1), W(1, 0), and W(0, 1) of Equations 3-1, 2, 3, and 4 applied. The resulting expression for $F_6^*(CL_1, CL_2)$ becomes (after Warner, 1974)

$$
\begin{aligned}
F_6^* = {} & [1-CL(1)]\{B_8-.5[\varepsilon_{wc}(6,8)(B_8-B_6)+\varepsilon_{wc}(4,6)(B_6-B_4) \\
& + (\varepsilon_{wc}(4,6)+\varepsilon_{wc}(2,6))(B_4-B_2)+(\varepsilon_{wc}(2,6)+\varepsilon_{wc}(1,6))(B_2-B_1) \\
& + \tilde{\varepsilon}_{wc}((0,6),T_1)*B_1]\}+(1-CL(1))(1-CL(2))\{(B_{10}-B_8)[1. \\
& - .5(\varepsilon_{wc}(6,8)+\varepsilon_{wc}(6,10))]\}+CL(1)\{(B_8-B_6)* \\
& [1-.5\varepsilon_{wc}(6,8)]\}+CL(1)(1-CL(2))\{(B_{10}-B_8)* \\
& [1-.5(\varepsilon_{wc}(6,8)+\varepsilon_{wc}(6,10))]\}.
\end{aligned}
\tag{3-10}
$$

2. Net Flux With Clear Skies $F_6^*(0, 0)$

As was described in Section III.B.5 concerning the use of the composite case (Equation 3-9), Equation 3-10 can be reduced to give expressions for F_6^* for the various cloud-cover cases (0, 0), (1, 1), (1, 0), and (0, 1). The resulting expressions are depicted as the unhatched areas in Figs. 5 (a), (b), (c), and (d). For the clear sky case of F_6^*, Equation 5-10 would be employed with CL(1) = CL(2) = 0.0. This is depicted by the unhatched area in Fig. 5 (a).

3. Net Flux With Overcast Clouds in Both Layers F_6*(1, 1)

For this case, Equation 3-10 would be used with CL(1) = CL(2) = 1.0. This is depicted by the unhatched area in Fig. 5 (b).

4. Net Flux With Overcast Clouds in Upper Layer Only F_6*(1, 0)

The expression needed in this case, and which is depicted by the unhatched area in Fig. 5 (c), is formulated by using Equation 3-10 and setting CL(1) = 1.0 and CL(2) = 0.0.

5. Net Flux With Overcast Clouds in Lower Layer Only F_6*(0, 1)

The expression needed in this case, representable by the unhatched area in Fig. 5 (d), is formulated by using Equation 3-10 and setting CL(1) = 0.0 and CL(2) = 1.0.

D. NET FLUX F_2*

A procedure analogous to the ones used in the computations of F_{10}* and F_6* net fluxes can be used in calculation the net flux at level k = 2. F_2* is represented pictorially by the weighted sum of the unhatched areas of Figs. 6 (a), (b), (c), and (d). Once these areas have been computed with the proper weighting factors applied, as was done similarly in Equations 3-9 and 3-10, the following general expression for the composite result for F_2* results

$$
\begin{aligned}
F_2^* = {} & [1-CL(1)]\{B_8 - .5[\varepsilon_{wc}(2,4)(B_4-B_2)+(\varepsilon_{wc}(2,4) \\
& + \varepsilon_{wc}(2,6))(B_6-B_4)+(\varepsilon_{wc}(2,6)+\varepsilon_{wc}(2,8))* \\
& (B_8-B_6)+\varepsilon_{wc}(1,2)(B_2-B_1)+\tilde{\varepsilon}_{wc}((0,2),T_1)*B_1)]\} \qquad (3\text{-}11)
\end{aligned}
$$

$$\begin{aligned}&+ (1-CL(1))(1-CL(2))*\{(B_{10}-B_8)[1-.5(\varepsilon_{wc}(2,8) \qquad (3\text{-}11)\\&+ \varepsilon_{wc}(2,10))]\}+CL(1)\{B_4-.5[\varepsilon_{wc}(2,4)(B_4-B_2)\\&+ \varepsilon_{wc}(1,2)(B_2-B_1)+\tilde{\varepsilon}_{wc}((0,2),T_1)*B_1]\}\end{aligned}$$

Equation 3-11 can also be derived in the computation of the net fluxes for the general cloud-cover cases once the proper weight factors for the simplified net fluxes are introduced. These simplified F_2* cases correspond to the (0, 0), (1, 1), (1, 0), (0, 1) cloud-overcast/clear combinations and are represented by the notation F_2*(0, 0), F_2*(1, 1), F_2*(1, 0), F_2*(0, 1), respectively. The corresponding chart depictions are displayed in Fig. 6 (a), (b), (c), (d), respectively.

E. APPLICATION TO HEAT BALANCE COMPUTATIONS

In order to compute the heat balance of the atmosphere, layers (2, 6) and (6, 10) are treated as subject to solar heating (Section IV). In order to complete the atmospheric radiational balance, the long-wave mean cooling rate in the FNWC model was computed as follows (after Kaitala [1974]):

$$F26 = F_2^* - F_6^* \qquad (3\text{-}12(a))$$

$$F610 = F_6^* - F_{10}^* \qquad (3\text{-}12(b))$$

where the combination 26 and 610 indicates the layer boundaries. Equations 3-12(a) and (b) represent the cooling effects by terrestrial radiation in the indicated layers, which is applicable at the time of the analysis. The radiative balance at the surface is computed using the absorbed solar insolation (Section IV.B-C) and the net flux F_{10}* from Equation (3-9). A complete heat balance at the surface is computed by subtraction of the

evaporative and sensible heat transport (Section V) from the surface radiative "balance." All these balances are displayed in cross sectional display forms in Section VI. The IR-cooling analysis was carried out at each gridpoint and the cooling rates were stored by gridpoint along each meridian. The zonally-averaged atmospheric balances are detailed in Sections VII and VIII for 16 January 1974.

F. STATISTICAL RESULTS AND COMPARISONS

A statistical test of the $F_{10}{}^*$ numerical results (Equation 3-9) was conducted by utilizing a linear regression program for regressing the 93 values of $F_{10}{}^*$ on the corresponding sample values of B_{10} and $B_{10}\sqrt{e}$ as predictors. The program used was based on the BMD02R in the Biomedical set of programs (after DIXON, 1973). The resulting form was

$$F_{10}{}^* = B_{10}\ (a + b\sqrt{e}) \qquad (3\text{-}13)$$

where B_{10} = Stephen-Boltzman blackbody radiation at the surface with temperature T_{10}. $B_{10} = St * T_{10}{}^4$

e = surface layer vapor pressure (mb).

a and b in Equation 3-13 are the desired regression coefficients and are dependent on B_{10} and $B_{10}\sqrt{e}$ (after Brunt, 1932). The predictand used for the regression was $F_{10}{}^*$, which included the downward contribution of CO_2 as well as that of water vapor in the computation of net flux at level 10. The statistical equation found in this study is Equation 3-14 where R_m is the multiple correlation coefficient.

$$\begin{aligned} F_{10}{}^* &= .3564B_{10} - .0224B_{10}\sqrt{e} \\ R_m &= .9955. \end{aligned} \qquad (3\text{-}14)$$

The high value of the R_m shows that B_{10} and $B_{10}\sqrt{e}$ are good predictors of $F_{10}*$ and therefore of F_d obtained from $F_{10}* = B_{10} - F_d$. Introduction of $F_{10}*$ into 3-14 permits solution of the latter for the downward flux at the surface. F_d is given by

$$F_d = B_{10}\{(1-a)-b\sqrt{e}\}$$

or (3-15)

$$F_d = B_{10}(.6436 + .0224\sqrt{e}).$$

Equation 3-15 is to be compared with a similar result after Swinbank [1963]

$$F_d = B_{10}(.64 + .037\sqrt{e}). \tag{3-16}$$

In summary, the high value of the correlation coefficient of Equation 3-14 along with a strong similarity between Equations 3-15 and 3-16 seems to indicate that Equation 3-14 may be regarded as an oceanic version of the Brunt downward-flux equation. Also, it is noted that F_d depends most strongly upon B_{10} and only slightly on $(B_{10}\sqrt{e})$. This was to be expected over the oceanic regime where nearly constant relative humidities exist over large, expansive areas.

A second statistical test was based upon a possible relationship between cloudy sky and clear sky cases of $F_{10}*$. In this test, the ratio $F_{10}*(CL)/F_{10}*(0, 0)$ was used as the predictand. The predictor was an approximation to the composite total opaque cloud at each gridpoint, defined as:

$$CL = CL(1) + CL(2)(1 - CL(1)). \tag{3-17}$$

The regression was run twice, first utilizing $F_{10}*(CL)$ computed using the amounts of CL(1) and CL(2) as calculated from

the Smagorinsky formulas (Equations 2-14(a), (b)) and second, utilizing $F_{10}^*(CL)$ computed from the two-thirds amounts of CL(1) and CL(2). The resulting regression formulas based upon a best-fit to the 93 soundings used in this study were listed in (3-18, 3-19)

$$\text{FULL CL:} \quad F_{10}^*(CL) = F_{10}^*(0,\ 0)(1-.75CL),\ R = .9916 \tag{3-18}$$

$$\text{2/3 CL:} \quad F_{10}^*(CL) = F_{10}^*(0,\ 0)(1-.73CL),\ R = .9936. \tag{3-19}$$

A comparison equation after Sverdrup [1942] is included as (3-20)

$$F_{10}^*(CL) = F_{10}^*(0,\ 0)(1-.83CL). \tag{3-20}$$

The high correlation coefficients found with Equation 3-18 and 3-19 along with the similarity to the Equation 3-20 (after Sverdrup, 1942), indicates the general capability of the IR-radiative model employed in this study to account for the effective net radiation at the surface, $F_{10}^*(CL_1,CL_2)$, both in the completely clear and cloudy-sky cases.

The mean values of the parameters in Equations 3-18 and 3-19 over the 93 gridpoint soundings were as follows:

FULL-CLOUD STATISTICS	REDUCED-CLOUD STATISTICS
$\overline{F_{10}^*(CL)} = .0749\ \ell y\ min^{-1}$	$\overline{F_{10}^*(CL)} = .0950\ \ell y\ min^{-1}$
$\overline{F_{10}^*(0,\ 0)} = .1518\ \ell y\ min^{-1}$	$\overline{F_{10}^*(0,\ 0)} = .1518\ \ell y\ min^{-1}$
$\overline{CL} = .6951$	$\overline{CL} = .5190$

In the above table, superior-bar symbols denote sample means. These results indicate that the surface net flux is decreased by the respective ratios (.0769/.1518) = .507 with $\overline{CL}$ = .6951 and (.0568/.1518) = .3740 with $\overline{CL}$ = .5190. These results

indicate that the downward flux $F_{10}\downarrow(CL)$ is, on the average, 50.7 percent larger than the clear-sky case utilizing the cloud-parameterization model (Equations 2-14(a), (b)) in this study with full cloud amounts. On the other $F_{10}\downarrow(CL)$ for the two-thirds cloud-model, the downward flux is increased by only 37.4 percent relative to the clear-sky case.

G. COMPARISONS WITH CLIMATOLOGICAL RESULTS OF F_2

Comparison was made of F_2 by the model-computations with satellite measurements of total long-wave flux to space after Raschke *et al.* [1973] for the NIMBUS III period 21 January - 3 February 1970. F_2 is used instead of F_2^* since the satellite does not measure the downward flux at k = 2. F_2 is computed using Equation 3-11, which was also used for F_2^* but omitting those emissivity-terms involving levels above k = 2, that is $\varepsilon_{wc}(2, 1)$ and $\varepsilon_{wc}(2, 0)$, from Equation 3-11. These terms are associated with downward flux at k = 2. The results for 16 January 1974 were computed both for the full-cloud and the two-thirds cloud-amount cases, based upon all gridpoint soundings. These F_2 - values were then interpolated to whole multiple of 5° latitude along each of the four meridians, and the results latitudinally averaged to get a "zonally-averaged" value valid for each 5° latitude band used in this study.

Table III (a) shows the zonally-averaged F_2 - values compared with those after Raschke *et al.* For consistency in comparison of the F_2 results deduced here with those reported by Raschke, the latter's results were obtained by interpolation from charts using the same oceanic meridians as those

	Radiative Statistics			Cloud Statistics	
Lat	F_2 (FULL-CL)	F_2 (2/3-CL)	F_2 (Raschke)	FULL-Cloud CL AVG.	2/3-Cloud CL AVG.
20S	.311	.325	.370	.932	.758
15	.321	.334	.378	.927	.733
10	.344	.354	.377	.867	.634
5	.354	.363	.347	.746	.536
0	.361	.369	.351	.790	.556
5	.371	.378	.368	.766	.527
10	.382	.387	.388	.557	.376
15	.386	.393	.394	.532	.342
20	.390	.388	.391	.443	.279
25	.361	.362	.371	.463	.320
30	.354	.328	.344	.559	.411
35	.336	.342	.319	.516	.382
40	.315	.319	.304	.628	.529
45	.278	.270	.292	.833	.740
50	.264	.280	.270	.911	.759
55	.217	.233	.255	.931	.749
60	.209	.226	.258	.764	.528
65N	.235	.235	.230	0.0	0.0
Wt. Avg.	.333	.338	.344	.688	.514

Table III(a). Comparison of zonally-averaged longwave flux to space, F_2, as found by this study for both full-CL and 2/3-CL cloud cases for 16 January 1974, and by Raschke et al. (1973) based upon NIMBUS III measurements. Also included are composite cloud amount fractions used in the two cloud models of this study. Flux values in ly min^{-1}.

used in this study. For further insight into the comparisons, the cloud statistics, CL and 2/3-CL values are listed at each latitude, where CL is given by Equation 3-17. In the bottom line of each column in Table III (a) is listed the cosine-weighted mean of each set of the column values over the listed latitude range. The resulting oceanic-means of F_2 obtained by the various techniques are as follows:

F_2(Full cloud amount this study) = .333 ℓy min^{-1}
F_2(2/3 cloud amount this study) = .338 ℓy min^{-1}
F_2(after Raschke) = .344 ℓy min^{-1}.

Note that the Raschke results do not correspond to specific known CL - values. The only conclusion that can be drawn from Table III (a) is that both cloud-amount systems give F_2 results which are reasonably close to the values reported by Raschke. This is especially true in the subtropics, 15°-20°N, where peak values of F_2 are found, and in high latitudes where minimum values of F_2 (after Raschke, 1973), are found. By these results alone, neither the full-cloud model nor the 2/3 CL can be selected as preferable. The limitations of the comparisons made here are obvious, when it is realized that at latitudes between 20°S-5°S and between 60°N-65°N in Table III (a), fewer than 4 meridional lines enter into the zonal averages listed. For all other latitudinal average values, four meridional lines were used in this averaging. These same limitations will apply to Table III (b) below. Note finally that the model results F_2 (full) and F_2 (2/3 CL) are based upon a single-day's observations, 16 January 1974.

Lat	F_{10}^* (FULL CL)	F_{10}^* (2/3 CL)	F_{10}^* (Budyko)
20S	.054	.078	.091
15	.050	.079	.092
10	.055	.086	.083
5	.063	.090	.085
0	.052	.082	.084
5	.056	.086	.080
10	.085	.107	.086
15	.094	.115	.094
20	.102	.120	.102
25	.104	.120	.098
30	.096	.111	.099
35	.107	.122	.102
40	.096	.108	.109
45	.056	.067	.098
50	.054	.069	.099
55	.052	.068	.102
60	.085	.106	.104
65N	.095	.095	.095
Wt. Avg.	.075	.096	.094

Table III(b). Comparison of zonally-averaged net fluxes at the surface F_{10}^* as found by this study for both full-CL and 2/3-CL cloud cases for 16 January 1974, and comparative values after annual climatology of Budyko (1956). Flux values in ly min^{-1}.

H. COMPARISONS WITH CLIMATOLOGICAL RESULTS OF $F_{10}*$

Table III (b) depicts the zonally-averaged values of the $F_{10}*$ at the earth's surface obtained in this study using both full-cloud model and the two-thirds cloud model. A comparison of the model-computed $F_{10}*$-values for the full and two-thirds cloud cases is then made with annual mean values of $F_{10}*$ obtained from climatological studies (Budyko, 1956). The $F_{10}*$ values shown in Table III (b) were computed from Equation 3-9 using the full CL_1,CL_2 values or the reduced ($2/3CL_1$, $2/3CL_2$) in the respective cloud-models. Since Budyko's mean values of $F_{10}*$ were based on annual climatology, his overall latitudinal range of $F_{10}*$ values is not as great as that of $F_{10}*$ by either cloud-model presented in Table III (b) for 16 January 1974.

It is to be noted that the locations of highest values of $F_{10}*$ after Budyko agree with those computed for both $F_{10}*$ (CL) and $F_{10}*(2/3\ CL)$, namely in the subtropics (latitude 20°N), and again in the latitude range 35-40°N. The "hemispheric" weighted mean of $\overline{F_{10}*} = .096$ ℓy min^{-1} by the reduced-cloud model is slightly greater than the cosine-weighted mean of Budyko (.094 ℓy min^{-1}). However, the weighted mean of $F_{10}*(CL)$ resulting from the full-cloud model is considerably smaller, $\overline{F_{10}*(CL)} = .075$ ℓy min^{-1}. The chief differences in $F_{10}*(CL)$ as a function of latitude compared with that of Budyko is accounted for by the marked minimum in $F_{10}*$ corresponding to the relatively high composite CL-amounts in low-latitudes (from 20S to 5N) and again in the latitude band 45-55°N where in both areas typical minimum values of $F_{10}*(CL)$

$\doteq$ .055 ℓy min^{-1} occur. Such a minimum of F_{10}* in the regions 45-55°N is generally associated with the location of the polar-front zone. However, in this same region the 2/3-CL model gives average values of $F_{10}* \doteq .068$ ℓy min^{-1}. The zonal-mean values of CL and 2/3-CL applicable to Table III (b) by latitude are exactly as listed in Table III (a). It is not clear from the comparisons of Table III (b) whether the higher values of F_{10}* deduced from the 2/3-CL model represents a closer approximation to reality than the F_{10}*(CL) values resulting from Equation 3-9 with the full-cloud model values.

It is to be expected that analogous comparisons made using the solar-insolation model (summarized in Table IV) will indicate some relative advantage for using the full or two-thirds cloud model.

IV. SOLAR RADIATION

A. PARTITION OF SOLAR INSOLATION

The solar constant assumed in this study at level k = 0 (top of atmosphere) was 2.00 ℓy min^{-1} (Joseph, 1971). This flux-value was further depleted by 4% to account for the attenuation caused by oxygen and ozone above the tropopause. This left the value S = 1.92 ℓy min^{-1} at level k = 2 to be used in this study as the effective solar constant.

Equation (4-1) was then utilized to compute the effective solar insolation at the tropopause (k = 2) as follows:

$$F(2) = S \left[\frac{r}{r_m} \right]^{-2} \text{Cos } z \qquad (4\text{-}1)$$

where S = effective solar constant at k = 2

Cos z = cosine of the zenith angle for the Julian date used

r/r_m = ratio of the actual earth-sun distance to the mean earth-sun distance for the Julian date used in this study.

The Smithsonian Meteorological Tables (List, 1958) gives the ratio r/r_m and the solar declination δ for 16 January, 0000GMT, as these values are employed. These values are, respectively:

$$\frac{r}{r_m} = .983715$$

$$\delta = -21.08 \text{ degrees of lat.}$$

δ is used in evaluating the cosine of the solar zenith angle, given by

$$\text{Cos } z = \text{Sin } \phi \text{ Sin } \delta + \text{Cos } \phi \text{ Cos } \delta \text{ Cos } h \quad (4\text{-}2)$$

where ϕ is the latitude and h is the hour angle of the sun

relative to the meridional data lines. For example, Fig. 1 makes it clear that for

line 1 $h = 55°$
line 2 $h = 10°$
lines 3, 4 $h = 35°$

at the times of the synoptic charts (0000GMT and 1200GMT, respectively). Sin ϕ was computed according to the standard polar stereographic projection formula applicable to the FNWC base chart given by

$$\text{Sin } \phi = \frac{r_E^{\,2} - [(I-32)^2 + [(J-32)^2]}{r_E^{\,2} + [(I-32)^2 + [(J-32)^2]} \qquad (4\text{-}3)$$

where $r_E^{\,2} = 973.752$. Thus Sin ϕ assumes the following functional form in terms of the FNWC grid-coordinate I (Fig. 1):

Lines 1, 3, 4

$$\text{Sin } \phi = \frac{973.752-2(32-I)^2}{973.752+2(32-I)^2} \qquad (4\text{-}4 \text{ (a)})$$

Line 2

$$\text{Sin } \phi = \frac{973.752-(32-I)^2}{973.752+(32-I)^2} \qquad (4\text{-}4 \text{ (b)})$$

or, conversely I is given in terms of ϕ by

Lines 1, 3, 4 $$I = 32 - 22.065\left[\frac{\text{Cos } \phi}{1 + \text{Sin } \phi}\right] \qquad (4\text{-}4 \text{ (c)})$$

Line 2 $$I = 32 - 31.205\left[\frac{\text{Cos } \phi}{1 + \text{Sin } \phi}\right] \qquad (4\text{-}4 \text{ (d)})$$

$$I = \begin{array}{l} 1,\ldots, 25 \text{ for Lines 1, 2} \\ 9,\ldots, 25 \text{ for Line 3} \\ 63,\ldots, 38 \text{ for Line 4.} \end{array}$$

For lines 1, 2, and 3 the gridpoint soundings correspond to 0000GMT 16 January when solar noon occurs at the 180th

meridian. Line 4 gridpoint soundings correspond to 1200 GMT, 16 January, when solar noon was at the Greenwich meridian.

A very simple partition of solar insolation was utilized in this study after Joseph [1971]. It consisted of dividing the insolation F(2) into two parts at level k = 2. One part was considered to include all wavelengths $\lambda > .9$ μm where absorption by water vapor and carbon dioxide bands are the most prevalent attenuation processes in clear air. This part of solar insolation was listed as F(A) energy and considered subject to water-vapor absorption but not to Rayleigh scattering. For those wavelengths $\lambda \leq .9$ μm, absorption of the solar insolation energy by water vapor was considered negligible. This part of the solar insolation band was listed as F(S) and was subject only to Rayleigh scattering attenuation in clear air. The two partitions are formulated as follows:

$$F(A) = .349\ F(2) \qquad (4\text{-}5\ (a))$$

$$F(S) = .651\ F(2). \qquad (4\text{-}5\ (b))$$

In this study, the introduction of two cloud decks produced cloud-reflectivity effects upon both the F(A) and F(S) solar energy insolations. However, in the clear areas around any gridpoint the absorption-attenuation only applies to the F(A) insolation while the Rayleigh scattering-attenuation applies to the F(S) insolation only.

B. DISPOSITION OF F(S) INSOLATION

In the treatment of the F(S) insolation, Joseph [1971] determined that Rayleigh scattering reflectance in clear skies

(after Coulson, 1959) could be effectively approximated by least squares in the following form

$$\alpha(R) = .085 + .25074\ [\log\ (\frac{\pi}{P_o}\ \mathrm{Sec}\ z\ )] \qquad (4\text{-}6)$$

where $P_o = 1013.25$ mb. In Equation 4-6, $\pi/P_o \doteq 1$ in view of the fact that mean sea level pressure π is close to 1000 mb. Also

$$\mathrm{Sec}\ z = (\mathrm{Cos}\ z)^{-1}$$

with Cos z given by Equation 4-2.

The surface albedo $\alpha(G)$ is another reflective parameter utilized in this study. Over oceanic areas the following formula for $\alpha(G)$ after Gates *et al.* [1971], was utilized:

$$\alpha(G) = \max\ \{.06,\ .06 + .54\ (.7 - \mathrm{Cos}\ z)\}. \qquad (4\text{-}7)$$

1. Clear Sky Case

In the clear sky (0, 0) case the F(S) insolation was subjected only to Rayleigh scattering reflectance $\alpha(R)$ and to surface reflectance $\alpha(G)$. Considering the likelihood of a succession of multiple reflections between earth and atmosphere, the F(S) insolation actually penetrating the earth's surface after scattering is given by

$$IS10(0,0) = F(S)[1-\alpha(R)][1+\alpha(R)\alpha(G)+\cdots(\alpha(R)\alpha(G))^n$$
$$+\cdots]*(1-\alpha(G)) \qquad (4\text{-}8\ (a))$$

that is, by

$$IS10(0,0) = F(S)[1-\alpha(R)][1-\alpha(G)]/[1-\alpha(R)\alpha(G) \qquad (4\text{-}8\ (b))$$

2. Cloudy-Sky Cases

In the three cases in which clouds were present, F(S) insolation absorbed by the ground at each gridpoint was

computed using a variation of the following equation (after Arakawa, 1972):

$$\begin{aligned} IS10(1,1) = {} & F(S)(1-R(1))(1-R(2))(1-\alpha(G)) \\ & *\{1-[(R(1)R(2)+R(2)\alpha(G)+R(1)\alpha(G) \\ & + 2R(1)R(2)\alpha(G)]\}^{-1}. \end{aligned} \tag{4-9}$$

As indicated by the notation (1, 1), denoting CL(1) = CL(2) = 1.0. Equation 4-9 is the formula used in calculating F(S) insolation absorbed by the ground in the case where overcast clouds are present at both levels of Fig. 2. Also in Equation 4-9, constant cloud-reflectance values were chosen, namely R(1) = .54 for the mid-level clouds between k = 4 and 6, and R(2) = .66 for the low-level clouds between k = 8 and 9. Both cloud-reflectance values are as suggested by C. D. Rodgers [1967].

For the other cloud cases, the following changes were applied to Equation 4-9. In the (1, 0) case (CL(1) = 1.0, CL(2) = 0.0), consider that R(2) = 0 in (4-9), from which it follows that

$$IS10(1, 0) = F(S)(1-R(1))(1-\alpha(G))/[1-R(1)\alpha(G))]. \tag{4-10}$$

In the case (0, 1), R(1) = 0.0 in (4-9) so that

$$IS10(0, 1) = F(S)(1-R(2))(1-\alpha(G))/[1-R(2)\alpha(G)]. \tag{4-11}$$

3. Composite F(S) Insolation

Equations (4-8), (4-9), (4-10), and (4-11) were utilized in the computation of the cloud-weighted F(S) insolation penetrating the earth's surface considering the areal-weights of the cloud combinations denoted by (0, 0), (1, 1), (1, 0) and (0, 1) about a gridpoint. The resultant

F(S) insolation penetrating the earth's surface denoted by IS10 is therefore expressible as

$$\begin{aligned} IS10(CL(1), CL(2)) = {} & IS10(0, 0)\ W(0, 0) \\ & + IS10(1, 1)\ W(1, 1) \\ & + IS10(1, 0)\ W(1, 0) \\ & + IS10(0, 1)\ W(0, 1). \end{aligned} \tag{4-12}$$

Here the weighting factors W(0, 0), W(1, 1), W(1, 0) and W(0, 1) are as computed in Equations 3-1, 3-2, 3-3, and 3-4 respectively. Note finally that the part of F(S) insolation reflected to space is found by subtracting IS10(CL(1), CL(2)) from F(S).

C. DISPOSITION OF F(A) INSOLATION

The fractional portion of the solar insolation subject to absorption by atmospheric water-vapor and carbon dioxide are covered in the following subsections.

1. The Clear-Sky Case (0, 0)

The Manabe-Möller absorptivity function provided the necessary absorptivity values for the key layers in this case. The form of this absorptivity function is

$$\underline{a}(2, k) = .271[U(2, k) \mathrm{Sec}\ z]^{.303}. \tag{4-13}$$

Here $\underline{a}$ is the absorptivity applied to the pressure-scaled water vapor mass between levels 2 and k (Fig. 2) along the zenith slant-path angle z. The resultant absorbed insolational energy in the particular layer (2, k) is then given by the Manabe-Möller relation

$$A(2, k) = 0.271F(A)[U(2, k)\ \mathrm{Sec}\ z]^{.303}. \tag{4-14}$$

The two layers of interest in which absorption was computed were (2, 6) and (2, 10). The absorbed insolation in the layer (6,10) was then computed by

$$A(6, 10) = A(2, 10) - A(2, 6). \qquad (4\text{-}15)$$

It is noted here that the water-vapor mass above level 2 was assumed negligible in this study.

By subtracting A(2, 10) from F(A), the direct transmission of F(A) insolation impinging at the earth's surface was determined. The transmission of F(A) insolation is then further reduced by the transmissivity $(1-\alpha(G))$, after surface-reflectance which leads to the earth-absorbed result

$$IA10(0, 0) = F(A)\{1-.271[U(2,10)\mathrm{Sec}\ z]^{.303}\}(1-\alpha(G)). \qquad (4\text{-}16\ (a))$$

The transmitted energy impinging upon the earth just prior to absorption is

$$TRANA(0, 0) = IA10(0, 0)\ /\ [1-\alpha(G)]. \qquad (4\text{-}16\ (b))$$

2. Cloudy Cases

In order to compute meaningful dispositions of F(A) insolation in cloudy-sky cases, cloud reflectivities and cloud absorptivities after C. D. Rodgers [1967] were utilized. The reflectance-values used here are different from those suggested by Rodgers for the F(S) wavelengths. The cloud reflectivities used here are RA(1) = .46 and RA(2) = .50. In this case there are also cloud-absorptivities to be considered. These were taken as A(1) = .20 and A(2) = .30, respectively. In the following discussions the cloud conditions are considered totally overcast in each of layers

indicated when the notations ((1, 1), (0, 1), and (1, 0)) are utilized.

Schematic representations of the computations performed in the various cases ((1, 1), (0, 1), (1, 0)) are displayed in Figures 7, 8, and 9. These figures suggest the parameters required in computing the disposition of incoming F(A)-insolation from level k = 2 to the earth's surface (k = 10).

Figure 7 depicts the disposition of F(A) insolation in the overcast case with both high and low cloud layers (1, 1). Figure 8 shows the case (1, 0) with an upper overcast only. Figure 9 displays the case (0, 1) for a low overcast. The equations (after Warner, 1974) which relate to the parameters in these figures are listed in Appendix B-1, B-2, B-3, respectively.

In Figs. 7, 8, and 9, the insolations, A24, A46, A68, A89, and A910, etc., represent the insolation absorbed in the layers concerned. Symbols F2, F4, F6, F8, and F9, etc., depict the streams of insolation passing through the indicated level. A vertical arrow implies the direction of insolation passage, i.e., ↓ denotes downward insolation, ↑ upward-reflected insolation, and ↓↓ downward-reflected insolation. The absorption quantity A(6, 8)↓↓, for example, indicates absorbed energy remaining in (6, 8) from a downward reflected beam.

Since multiple reflections occur between the earth's surface and a cloud base, or between cloud-layers in this model, the insolational amount reaching the lowermost reflecting

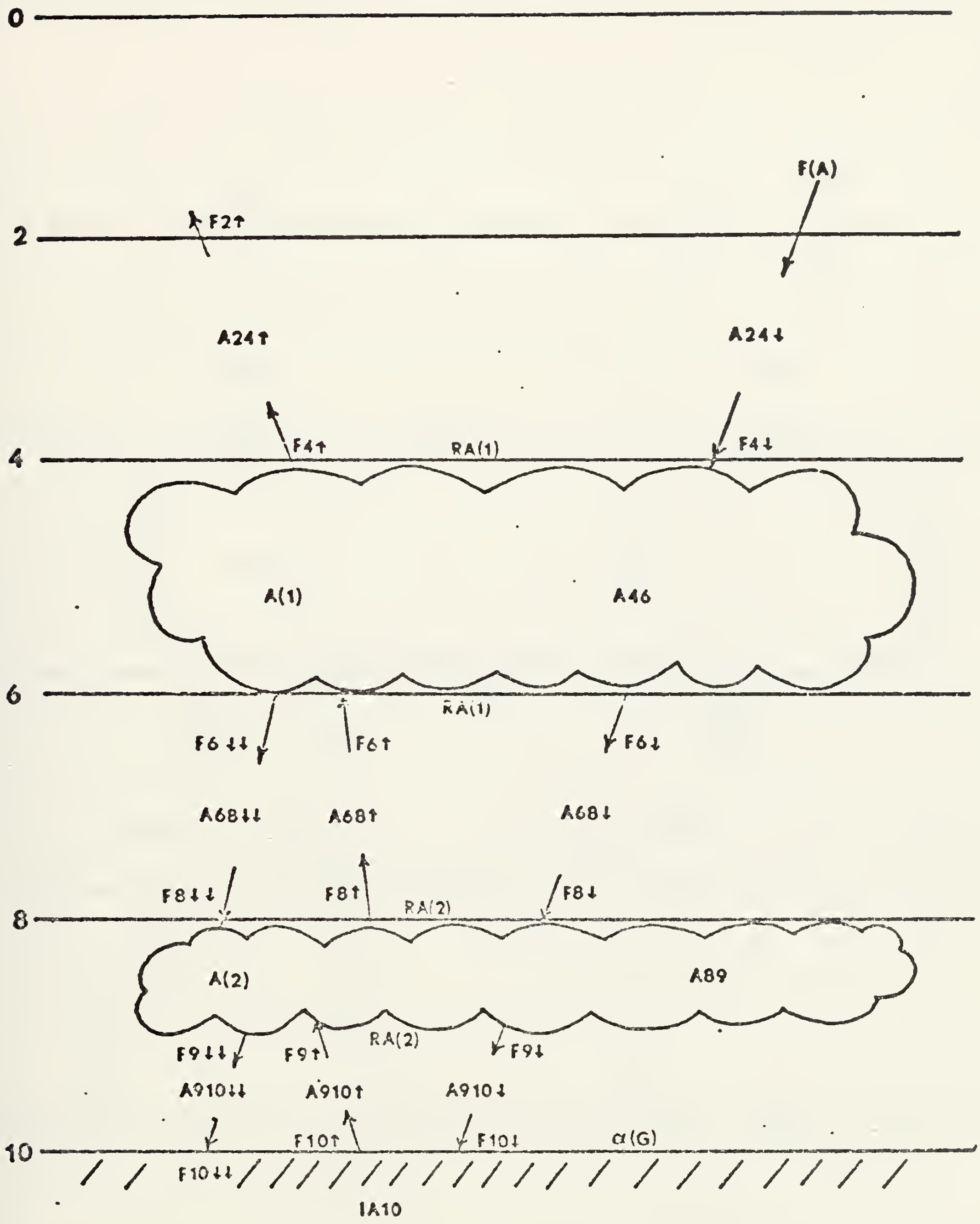

Figure 7 Schematic representation of F(A) insolation disposition in the case of two overcast layers.

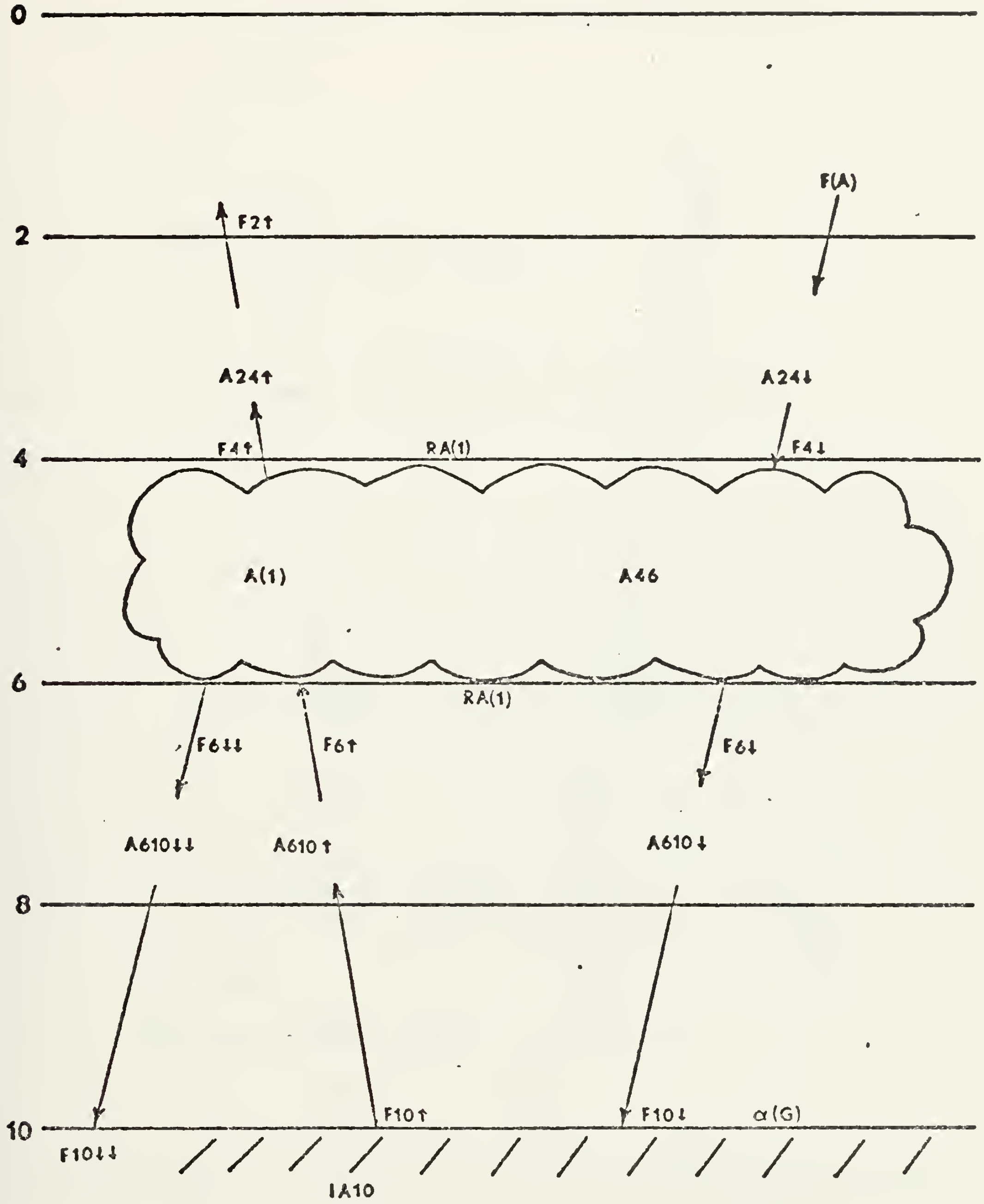

Figure 8 Schematic representation at F(A) insolation disposition with an upper overcast layer only.

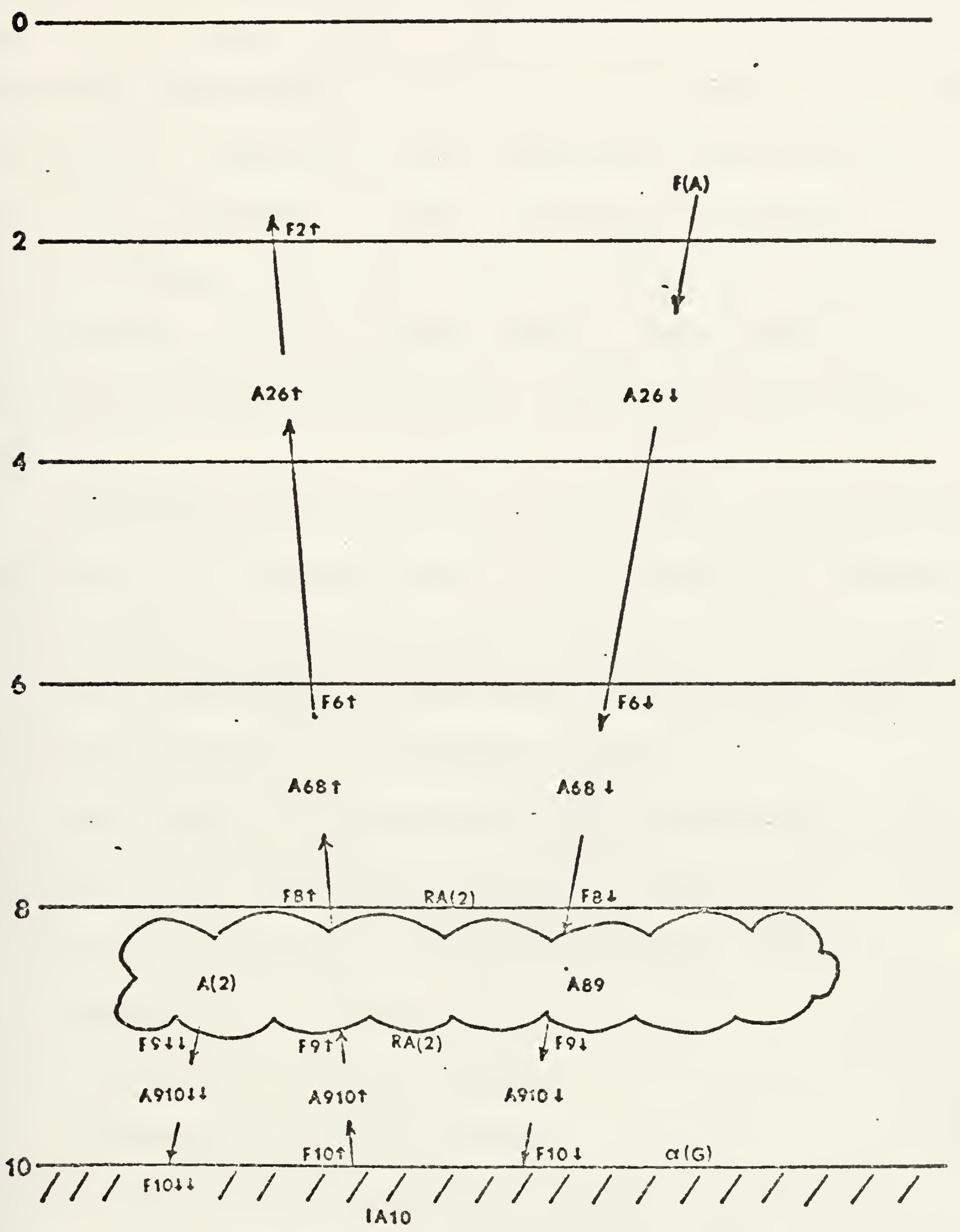

Figure 9 Schematic representation of F(A) insolation disposition with a lower overcast layer only.

surface is affected by the downward reflected beams. Additional insolational amounts remaining after more than two reflections are negligible and are not included in the models (Appendix B). Also note that insolation reflected upward from a lower interface, either cloud-top or ground, to the base of a higher cloud deck was not subjected to absorption by or transmission through the cloud. This simplification resulted in slightly reduced F(A) insolation-reflectance to space.

A final point to note is that there are three contributions to the absorption of solar insolation within a layer between any two reflecting surfaces. In the Figs. 7, 8, 9, these contributions are identified by arrows which indicate the portion of path being crossed.

For each of the overcast-cloud combinations, the transmitted F(A) insolation arriving at the earth's surface may be defined using the following notation (TRANA) as

$$\mathrm{TRANA}(1,\ 1) = \mathrm{F10}\downarrow + \mathrm{F10}\downarrow\downarrow \tag{4-17}$$

$$\mathrm{TRANA}(1,\ 0) = \mathrm{F10}\downarrow + \mathrm{F10}\downarrow\downarrow \tag{4-18}$$

$$\mathrm{TRANA}(0,\ 1) = \mathrm{F10}\downarrow + \mathrm{F10}\downarrow\downarrow \tag{4-19}$$

where the right side parameters of (4-17), (4-18), and (4-19) are derived in Appendices (B-1), (B-2), and (B-3).

The F(A) insolation absorbed by the earth in each case is derived by

$$\mathrm{IA10}(1,\ 1) = \mathrm{F10}\downarrow\ (1-\alpha(G)) + \mathrm{F10}\downarrow\downarrow \tag{4-20}$$

$$\mathrm{IA10}(1,\ 0) = \mathrm{F10}\downarrow\ (1-\alpha(G)) + \mathrm{F10}\downarrow\downarrow \tag{4-21}$$

$$\mathrm{IA10}(0,\ 1) = \mathrm{F10}\downarrow\ (1-\alpha(G)) + \mathrm{F10}\downarrow\downarrow. \tag{4-22}$$

In the last three equations, the quantity $F10\downarrow\downarrow$ is small enough in each case, that no further reflections from the earth were considered.

3. Composite F(A) Layer-Absorptions and Surface-Absorption Insolation

As has been previously discussed, the standard grid-area weighting scheme of this study was applied to obtain composite values of the absorbed F(A) insolation in key layers and also within the earth's surface. The weighting factors applied to the corresponding overcast-combination absorption quantities provided the following composite results:

$$\begin{aligned} A26(CL(1),\ CL(2)) = {} & A26_{(0,\ 0)}W(0,\ 0) + A26_{(1,\ 0)}W(1,\ 0) \\ & + A26_{(0,\ 1)}W(0,\ 1) \qquad (4\text{-}23) \\ & + A26_{(1,\ 1)}W(1,\ 1) \end{aligned}$$

$$\begin{aligned} A610(CL(1),\ CL(2)) = {} & A610_{(0,\ 0)}W(0,\ 0) \\ & + A610_{(1,\ 0)}W(1,\ 0) \qquad (4\text{-}24) \\ & + A610_{(1,\ 1)}W(1,\ 1) + A610_{(0,\ 1)}W(0,\ 1) \end{aligned}$$

$$\begin{aligned} IA10(CL(1),\ CL(2)) = {} & IA10(0,\ 0)W(0,\ 0) \\ & + IA10(1,\ 0)W(1,\ 0) \\ & + IA10(0,\ 1)W(0,\ 1) \qquad (4\text{-}25) \\ & + IA10(1,\ 1)W(1,\ 1). \end{aligned}$$

The weighting factors W(0, 0),...,W(1, 1) were first listed in Equations 3-1, 3-2, 3-3, 3-4.

4. Absorptivity (ABA) by Layers

Here the (fractional) absorptivity as well as the actual insolation values absorbed in the layers are considered.

In the computation of absorptivity, the total undepleted insolation at the top (k = 0) is used. The following equation was utilized in this calculation:

$$\mathrm{FADJ} = 2.00(r/r_m)^{-2}\ \mathrm{Cos}\ z. \tag{4-26}$$

ABA, or the absorptivity of the troposphere was computed from the ratio of the insolation absorbed in the troposphere to the insolation incident at the top of the atmosphere rather than at k = 2:

$$\mathrm{ABA} = \frac{A(2,\ 6) + A(6,\ 10)}{\mathrm{FADJ}}\ . \tag{4-27}$$

D. ALBEDO (ALB) OF THE EARTH-TROPOSPHERE SYSTEM

In considering the planetary albedo, the absorptions of the earth-troposphere system in both the F(A) and F(S) insolational regions must be recalled by the program. Thus we define the reflected insolational energy in F(A) as REFA, and it is computed by

$$\mathrm{REFA} = F(A) - \mathrm{A26} - \mathrm{A610} - \mathrm{IA10}. \tag{4-28}$$

Likewise REFS, the reflected part of F(S) is defined by

$$\mathrm{REFS} = F(S) - \mathrm{IS10}. \tag{4-29}$$

It is understood that REFA, REFS are computed for appropriate CL_1, CL_2 at each gridpoint sounding considered.

Summing REFA and REFS gives REF:

$$\mathrm{REF} = \mathrm{REFS} + \mathrm{REFA}. \tag{4-30}$$

Finally the planetary albedo is related to FADJ through

$$\mathrm{ALB} = \frac{\mathrm{REF}}{\mathrm{FADJ}}\ . \tag{4-31}$$

E. COMPOSITE ABSORPTIVITY (ABG) BY THE EARTH-SURFACE; COMPOSITE ATMOSPHERIC TRANSMISSIVITY (ATRAN)

1. Absorptivity (ABG) of Earth

By summing the weighted values of F(S) and F(A) portions of the incoming insolation entering the earth, the total insolation absorbed at the earth's surface was computed. This quantity when divided by the extraterrestrial insolation gave the fractional absorptivity (ABG) of the earth's surface. The equation for ABG was

$$ABG = \frac{IA10 + IS10}{FADJ} \qquad (4\text{-}32)$$

where IA10, IS10, and FADJ were defined previously by Equations 4-25, 4-12, and 4-26, respectively.

2. Transmissivity (ATRAN) of the Troposphere

Also computed was the total insolational energy TRAN, incident at the earth's surface just before absorption by the surface. This calculation is given by

$$TRAN = TRANA + [IS10 \; / \; (1-\alpha(G)]. \qquad (4\text{-}33)$$

Here α(G) is as previously defined in Equation 4-7. TRANA is as defined by the weighted value of TRANA(0, 0), TRANA(1, 1), TRANA(1, 0) and TRANA(0, 1) given by Equations 4-16, 4-17, 4-18, and 4-19. Also note that the four terms of IS10 of (4-8), (4-9), (4-10), and (4-11) have the common factor (1-α(G)) in the numerator and therefore each F(S) insolation component at the earth just before absorption need only be divided by (1-α(G)). TRAN may thus be viewed as the total insolational energy incident at a pyrheliometer located at earth. The (fractional) transmissivity of the troposphere

(ATRAN) is then computed from

$$\text{ATRAN} \equiv \text{TRAN} \,/\, \text{FADJ}. \qquad (4\text{-}34)$$

Note finally that the major dispositions of the total insolation at the indicated map times have been identified by the fractional values, ALB, ABA, ABG, and ATRAN, each of which is a fractional value representing the reflectivity (albedo), absorptivity, or atmospheric transmissivity as the case may be.

3. Computational Check

The computational scheme utilized in this model was checked by summing the fractional values ALB, ABA, and ABG relative to the troposphere at each gridpoint. The value in each case must total .96, since as previously noted the attenuation of solar insolation was taken as four percent as it streamed through the stratosphere.

F. STATISTICAL ANALYSIS

In order to substantiate some of the computations performed in this section, several of the most important items computed were statistically analyzed using linear regression computer programs from the BMD set of statistical programs (Dixon, 1973).

1. Clear Sky Cases

Using ALB (0, 0, z), which is the clear sky case of albedo, as the predictand, and $\log_{10}$Sec z and its square as the predictor, the following best-fit equation resulted

$$\text{ALB}(0,\ 0,\ z) = .05705 + .54529 \log_{10}\text{Sec } z - .18885(\log \text{Sec } z)^2. \qquad (4\text{-}35)$$

$$R_m = .9918$$

where R_m represents the multiple correlation coefficient.

This result was as expected over the ocean where $\alpha(G)$ and $\alpha(R)$ involved logarithmic dependence on Sec z. Average values of ALB and $\log_{10}$Sec z were

$$\overline{ALB(0,0)} = .20350 \qquad \overline{\log_{10} \mathrm{Sec}\ z} = .34049.$$

Other clear sky regression tests made use of the water-vapor mass path length (M) defined by

$$M = (U\ \mathrm{Sec}\ z)^{\frac{1}{2}} \log_{10}(U\ \mathrm{Sec}\ z)^{\frac{1}{2}}. \qquad (4\text{-}36)$$

This parameterization of water vapor mass is similar to that developed by Hanson [1971], who used a similar M as a predictor in his empirical formulations of ABA for both clear and partly cloudy sky cases. In this study the two regressions attempted using M as a predictor were with ABA(0, 0, M) and ATRAN(0, 0, M) as predictands. The best-fit equations resulting were

$$ABA(0,\ 0,\ M) = .11478 + .04012\ M \qquad (4\text{-}37)$$

$$R_m = .9675$$

$$ATRAN(0,\ 0,\ M) = .77794 - .06337\ M \qquad (4\text{-}38)$$

$$R_m = .8575.$$

The means of ABA(0, 0, M) and ATRAN(0, 0, M) for the original 93 soundings were

$$\overline{ABA(0,\ 0,\ M)} = .15154$$

$$\overline{ATRAN(0,\ 0,\ M)} = .71987$$

$$\overline{M} = 1.83259\ (\mathrm{gm\ cm}^{-2})^{\frac{1}{2}}.$$

2. Relationships Between Albedo, Atmospheric Absorptivity, Atmospheric Transmissivity, and Ground Insolation in the Cloudy and Clear Sky Cases

In addition to the clear sky value of ALB, it was also possible to compute the composite cloudy sky case. A regression was formed showing the relationship between the ratio ALB(CL(1),CL(2))/ALB(0, 0) as the predictand and the total opaque cloud cover (CL) as the predictor. CL in this model is specified by Equation 4-39 below:

$$CL = CL(1) + CL(2) - CL(1)CL(2). \qquad (4\text{-}39)$$

CL, it was felt, gave a good approximation of the effective cloud-cover by the two layers of cloud amounts CL_1 and CL_2 by Equation 2-14 used in this model. As explained earlier in this study, a one-third reduction of both CL(1) and CL(2) after initial determination by Equation 2-14 was also tried in all computations involving cloud amounts. This test represented an initial attempt at tuning the cloud model for radiative calculations as will later be substantiated, and gave results in closer agreement with the latest literature on satellite reflectances. Thus all subsequent regressions involving CL will also include those best-fit equations formulated using a CL based also upon a one-third reduction of CL(1) and CL(2). A small letter subscript 'a' in the equation number will indicate those computations using full-cloud amounts while a small letter subscript 'b' will indicate those utilizing a one-third reduction in the cloud model amounts.

The first regression equations tested were those for ALB(CL) and ABA(CL) for the respective cases of "full" and

two-thirds cloud cover. The results are given in (4-40), 4-41). The symbol R_m once again signifies the multiple correlation of the statistical regressions.

$$ALB_a(CL(1)CL(2) = ALB(0,0)[1 + 3.59683CL - 1.7006CL^2] \qquad (4\text{-}40\ (a))$$

$$R_m = .8755$$

$$ALB_b(CL(1),CL(2) = ALB(0,\ 0)[1 + 4.13667CL - 3.18972CL^2] \qquad (4\text{-}40\ (b))$$

$$R_m = .8876.$$

The sample means of the values in Equations 4-40a and 4-40b are

Equation 4-40a		Equation 4-40b	
$\overline{ALB(CL(1),CL(2))}$	= .4298	$\overline{ALB(CL(1),CL(2))}$	= .3640
$\overline{ALB(0,\ 0)}$	= .2035	$\overline{ALB(0,\ 0)}$	= .2035
$\overline{CL}$	= .6951	$\overline{CL}$	= .5176

The correlation coefficient in Equation 4-40 appears to show strong dependence of ALB upon CL. Also note that ALB(CL(1), CL(2)) values computed here are slightly higher than reported by Raschke *et al.*, [1973], (ALB = .30) for essentially the same set of gridpoints during the NIMBUS III period 21 January through 3 February 1970. However, the one-third reduction-CL appears to give much closer albedo results, suggesting that the full cloud amounts of Smagorinsky by 2-14 are too high.

A second regression computed was between the ratio of tropospheric absorptivity of the cloudy air to that for the clear sky case, versus CL. The following best-fit equation resulted:

$$ABA_a(CL(1),CL(2)) = ABA(0,\ 0)[1 + .5043CL - .1326CL^2] \qquad (4\text{-}41\ (a))$$

$$R_m = .8989$$

$$ABA_b(CL(1),CL(2)) = ABA(0,\ 0)[1 + .5522CL - .2451CL^2] \qquad (4\text{-}41\ (b))$$

$$R_m = .8873$$

Mean statistics for this regression case are

Equation 4-41(a)		Equation 4-41(b)	
$\overline{ABA_a(CL(1),CL(2))}$	= .1916	$\overline{ABA_b(CL(1),CL(2)}$	= .1810
$\overline{ABA(0,\ 0)}$	= .1515	$\overline{ABA(0,\ 0)}$	= .1515
$\overline{CL_a}$	= .6951	$\overline{CL_b}$	= .5176

In (4-41), it is seen that the model specifies an increase in atmospheric (solar) absorptivity with increasing the cloud cover. This result is in agreement with studies of Plante [1972], Warner [1974], and with the earlier study of London [1957].

An analogous statistical regression was then developed for the cloudy-sky transmissivity relative to the clear-sky transmissivity. The resulting regressions were

$$ATRAN_a(CL(1),CL(2)) = ATRAN(0,0)[1-.6020CL - .0285CL^2] \qquad (4\text{-}42\ (a))$$

$$R_m = .9895$$

$$ATRAN_b(CL(1),CL(2)) = ATRAN(0,0)\ [1-.6833CL + .1246CL^2] \qquad (4\text{-}42\ (b))$$

$$R_m = .9862.$$

Equation 4-42a		Equation 4-42b	
$\overline{\mathrm{ATRAN}_a\mathrm{CL(1),CL(2)}}$	= .4440	$\overline{\mathrm{ATRAN}_b\mathrm{CL(1),CL(2)}}$	= .4957
ATRAN(0, 0)	= .7199	ATRAN(0, 0)	= .7199

If Equation 4-42b is terminated at the first power of CL, the result reduces to

$$\mathrm{ATRAN(CL(1),CL(2))} = \mathrm{ATRAN(0,\ 0)}[1-.5961\mathrm{CL}] \quad (4\text{-}43)$$

$$R_m = .9855.$$

The result (4-43) is in reasonable agreement with the Savino-Angstrom result which is

$$\mathrm{ATRAN(CL(1),CL(2))} = \mathrm{ATRAN(0,\ 0)}[1-(1-k)\mathrm{CL}] \quad (4\text{-}44)$$

Here k is a slowly increasing function of latitude, ranging from 0.35 to 0.50, according to Budyko [1956].

3. Some Conclusions

The statistical analyses performed seem to show agreement with observational results of other investigators. Thus the radiation model, with the solar seasonal effects imposed appears to be realistic. Further, the one-third reduction in amounts given by the cloud parameterization model appear to give even better agreement with the latest satellite findings.

G. ALBEDO COMPARISONS WITH PUBLISHED RESULTS

The tropospheric albedo computations of the solar-insolation model of this section have been presented for both the full-cloud and two-thirds CL cases, respectively. These albedos have been interpolated to whole multiples of 5° latitude between 20°S and 65°N. These computations were made for each of the four oceanic meridians and the resulting

zonally-averaged albedos are presented as a function of latitude in Table IV for both the full-CL and two-thirds CL cases, where comparison is also made with satellite climatology of Raschke *et al.* [1973], pertaining to the NIMBUS III averaged albedo measurements over the period 21 January - 3 February 1970. For sake of consistency the Raschke albedo analyses have been derived by interpolation to latitude using the same four meridians before applying the zonal-averaging process.

The model results under the headings "FULL-CL" and "2/3-CL" correspond to the composite cloud amounts previously listed in Table II(a) according to the equation

$$CL = CL_1 + CL_2 - CL_1 * CL_2 \qquad (3\text{-}17)$$

with either (CL_1, CL_2) by Equation 2-14 or (CL_1', CL_2') by Equation 2-15.

The most unusual results to be observed in Table IV are the small albedo-values ($\simeq .2$) between 20°S to 20°N after Raschke, as contrasted with the corresponding values (in the range .3 to .4) by 2/3-CL cloud model , and more markedly with those of the FULL-CL model (values in the range .35 to .5). The "hemispheric" cosine weighted mean albedos are as follows:

FULL-CL, $\overline{ALB} = .46$

2/3-CL, $\overline{ALB} \doteq .38$

RASCHKE-$\overline{ALB} = .30$

At every latitude ($\phi \lesssim 50°$) under comparison the 2/3-CL albedo computation is closer to Raschke's observations than is the full-CL value. At latitudes $\phi \gtrsim 55°$, there is evidence

Lat	ALBEDO (FULL-CL)	ALBEDO (2/3-CL)	ALBEDO (Raschke)	FULL-CL AMOUNT	(2/3-CL) AMOUNT
20S	.5462	.4458	.2195	.932	.758
15	.5380	.4336	.2050	.927	.733
10	.4901	.3859	.1875	.867	.634
5	.4334	.3432	.1967	.746	.536
0	.4447	.3478	.2325	.790	.556
5	.4290	.3362	.2225	.766	.527
10	.3532	.2859	.2050	.557	.376
15	.3517	.2895	.2075	.532	.342
20	.3390	.2868	.2450	.443	.279
25	.3664	.3151	.2925	.463	.320
30	.4217	.3668	.2725	.559	.411
35	.4145	.3703	.3375	.516	.382
40	.4595	.4275	.3925	.628	.529
45	.5558	.5151	.4250	.833	.740
50	.5682	.5186	.5325	.911	.759
55	.5717	.5218	.5929	.931	.749
60	.5180	.4848	.5600	.764	.528
65N	.4294	.4153	.7000	0.0	0.0
Wt. Avg	.4622	.3820	.3010	.688	.514

Table IV. Comparison of planetary albedo as found by this study for both full and two-thirds cloud models for 16 January 1974 and by Raschke et al. (1973) based upon NIMBUS III measurements. Also included are the globally weighted mean values at the base of the columns and the composite cloud amounts for both cloud cases.

of added surface-ice reflections contributing to the Raschke values of planetary albedo. This is especially true at the latitude 65°N where Raschke's results indicate ALB(65°N) = .7, whereas the model-computations with essentially zero cloud cover is close to .42. Part of the discrepancy with the model at high latitudes lies in the non-inclusion of a surface-ice reflectance parameter.

To summarize, apart from the region covered by sea-ice, there is a marked tendency for the 2/3-CL cloud model to give reduced albedos as suggested by Raschke *et al.* [1973], Von der Haar and Hanson [1969], and others. This result of the 2/3-CL model is especially more clearly defined in tropical latitudes where Von der Haar and Hanson [1969] have discussed the reality of both reduced cloud-covers and the resultant reduced global-albedo. These latter effects than must give rise to larger net radiation into the oceanic surface, which they also prescribe.

In Section VI, heat-budget computations along each of the four meridians are presented. These computations make use only of the 2/3-CL cloud model for purposes of radiative calculations. This selection (2/3-CL) is supported by the results of Section VII. However, it is felt that the grid-point method used here for 2/3-CL is not the final answer in the tropics. In the tropics the peculiar reflection-characteristics of cumulus convective elements must be more realistically accounted for than by the large-scale layering considered in the solar insolation model of this section.

V. SENSIBLE AND LATENT HEAT TRANSPORT AT THE SEA-AIR INTERFACE

A. GENERAL

In order to compute heat balances involving the atmosphere and the ocean-surface, it was necessary to compute vertical fluxes of sensible and of latent heat across the air-sea interface. The model adopted to describe the turbulent-fluxes in the planetary boundary layer was essentially that used in the FNWC primitive equation model as delineated by Kesel and Winninghoff [1972] and Kaitala [1974]. The model as used in this study was adapted in such a way that it gave similar quantitative bulk-transfer results across the air-sea interface as the model used by Kaitala [1974]. This was a major deviation from Warner's study [1974], where he required a positive sea-to-air sensible heat transport based primarily upon a semi-empirical Bowen ratio.

B. SENSIBLE HEAT TRANSPORT

As previously mentioned a slightly different modelling as compared to that of Kesel and Winninghoff [1972] was used in this study for the vertical distribution of sensible-heat convergence in the layer 800 to 1000 mb. In the presently operational heat-package of FNWC, as described by Kaitala [1974] and by Kesel and Winninghoff [1972], the planetary boundary layer sensible heat transport is given by

$$H_{\Gamma}(900) = \rho_{10} C_p \left(\frac{K^*}{1 + a^* \left(\frac{\theta_9 - \theta_g}{z_9 - z_{10}} \right.} \right) \left\{ \gamma_c - \frac{\theta_9 - \theta_x}{z_9 - z_{10}} \right\} . \qquad (5\text{-}1)$$

In (5-1), the parameters are as described below:

$C_p = .239$ cal $\text{gm}^{-1}(\text{deg. K})^{-1}$

$\theta_x = T_x$

γ_c = (the critical countergradient lapse rate) =

$3 \times 10^{-5}(\text{deg. K})\text{cm}^{-1}$

K* = (the neutral value of the eddy coefficient) =

$2 \times 10^{5}\text{cm}^{2}\text{sec}^{-1}$

a* = (a turbulent transfer coefficient) =

$5 \times 10^{4}\text{cm}(\text{deg. K})^{-1}$

ρ_{10} = (surface density) = $\rho_{10}(R_dT_{10})^{-1}$.

The other parameters in (5-1) are θ_9, which is the potential temperature at 900 mb, θ_x which is the potential temperature at the top of the constant flux layer, and θ_g which is the potential temperature at the surface.

Equation 5-1 was given by Kaitala [1974] as the planetary boundary layer equivalent of the bulk formula for H_Γ, given in terms of surface-layer parameters as

$$H_\Gamma = \rho_{10}C_pC_DV_s(T_g - T_x) \qquad (5\text{-}2)$$

where C_D is the drag coefficient, V_s = surface wind, and $(T_g - T_x)$ is proportional to the temperature lapse for the thin layer between the sea surface and the top of the constant-flux layer. If H_Γ of (5-1, 5-2) are always equal, then it follows that T_x may be solved from the identity, giving

$$T_x = \frac{C_pV_sT_g + \tilde{K}\,\frac{\theta_9}{\Delta z} - \tilde{K}\,\gamma_c}{\frac{\tilde{K}}{\Delta z} + C_DV_s} \qquad (5\text{-}3\ (a))$$

where

$$\tilde{K} = \frac{K^*}{1 + a^* \left(\frac{\theta_9 - \theta_g}{z_9 - z_{10}} \right)} \qquad (5\text{-}3\ (b))$$

$$\Delta z = z_9 - z_{10} = \frac{R_d}{g} \overset{9-10}{\overline{T}} \left(\ell n \frac{10}{9} \right) \qquad (5\text{-}3\ (c))$$

The requirement of identical values of H_Γ at level x and at level k = 9, with H_Γ decreasing to zero at k = 8, was interpreted by Kesel and Winninghoff [1972] as giving rise to sensible-heat convergence H_Γ, layer-centered at k = 9. Actually Fig. 10a suggests that the vertical convergence of sensible heat flux of amount H_Γ occurs in the layer (8, 9) when the assumption of constant heat flux in the layer (x, 9) is made. However, in the sensible-heat model visualized in this thesis, a linear decrease in H_Γ with pressure was assumed above level 'x', Fig. 10b. Note that level 'x' is assumed to occur so close to k = 10 that one may solve (5-1) for

$$H_\Gamma(k = 9) = \frac{1}{2} H_\Gamma \text{ (Bulk)}. \qquad (5\text{-}4)$$

Solution of (5-4) by use of (5-1), (5-2) gives the result

$$T_x = \frac{C_D V_s T_g + \frac{2 \tilde{K} \theta_9}{\Delta z} - 2 \tilde{K} \gamma_c}{\frac{2 \tilde{K}}{\Delta z}} . \qquad (5\text{-}5)$$

Equation 5-5 has the same format as (5-3). As was mentioned, Kaitala [1974] has suggested the use $K^* = 2 \times 10^5 \text{cm}^2 \text{sec}^{-1}$ in (5-3), and this would lead to identical values as the use of $K^* = 10^5 \text{cm}^2 \text{sec}^{-1}$ in (5-5). The latter K* value was tested by Warner [1974] who felt, with Kaitala, that either K* value

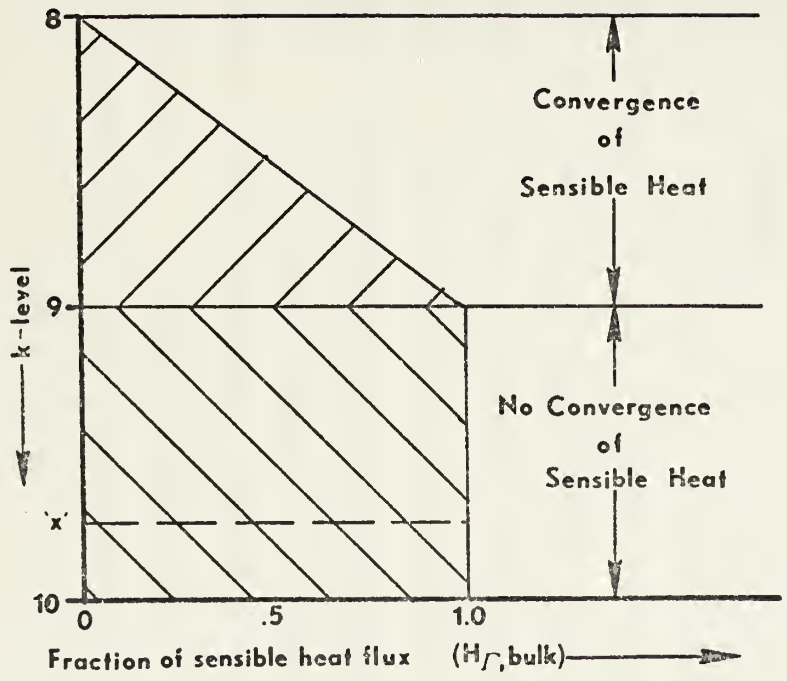
8
9
'x'
10
k-level
Convergence of Sensible Heat
No Convergence of Sensible Heat
0
.5
1.0
Fraction of sensible heat flux (H_Γ,bulk)

Figure 10(a). Schematic representation of the distribution of convergence of sensible heat after Kaitala (1974). Note 'x' is the level of the top of the constant flux layer.

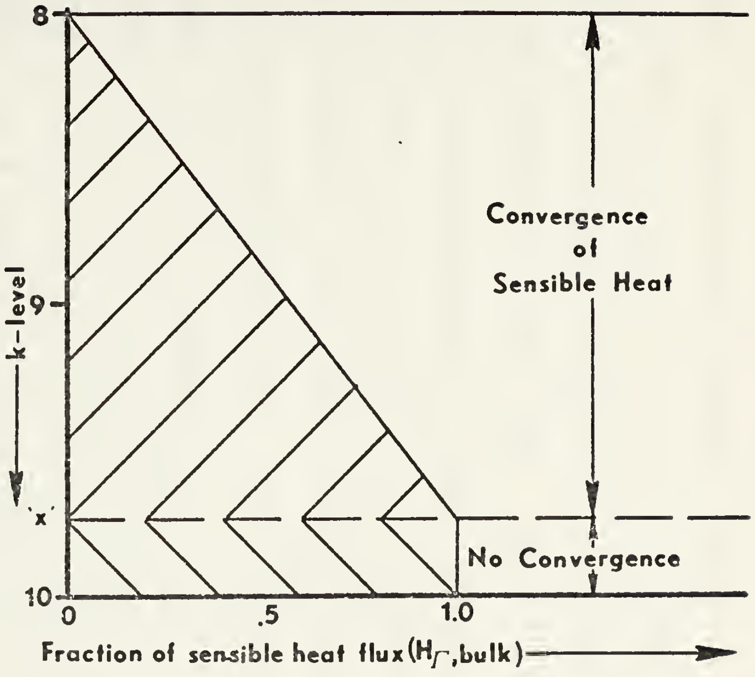
8
9
'x'
10
k-level
Convergence of Sensible Heat
No Convergence
0
.5
1.0
Fraction of sensible heat flux (H_Γ,bulk)

Figure 10(b). Schematic representation of convergence of sensible heat as used in this study.

was only an approximate choice of the eddy coefficient requiring at least some tuning, with a theoretical dependence upon the larger-scale synoptic parameters over the ocean.

The physical implications of condition (5-4) along with the linear decrease of $H_{\Gamma}(P)$ with pressure to zero at level k = 8 is depicted in Fig. 10b. This condition is compatible with uniform convergence of the sensible-heat flux H_{Γ} of the surface layer into the overlying layer (8, 10). Having uniform convergence from level x (near surface) to level 8 is equivalent to maintaining a "well mixed" boundary layer of thickness from the surface to 8.

With either case, Equation 5-3 or 5-5, the sensible heat convergences of Fig. 10-a and 10-b were considered applicable at level k = 9 and were considered to be identical. In this thesis the value of $2\tilde{K}$ in (5-5) was based upon an arbitrary choice $K^* = 10^5 \mathrm{cm}^2 \mathrm{sec}^{-1}$ in (5-3b), rather than $2 \times 10^5 \mathrm{cm}^2 \mathrm{sec}^{-1}$.

In order to evaluate H_{Γ}, it was necessary to derive the surface winds V_s by use of (2-21) at all gridpoints of the four oceanic meridians under study. This was done using Equations 2-16 and 2-20 with contour gradients extracted from the 1000 mb field except in the latitude band ±5°. Here, the January climatological values of gradient winds were taken from the Tropical Wind Atlas of Atkinson [1970].

Besides having computed the applicable surface winds V_s for use in (5-2), a modification to $C_D = 1.4 \times 10^{-3}$ (after Weiler and Burling, 1967) was introduced, as compared with $C_D = 2. \times 10^{-3}$ as suggested by Kaitala [1974].

After determination of T_x in Equation 5-5, H_Γ was then computed at each gridpoint using Equation 5-2. The values of H_Γ are used later in calculations of heat budgets in Sections VI and VIII.

C. EVAPORATIVE HEAT TRANSPORT

As in the case of sensible heat convergence, the latent heat transport by turbulence was assumed to be subject to uniform heat flux convergence throughout the layer 800-1000 mb (Fig. 11b). The total amount of latent heat removed by evaporation from the ocean surface was similar to that given by Kaitala [1974] using bulk transfer theory. While a turbulent model similar to Fig. 11b can be adopted, it is necessary to recognize that the realized latent heat may occur at arbitrary levels (for example, higher than k = 8) and therefore is not introduced at level k = 9. The basis of the turbulent latent-heat flux model adopted here is shown in Fig. 11b, where

$$E_{(900)} = \tfrac{1}{2}E(\text{Bulk}) \qquad (5\text{-}6)$$

and where the surface-layer bulk transfer of latent heat is given by

$$E \equiv E(\text{Bulk}) = L\rho_{10}\, C_D\, V_s(q_{10} - q_x). \qquad (5\text{-}7)$$

From the planetary boundary-layer transfer theory analog to $H_\Gamma(900)$, E(900) may be written

$$E_{(900)} = L\rho_{10}\, \tilde{K}\, \frac{(q_x - q_9)}{z_9 - z_{10}}\ . \qquad (5\text{-}8)$$

In (5-7), and (5-8), L is the latent heat of vaporization

$$L = 596.73 - .601T_{10}\ \text{cal gm}^{-1},\quad T_{10}\ \text{in °C.}$$

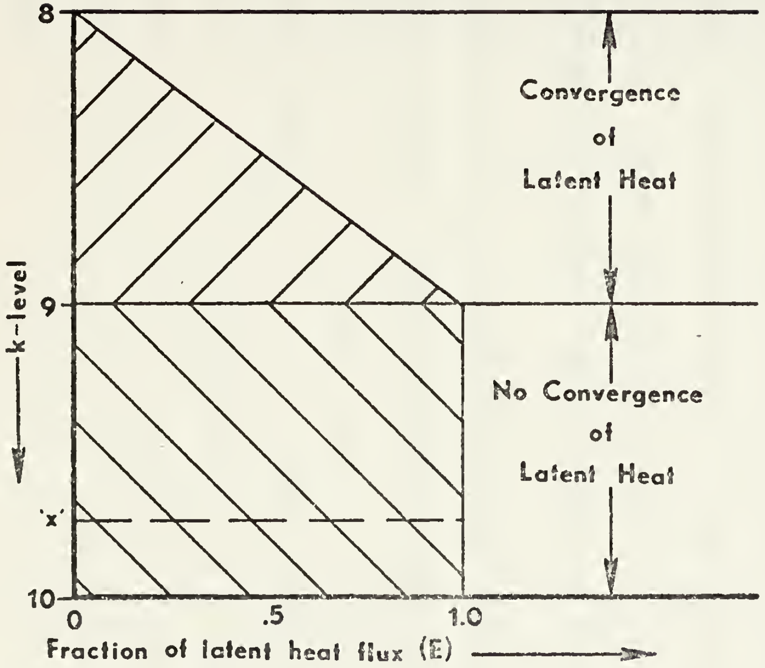
8
9
'x'
10
k-level
0
.5
1.0
Fraction of latent heat flux (E)
Convergence of Latent Heat
No Convergence of Latent Heat

Figure 11(a). Schematic representation of distribution of convergence of latent-heat flux after Kaitala (1974). Note 'x' is the level of the top of the constant flux layer.

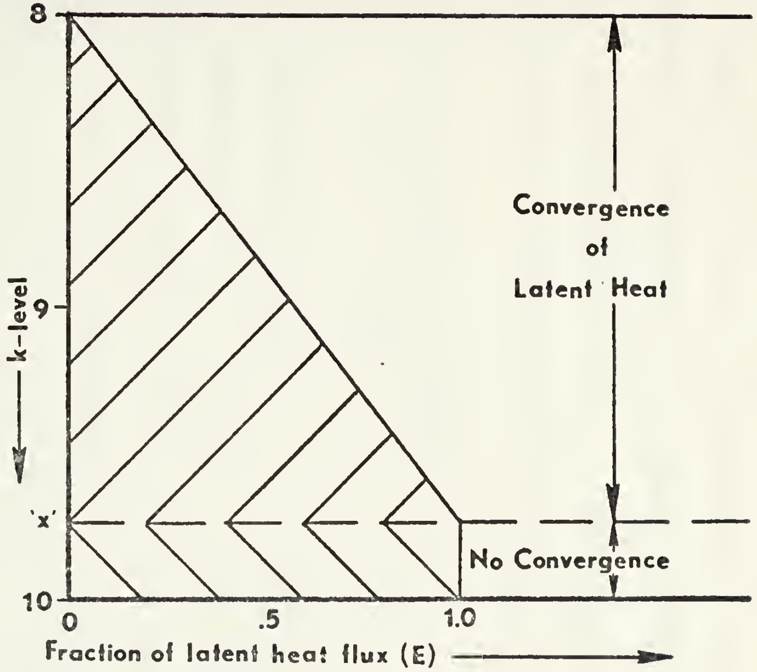

Figure 11(b). Schematic representation of distribution of convergence of latent-heat flux as used in this study.

Also in (5-8) q_9 and q_x are mixing ratios at the level k = 9 and at x, the top of the constant flux layer. The factor ½ which appears in the right side of (5-6) gives the type of latent heat convergence as shown in Fig. 11b, as against that of Kaitala (Fig. 11a). Combining Equations 5-6, 5-7, and 5-8 leads to the solution for q_x, namely

$$q_x = \frac{C_D V_s q_{10} + 2 \frac{\tilde{K}}{\Delta z} q_9}{C_D V_s + 2 \frac{\tilde{K}}{\Delta z}} \tag{5-9}$$

with Δz given by (5-3(c)). As in the case of T_x in Equation (5-5), the factor of 2 $\tilde{K}$ of (5-9) was taken equal to Kaitala's $\tilde{K}$ of Equation 5-3(b). This was done in this study by using a value of $K^* = 1. \times 10^5 \mathrm{cm}^2\mathrm{sec}^{-1}$ as against $2 \times 10^5 \mathrm{cm}^2\mathrm{sec}^{-1}$ suggested by Kaitala. Thus amounts computed for E of Equation (5-7) were equivalent to amounts computed using Kaitala's scheme (Equation 5-8) only the turbulent convergence of E was distributed differently in the planetary boundary layer. Thus after computing q_x (Equation 5-9), E was calculated at each gridpoint except those over ice by using Equation (5-7).

D. TURBULENT HEAT TRANSPORTS OVER AN ICE-COVERED OCEAN

Any gridpoint whose surface temperature was less than -5°C was considered to be over an ice-covered ocean for the purposes of calculating H_Γ and E. In this study there were four such gridpoints. In the handling of H_Γ, a formula adopted from Kaitala [1974] was first utilized to describe heat conduction into the ice (HICE), from the warmer water beneath the ice surface:

$$\mathrm{HICE} = \mathrm{BBB}^*(T_o - T_g) \tag{5-10}$$

where BBB is an ice conduction coefficient (697.83 ergs $cm^{-2}sec^{-1}(deg. K)^{-1}$), T_o is the freezing point of sea water (271.3 deg. K), and T_g is the surface temperature. HICE is then utilized in the following surface heat-balance equation to determine the summation of the sensible heat flux H_Γ plus the latent heat flux:

$$H_\Gamma + E = HICE + QABG - F_{10}*. \qquad (5\text{-}11)$$

A Bowen ratio r as described by Kaitala [1974] was then calculated using Equation 5-12, where the right side is an empirical least-squares best-fit applicable over continental and ice-covered ocean areas.

$$r(\phi) \equiv \frac{H_\Gamma}{E} = 9.6|\text{Sin } \phi|^2 - 7.93|\text{Sin } \phi| + 2.0. \qquad (5\text{-}12)$$

Here ϕ is the latitude of the gridpoint, and r was never allowed to exceed 1.33. This restraint on r meant that E was always bounded by

$$E \leq .75 H_\Gamma \qquad (5\text{-}13)$$

(cf. Kaitala, 1974). From the definition of the Bowen ratio (r) as a function of Sin ϕ, and using the following equation for the combined interface fluxes $H_\Gamma + E$ as

$$H_\Gamma + E = H_\Gamma \left(1 + \frac{1}{r}\right) \qquad (5\text{-}14)$$

one obtains simply

$$H_\Gamma = \frac{r}{r+1} (H_\Gamma + E). \qquad (5\text{-}15)$$

Since both the Bowen ratio (r) and $H_\Gamma + E$ are known at each gridpoint, H_Γ is easily determined from (5-14). Then a simple rearrangement of terms in the Bowen ratio definition permitted

the computation of E. This is given by

$$E = \frac{H_\Gamma}{r(\phi)} \quad . \qquad (5\text{-}16)$$

Equations 5-10 and 5-11 always gave negative or downward values of sensible and evaporative heat fluxes at the four gridpoints involving ice-covered oceans since QABG - F_{10}^* was dominantly negative. Further, evaporation never exceeded 75% of H_Γ in magnitude. These negative values appear to agree generally with those arrived at in the work of Vowinckel and Taylor [1964] which dealt in part with evaporative and sensible heat fluxes over an ice-covered Polar Ocean areas in winter.

E. LARGE-SCALE TURBULENT HEAT FLUX ACROSS THE AIR-SEA INTERFACE

At each gridpoint, it is possible through the adaptation of the turbulent boundary layer model to include heating rates across the air-sea interface. For use in Section VI, we compute the values of H_Γ as the convergence of sensible-heating rate for the layer (8, 10) through Equations 5-2,..., 5-5. Also for Section VI, the combination E + H_Γ considered primarily as a heat loss at the ocean surface is computed at each gridpoint by use of Equations 5-7, 5-9. For the over-ice cases H_Γ + E is determined by (5-11), while H_Γ results from (5-12) and (5-14). In any case, the model governing these heating rates, H_Γ and E has been extracted from the FNWC operational turbulent-boundary layer model and appended to the radiational model (with the 2/3-CL case) for operational computations at each gridpoint of the four meridians of interest.

The values of H_Γ turned out to be in general small and negative in low latitudes reflecting computed negative values of $T_g - T_x$. However, in the data-rich mid-latitude cross sections where both strong surface winds and relatively warm ocean temperatures coexist, H_Γ is positive and larger and dominates the net atmospheric heating in layer (8, 10). Regardless of the inconsistency in the sign of H_Γ, the values of $E + H_\Gamma$ seems to be reasonable heat-loss rates at the ocean surface at all latitudes insofar as comparison with other sources of data (Budyko, 1956) are relevant.

Finally in the large-scale sense $H_\Gamma + E$ is included as a (positive) contribution to the heat budget of the tropospheric column even though it is not known precisely at what level the latent heat flux E will be realized.

VI. MERIDIONAL CROSS-SECTIONAL DEPICTION OF THE HEAT BUDGET SYSTEM COMPUTATIONS

A. GENERAL

The general design of this section is to utilize all computational subroutines explained in Sections III, IV and V in computations of a single time-step of the heating model developed for use in the FNWC prediction model. It was decided after the testing of F_2 and of ALB with the corresponding values of Raschke *et al.* [1973] that only the two-thirds cloud model would be displayed in the meridional cross-sections depicting the single time-step computations of the heating package of the FNWC prediction system (Figs. 12, 13(a), 13(b), 14(a), 14(b), 15(a), 15(b), 16(a), and 16(b)). The appropriate radiative calculations with two-thirds CL were thus performed at each gridpoint of the four meridians used for presentation purposes in this section. However, the same type computations were made with full-cloud cover so that the mean radiative balances could be compared layer-by-layer and at the levels k = 2 and k = 10. Both sets of computations were zonally-averaged and used to get mean radiation meridional cross-sections displayed in Section VII (Figs. 17, 18(a), 18(b), 19(a), and 19(b)).

In this study, the FNWC gridpoint processed analyses for 0000GMT, 16 January 1974 were used at the three Pacific cross-sections, while that for 1200GMT, 16 January 1974, was used for the single Atlantic meridian. In any case, the set of

k		LAT.	latitude of the gridpoints in 5° increments
	a)	QAVE	24-hour averaged insolation at level k=2
	b)	QREF	Reflected average insolation at level k=2
	c)	F_2*	Net Outgoing long-wave flux at level k=2
2	d)	BALT	averaged earth-tropospheric gain or loss (a-b-c)
	e)	Q26	averaged solar insolation absorbed by layer (2,6), positive heating
	f)	F26	IR flux loss by layer (2,6)
6	g)	BAL26	averaged radiative cooling in layer (2,6) (e-f)
		2/3 CL(1)	upper layer (4,6) cloud amount
		2/3 CL(2)	lower layer (8,9) cloud amount
	h)	Q68	averaged solar insolation absorbed by layer (6,8)
	i)	F68	IR flux loss by layer (6,8)
	j)	BAL68	averaged radiative cooling in layer (6,8) (h-i)
8			
	k)	Q810	averaged solar insolation absorbed by layer (8,10)
	l)	F810	IR flux loss by layer (8,10)
	m)	H_Γ	sensible heat gain in layer (8,10)
	n)	BAL810	averaged heat balance in layer (8,10) (k-l+m)
10			
	o)	QABG	averaged solar insolation absorbed by surface
	p)	$F_{10}*$	net long-wave flux at earth's surface
	q)	$E+H_\Gamma$	combined heat loss due to evaporation and sensible heat transport
	r)	BALB	averaged warming or cooling at earth's surface (o-p-q)

Figure 12. Key to Meridional cross-sections for Figs. 7,...,10. All radiative and turbulent transfer values are in ly min^{-1} for the levels or layers considered. The reduced cloud amounts 2/3 CL(1) and 2/3 CL(2) are given by Eq. (2-15).

meridians was considered as representative of 16 January data when converted to heating-rate calculations.

Figure 12 depicts in symbolic language the key to the computational entries in Figs. 13, 14, 15, and 16. In actuality, this key list represents computations made at each (I, J) gridpoint sounding from data in the form of Table I(b). It covers those computations proceeding from the top of the troposphere to the ocean surface, including sensible and latent heat transfers (Equations 5-2, 5-7). For simplicity and ease of climatological data comparison, Figs. 13, 14, 15, and 16 were developed by interpolating gridpoint results to whole 5° latitude increments. The interpolation routine utilized was the Lagrangian cubic interpolation scheme. It has the form

$$Q(I) = Q_1 \frac{(I-2)(I-3)(I-4)}{(I-2)(I-3)(I-4)} + Q_2 \frac{(I-1)(I-3)(I-4)}{(2-1)(2-3)(2-4)} \qquad (6\text{-}1)$$

$$+ Q_3 \frac{(I-1)(I-2)(I-4)}{(3-1)(3-2)(3-4)} + Q_4 \frac{(I-1)(I-2)(I-3)}{(4-1)(4-2)(4-3)}$$

where I is determined from an equation similar to (4-3(c)), Q(I) is the desired interpolated value of the heating parameter at a non-integral grid-value I that corresponds to a whole latitude of 5°. In (6-1), the indices 1, 2, 3, and 4 are for any four increasing successive integral values of I along gridpoint lines. The symbol I in (6-1) is usually applied between points 2 and 3, but this interpolation scheme may also be applied with good accuracy to an I-value which is non-centered in the I-array (1, 2, 3, 4). In order to complete the interpolation to latitude, the array is applied sequentially to successive sets of integral I-values along each meridian.

B. EXPLANATION OF TERMS IN FIGURE 12

1. Cross-Section at Level k = 2

It should be explained here that all insolational parameters enumerated upon in Section IV dealt with the specific time of day that corresponded to the hour angle h at the instantaneous times under consideration. The resultant incident solar insolation dealt with is then by Equation 4-1

$$F(2) = S(\frac{r}{r_m})^{-2} \text{ Cos } z.$$

In order to avoid reference to specific map times, the applicable solar hour-angles were: h = 35°, 10°, 55°, and 35°, respectively, for cross-sections 1, 2, 3, 4, depicted in Figs. 13, 14, 15, and 16.

Regarding the first symbol at level k = 2 in Fig. 12, note QAVE and not F(2) is displayed. This is because averages over the 24-hour day (16 January 1974) are considered more meaningful for the data day under consideration, and hence are presented in this form in Figs. 13, 14, 15, and 16. QAVE is the 24 hour average of F(2) found by using a similar form of Equation 4-1 but replacing Cos z by $\overline{\text{Cos } z}$ as in (6-2)

$$\text{QAVE} = F(2)\left(\frac{\overline{\text{Cos } z}}{\text{Cos } z} \right) \tag{6-2}$$

where

$$\overline{\text{Cos } z} = \frac{[H \text{ Sin } \phi \text{ Sin } \delta + \text{Cos } \phi \text{ Cos } \delta \text{ Sin } H]}{\pi} \tag{6-3}$$

H(hour angle at sunset) = arc Cos[- Tan ϕ Tan δ]

ϕ = latitude

δ = solar declination for 16 January 1974.

$\overline{\text{Cos } z}$ is equal to the 24-hour average cosine of the zenith angle. The 24-hour time-averaging period is considered consistent with the longwave flux divergences, which change slowly with the time of day. This conversion to expected daily averaged heat-transfer quantities is compatible with the determination of a heat budget for the given date (e.g., 16 January 1974).

In keeping with the concept of using 24-hour averages, other parameters for level k = 2 are defined as follows:

$$\text{QREF} = \text{REF}(t)\left(\frac{\overline{\text{Cos } z}}{\text{Cos } z} \right) \qquad (6\text{-}4)$$

where

$$\text{REF}(t) = F(2) - \text{A26} - \text{A610} - (\text{IA10} + \text{IS10}). \qquad (6\text{-}5)$$

Here REF(t) is the instantaneous solar-reflected insolation at the gridpoint as given in 4-30 and QREF is its 24-hour average, assuming that planetary albedo remains constant for the 24-hour period, even though it was calculated for the indicated solar time at each meridian.

The same principle will be used with regard to all other solar disposition parameters in converting from time-dependent values at solar time t to 24-hour averaged values. Thus in the following Equations 6-7, 6-9 below Q26(t) becomes Q26, and Q610(t) becomes Q610. Superior bars $\overline{(\ )}$ will not be explicitly shown in the values presented in the cross-sections key, Fig. 12, but will be understood in what follows. Finally, the 24-hour average "system" balance BALT is computed from

$$\text{BALT} = \text{QAVE} - (\text{QREF} + F_2{*}) \qquad (6\text{-}6)$$

for the tropopause level k = 2 at the indicated latitude. In computing this balance the value of F_2^* was introduced from Equation 3-11. Net terrestrial fluxes "F*" such as F_2^* that appear in Fig. 12 were considered to be constant throughout the 24-hour period which would be approximately true if the cloud-covers were representative of the period.

2. Cross-Section in Layer (2, 6)

Referring to Fig. 12 the following definitions apply. In this layer all the heat-transfers shown are assumed to be radiative only in our version of the FNWC heating model. The averaged radiative cooling (heating) rate is given by

$$BAL26 = Q26 - F26 \tag{6-7}$$

where

Q26 = daily average absorption in layer (2,6) and is defined relative to A26(t) by a transformation similar to Equation 6-2

F26 = terrestrial cooling rate given by Equation 3-12 (a).

3. Cross-Section in Layer (6, 10)

When considering radiative transfers only in the layer (6, 10) the 24-hour average radiative cooling is given by

$$BAL610 = Q610 - F610 \tag{6-8}$$

where Q610 is the sum of Q68 and Q810 in Fig. 12. BAL68 has been taken as one-half of BAL610. However

$$BAL810 = Q810 - F810 + H_\Gamma = BAL68 + H_\Gamma. \tag{6-9}$$

Here H_Γ is the sensible heat flux transported to (8, 10) by Equation 5-2. Likewise, F610 is the sum of F68 and F810, terrestrial flux loss values for the respective layers. Note here that the parameter BAL610 remained negative at all gridpoints

of Figures 13 through 16 when considering radiative transfers only.

4. Cross-Section at Air-Sea Interface (k = 10)

The heat balance at the earth's surface (BALB) consisted of the following equation

$$\mathrm{BALB} = \mathrm{QABG} - F_{10}{}^{*} - (H_{\Gamma} + E). \qquad (6\text{-}10)$$

Here QABG is the 24-hour average insolation absorbed by the surface as

$$\mathrm{QABG} = \mathrm{QABG}(t)\ [\overline{\mathrm{Cos}\ z} / \mathrm{Cos}\ z] \qquad (6\text{-}11)$$

$(E + H_{\Gamma})$ is the sum of the turbulent heat transfers which were computed from the bulk formulas as explained in Section V.B. and V.C.

C. MERIDIONAL CROSS-SECTIONS OF THE VERTICAL HEAT BUDGET FOR 16 JANUARY 1974

Figures 13, 14, 15, and 16 as explained represent the single-time step of heating computations for each of the four meridians used in this study. Note that the four Figures (13-16) are divided into a and b parts with section (a) showing "tropical" results and (b) mid-to-high-latitude results. While the results depicted in these cross-sections are exhibited as representing daily-averaged values, they are actually based upon heat-budget parameters at the specific map time 0000GMT and/or 1200GMT on 16 January 1974. Hence, if the results are to be used as part of the "heat-package" subroutine of FNWC, all solar-radiative absorption and-reflectance terms must be recovered as functions of GMT e.g.,

$$F(2,\ t) = \mathrm{QAVE} * [\mathrm{Cos}\ z / (\overline{\mathrm{Cos}\ z})]$$

LAT.	-20.0	-15.0	-10.0	-5.0	0.0	5.0	10.0	15.0	20.0	25.0
	0.6812 0.3418 0.2943 0.0450	0.6646 0.3288 0.2958 0.0401	0.6437 0.2863 0.3111 0.0462	0.6184 0.2482 0.3322 0.0380	0.5893 0.2273 0.3531 0.0088	0.5563 0.2165 0.3724 -0.0327	0.5197 0.1725 0.3847 -0.0375	0.4799 0.1452 0.3942 -0.0596	0.4372 0.1196 0.3918 -0.0741	0.3920 0.1336 0.3276 -0.0692
2										
	0.0668 0.1244 -0.0574	0.0656 0.1246 -0.0590	0.0612 0.1199 -0.0586	0.0550 0.1155 -0.0604	0.0482 0.1125 -0.0643	0.0423 0.1088 -0.0665	0.0375 0.1060 -0.0686	0.0327 0.1065 -0.0739	0.0309 0.1023 -0.0714	0.0384 0.1052 -0.0669
	(0.436)	(0.434)	(0.358)	(0.246)	(0.138)	(0.054)	(0.005)	(0.0)	(0.0)	(0.224)
6										
	(0.753)	(0.722)	(0.580)	(0.494)	(0.503)	(0.555)	(0.358)	(0.204)	(0.034)	(0.0)
	0.0379 0.0507 -0.0128	0.0365 0.0502 -0.0137	0.0349 0.0563 -0.0214	0.0352 0.0676 -0.0324	0.0377 0.0810 -0.0434	0.0399 0.0907 -0.0508	0.0347 0.0859 -0.0513	0.0300 0.0811 -0.0512	0.0238 0.0725 -0.0486	0.0150 0.0510 -0.0360
8										
	0.0379 0.0507 0.0254 0.0126	0.0365 0.0502 0.0201 0.0064	0.0349 0.0563 0.0139 -0.0075	0.0352 0.0676 -0.0036 -0.0360	0.0377 0.0810 -0.0102 -0.0536	0.0399 0.0907 -0.0014 -0.0521	0.0347 0.0859 -0.0051 -0.0564	0.0300 0.0811 -0.0069 -0.0581	0.0238 0.0725 -0.0108 -0.0594	0.0150 0.0510 -0.0214 -0.0575
10										
	0.1967 0.0683 0.2011 -0.0730	0.1971 0.0706 0.1682 -0.0418	0.2264 0.0787 0.2126 -0.0650	0.2449 0.0816 0.1148 0.0485	0.2383 0.0785 0.0750 0.0849	0.2177 0.0823 0.0787 0.0568	0.2404 0.1068 0.1193 0.0143	0.2421 0.1254 0.1206 -0.0040	0.2391 0.1445 0.0857 0.0088	0.1900 0.1203 0.0550 0.0147

Figure 13(a). 125°W Longitudinal cross-section, tropical section. Refer to Fig. 12 for key. Values computed from data for 16 January 1974 for two-thirds case only.

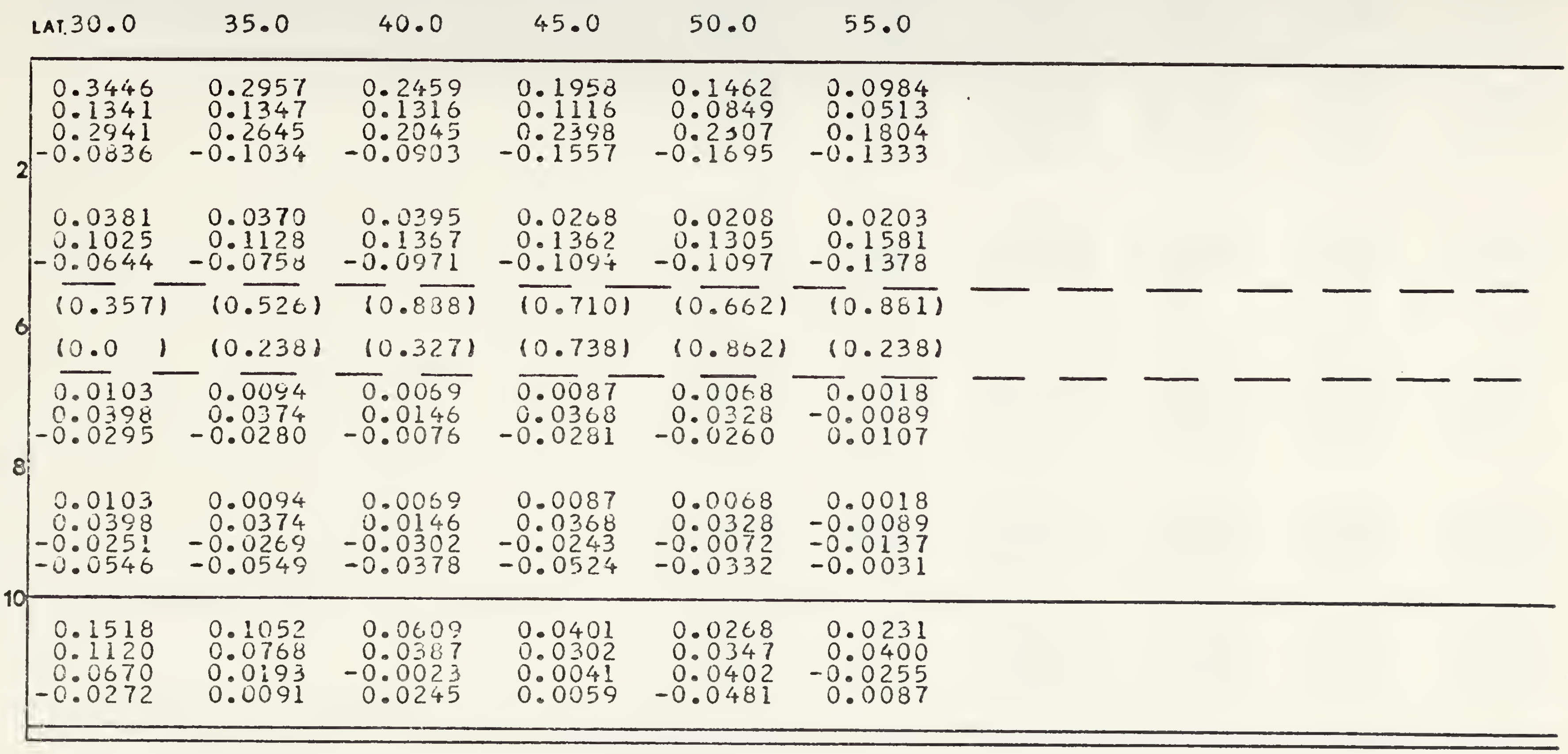

LAT. 30.0	35.0	40.0	45.0	50.0	55.0
0.3446 0.1341 0.2941 -0.0836	0.2957 0.1347 0.2645 -0.1034	0.2459 0.1316 0.2045 -0.0903	0.1958 0.1116 0.2398 -0.1557	0.1462 0.0849 0.2307 -0.1695	0.0984 0.0513 0.1804 -0.1333
0.0381 0.1025 -0.0644	0.0370 0.1128 -0.0758	0.0395 0.1367 -0.0971	0.0268 0.1362 -0.1094	0.0208 0.1305 -0.1097	0.0203 0.1581 -0.1378
(0.357)	(0.526)	(0.888)	(0.710)	(0.662)	(0.881)
(0.0)	(0.238)	(0.327)	(0.738)	(0.862)	(0.238)
0.0103 0.0398 -0.0295	0.0094 0.0374 -0.0280	0.0069 0.0146 -0.0076	0.0087 0.0368 -0.0281	0.0068 0.0328 -0.0260	0.0018 -0.0089 0.0107
0.0103 0.0398 -0.0251 -0.0546	0.0094 0.0374 -0.0269 -0.0549	0.0069 0.0146 -0.0302 -0.0378	0.0087 0.0368 -0.0243 -0.0524	0.0068 0.0328 -0.0072 -0.0332	0.0018 -0.0089 -0.0137 -0.0031
0.1518 0.1120 0.0670 -0.0272	0.1052 0.0768 0.0193 0.0091	0.0609 0.0387 -0.0023 0.0245	0.0401 0.0302 0.0041 0.0059	0.0268 0.0347 0.0402 -0.0481	0.0231 0.0400 -0.0255 0.0087

Figure 13(b). 125°W Longitudinal cross-section, higher latitude section. Refer to Fig. 12 for key. Values computed from data for 16 January 1974.

LAT.	0.0	5.0	10.0	15.0	20.0	25.0
	0.5892	0.5563	0.5198	0.4799	0.4372	0.3919
	0.1693	0.1575	0.1237	0.1293	0.1375	0.1497
	0.3502	0.3693	0.3992	0.4003	0.3933	0.3576
	0.0697	0.0295	-0.0032	-0.0498	-0.0937	-0.1153
2						
	0.0483	0.0421	0.0338	0.0297	0.0286	0.0309
	0.1124	0.1098	0.1063	0.1109	0.1144	0.1208
	-0.0640	-0.0678	-0.0725	-0.0812	-0.0857	-0.0899
	(0.201)	(0.111)	(0.0)	(0.0)	(0.0)	(0.124)
6						
	(0.294)	(0.351)	(0.313)	(0.372)	(0.495)	(0.599)
	0.0283	0.0303	0.0297	0.0263	0.0290	0.0266
	0.0695	0.0815	0.0925	0.0869	0.0951	0.0907
	-0.0412	-0.0512	-0.0630	-0.0606	-0.0661	-0.0641
8						
	0.0283	0.0303	0.0297	0.0263	0.0290	0.0266
	0.0695	0.0815	0.0925	0.0869	0.0951	0.0907
	-0.0134	-0.0145	-0.0157	0.0041	-0.0066	-0.0242
	-0.0545	-0.0657	-0.0787	-0.0565	-0.0727	-0.0883
10						
	0.3151	0.2961	0.3030	0.2681	0.2130	0.1581
	0.0991	0.0964	0.1079	0.1155	0.0887	0.0553
	0.0809	0.0731	0.0878	0.2064	0.1061	0.0180
	0.1349	0.1265	0.1073	-0.0539	0.0182	0.0847

Figure 14(a). 170°W Longitudinal cross-section, tropical section. Refer to Fig. 12 for key. Values computed from data for 16 January 1974.

	LAT 30.0	35.0	40.0	45.0	50.0	55.0	60.0	65.0
2	0.3446 0.1608 0.2783 -0.0945	0.2957 0.1264 0.3450 -0.1757	0.2459 0.1227 0.3478 -0.2245	0.1958 0.1009 0.3241 -0.2292	0.1462 0.0760 0.3280 -0.2579	0.0984 0.0503 0.2445 -0.1964	0.0542 0.0252 0.1673 -0.1383	0.0170 0.0074 0.2355 -0.2258
	0.0366 0.1334 -0.0968	0.0186 0.1084 -0.0898	0.0081 0.0772 -0.0692	0.0075 0.0798 -0.0723	0.0058 0.0748 -0.0690	0.0084 0.0903 -0.0819	0.0062 0.0687 -0.0625	0.0011 0.0628 -0.0618
6	(0.521)	(0.066)	(0.0)	(0.0)	(0.0)	(0.293)	(0.564)	(0.0)
	(0.559)	(0.661)	(0.861)	(0.851)	(0.869)	(0.574)	(0.0)	(0.0)
8	0.0164 0.0498 -0.0334	0.0208 0.0906 -0.0697	0.0216 0.1072 -0.0856	0.0150 0.0896 -0.0746	0.0119 0.0928 -0.0807	0.0048 0.0335 -0.0287	0.0007 0.0005 0.0001	0.0004 0.0396 -0.0392
10	0.0164 0.0498 -0.0272 -0.0607	0.0208 0.0906 -0.0175 -0.0872	0.0216 0.1072 0.0537 -0.0319	0.0150 0.0896 0.1019 0.0273	0.0119 0.0928 0.0869 0.0061	0.0048 0.0335 0.1037 0.0750	0.0007 0.0005 -0.0571 -0.0570	0.0004 0.0396 -0.0504 -0.0896
	0.1144 0.0451 0.0126 0.0566	0.1090 0.0554 0.0263 0.0273	0.0721 0.0562 0.2289 -0.2130	0.0573 0.0651 0.2543 -0.2621	0.0404 0.0678 0.1795 -0.2068	0.0301 0.0871 0.1968 -0.2539	0.0214 0.0976 -0.0848 0.0085	0.0078 0.0934 -0.0713 -0.0143

Figure 14(b). 170°W Longitude cross-section, higher latitude section. Refer to Fig. 12 for key. Values computed from data for 16 January 1974.

LAT.	-5.0	0.0	5.0	10.0	15.0	20.0	25.0
	0.6049	0.5722	0.5563	0.5197	0.4799	0.4372	0.3920
	0.1910	0.1979	0.2043	0.1617	0.1759	0.1401	0.0984
	0.3631	0.3980	0.4018	0.4070	0.3981	0.4062	0.4074
2	0.0508	-0.0237	-0.0498	-0.0490	-0.0940	-0.1090	-0.1139
	0.0507	0.0400	0.0377	0.0343	0.0327	0.0257	0.0207
	0.1185	0.1130	0.1186	0.1161	0.1149	0.1160	0.1255
	-0.0678	-0.0730	-0.0809	-0.0818	-0.0823	-0.0904	-0.1048
	(0.170)	(0.0)	(0.0)	(0.0)	(0.0)	(0.0)	(0.0)
6	(0.395)	(0.589)	(0.641)	(0.480)	(0.599)	(0.415)	(0.140)
	0.0348	0.0428	0.0433	0.0364	0.0356	0.0279	0.0160
	0.0761	0.1054	0.1082	0.0971	0.1021	0.0893	0.0537
8	-0.0412	-0.0626	-0.0649	-0.0608	-0.0665	-0.0615	-0.0376
	0.0348	0.0428	0.0433	0.0364	0.0356	0.0279	0.0160
	0.0761	0.1054	0.1082	0.0971	0.1021	0.0893	0.0537
	-0.0102	-0.0108	-0.0110	-0.0050	-0.0054	0.0119	0.0436
10	-0.0514	-0.0734	-0.0759	-0.0658	-0.0719	-0.0496	0.0060
	0.2936	0.2488	0.2279	0.2509	0.2004	0.2156	0.2406
	0.0924	0.0743	0.0668	0.0967	0.0791	0.1114	0.1746
	0.0950	0.0735	0.0689	0.1876	0.1306	0.2131	0.2495
	0.1062	0.1010	0.0922	-0.0334	-0.0092	-0.1089	-0.1834

Figure 15(a). 145°E Longitudinal cross-section, tropical section. Refer to Fig. 12 for key. Values computed from data for 16 January 1974.

	LAT 30.0	35.0	40.0	45.0	50.0	55.0
2	0.3446 0.0971 0.3612 -0.1136	0.2957 0.0923 0.3612 -0.1577	0.2459 0.0881 0.3330 -0.1752	0.1958 0.1158 0.2206 -0.1407	0.1462 0.0781 0.2122 -0.1441	0.0984 0.0552 0.2011 -0.1580
	0.0216 0.1149 -0.0933	0.0137 0.0946 -0.0809	0.0093 0.0783 -0.0691	0.0167 0.1094 -0.0927	0.0138 0.0998 -0.0860	0.0106 0.0976 -0.0869
6	(0.0)	(0.0)	(0.0)	(0.656)	(0.612)	(0.618)
	(0.166)	(0.189)	(0.220)	(0.869)	(0.403)	(0.491)
	0.0147 0.0423 -0.0277	0.0138 0.0434 -0.0296	0.0109 0.0439 -0.0330	0.0089 0.0361 -0.0272	0.0051 0.0210 -0.0160	0.0038 0.0240 -0.0202
8	0.0147 0.0423 0.1141 0.0864	0.0138 0.0434 0.1700 0.1404	0.0109 0.0439 0.2067 0.1736	0.0089 0.0361 0.0174 -0.0098	0.0051 0.0210 0.0450 0.0290	0.0038 0.0240 0.0179 -0.0023
10	0.1966 0.1616 0.5108 -0.4758	0.1621 0.1797 0.5258 -0.5434	0.1268 0.1668 0.4433 -0.4833	0.0454 0.0391 0.0562 -0.0498	0.0441 0.0703 0.1225 -0.1487	0.0251 0.0557 0.0636 -0.0942

Figure 15(b). 145°E Longitudinal cross-section, higher latitude section. Refer to Fig. 12 for key. Values computed from data for 16 January 1974.

LAT.	-20.0	-15.0	-10.0	-5.0	0.0	5.0	10.0	15.0	20.0	25.0
	0.6812 0.2655 0.3246 0.0911	0.6646 0.2475 0.3469 0.0702	0.6437 0.2105 0.3819 0.0513	0.6184 0.1931 0.3716 0.0538	0.5893 0.2193 0.3520 0.0180	0.5563 0.1697 0.3535 0.0330	0.5197 0.1365 0.3497 0.0336	0.4799 0.1054 0.3666 0.0079	0.4372 0.1044 0.3811 -0.0483	0.3920 0.1124 0.3565 -0.0769
2										
	0.0603 0.1183 -0.0580	0.0535 0.1155 -0.0620	0.0435 0.1083 -0.0648	0.0458 0.1117 -0.0658	0.0489 0.1187 -0.0698	0.0461 0.1141 -0.0680	0.0437 0.1122 -0.0685	0.0355 0.1041 -0.0687	0.0282 0.1000 -0.0717	0.0283 0.1056 -0.0773
	(0.318)	(0.205)	(0.033)	(0.095)	(0.194)	(0.183)	(0.203)	(0.101)	(0.006)	(0.105)
6										
	(0.496)	(0.525)	(0.522)	(0.438)	(0.538)	(0.343)	(0.187)	(0.104)	(0.184)	(0.186)
	0.0354 0.0590 -0.0236	0.0390 0.0721 -0.0331	0.0448 0.0909 -0.0461	0.0385 0.0818 -0.0433	0.0368 0.0782 -0.0415	0.0297 0.0706 -0.0408	0.0235 0.0601 -0.0366	0.0207 0.0619 -0.0412	0.0219 0.0734 -0.0515	0.0188 0.0607 -0.0419
8										
	0.0354 0.0590 0.0023 -0.0214	0.0390 0.0721 0.0041 -0.0291	0.0448 0.0909 0.0007 -0.0454	0.0385 0.0818 -0.0045 -0.0478	0.0368 0.0782 -0.0081 -0.0496	0.0297 0.0706 -0.0087 -0.0496	0.0235 0.0601 -0.0099 -0.0466	0.0207 0.0619 -0.0017 -0.0429	0.0219 0.0734 0.0027 -0.0489	0.0188 0.0607 0.0127 -0.0291
10										
	0.2843 0.0882 0.0794 0.1169	0.2856 0.0872 0.1754 0.0231	0.3000 0.0917 0.1252 0.0832	0.3025 0.0964 0.1493 0.0568	0.2475 0.0769 0.1061 0.0645	0.2810 0.0982 0.0957 0.0871	0.2925 0.1172 0.1551 0.0202	0.2976 0.1387 0.1869 -0.0279	0.2607 0.1343 0.1671 -0.0406	0.2136 0.1294 0.1804 -0.0962

Figure 16(a). 35°W Longitudinal cross-section, tropical section. Refer to Fig. 12 for key. Values computed from data for 16 January 1974.

	LAT. 30.0	35.0	40.0	45.0	50.0	55.0	60.0
	0.3446 0.1137 0.3384 -0.1075	0.2957 0.0846 0.3729 -0.1619	0.2459 0.0781 0.3534 -0.1857	0.1958 0.0751 0.3489 -0.2282	0.1462 0.0643 0.3354 -0.2534	0.0984 0.0486 0.2813 -0.2314	0.0541 0.0273 0.2751 -0.2482
2							
	0.0259 0.1058 -0.0798	0.0167 0.0916 -0.0749	0.0143 0.0915 -0.0772	0.0108 0.0933 -0.0825	0.0080 0.0850 -0.0769	0.0080 0.0898 -0.0818	0.0044 0.0768 -0.0724
	(0.162)	(0.032)	(0.061)	(0.012)	(0.0)	(0.254)	(0.265)
6							
	(0.207)	(0.052)	(0.054)	(0.264)	(0.454)	(0.427)	(0.341)
	0.0158 0.0525 -0.0367	0.0105 0.0521 -0.0417	0.0089 0.0458 -0.0368	0.0108 0.0606 -0.0499	0.0101 0.0741 -0.0641	0.0053 0.0505 -0.0452	0.0029 0.0422 -0.0392
8							
	0.0158 0.0525 0.0286 -0.0081	0.0105 0.0521 0.0865 0.0449	0.0089 0.0458 0.1469 0.1100	0.0108 0.0606 0.1637 0.1139	0.0101 0.0741 0.0995 0.0354	0.0053 0.0505 0.0404 -0.0048	0.0029 0.0422 0.1120 0.0728
10							
	0.1735 0.1277 0.2090 -0.1632	0.1734 0.1769 0.3649 -0.3684	0.1356 0.1704 0.5185 -0.5533	0.0883 0.1343 0.5544 -0.6005	0.0538 0.1023 0.4183 -0.4667	0.0313 0.0905 0.2664 -0.3257	0.0165 0.1139 0.3160 -0.4134

Figure 16(b). 35°W Longitudinal cross-section, higher latitude section. Refer to Fig. 12 for key. Values computed from data for 16 January 1974.

and

$$QREF(t) = QREF * [\text{Cos } z / \overline{(\text{Cos } z)}\ ]$$

etc. These solar disposition terms may then be utilized in connection with a one-hour time-step application of the thermodynamic equation of the set of primitive equations used in the FNWC prediction-process. The purpose for leaving all results of Figures 13,..., 16 in the form of daily-averages was primarily so that these figures could be compared with climatology where available of the zonally-averaged heat budget of the ocean-atmosphere system for January.

Finally while only the (2/3)-CL cloud model results have been depicted in Figs. 13, 14, 15,16. An analogous set of heat-budget cross-sections were developed for the full-CL model. These are not presented here because of the sheer volume of the results. However, certain radiative terms in both the (2/3)-CL and full-CL cross-section sets have been extracted from both sets for purposes of presenting zonal comparisons of the purely radiative-heat-budget of the FNWC data as it was applicable to 16 January 1974. The comparative zonally-averaged radiative cross-sections are presented in Figs. 18 and 19 of Section VII.

VII. ZONALLY-AVERAGED RADIATIONAL BALANCE OF THE OCEAN-ATMOSPHERE SYSTEM

A. GENERAL

In order to depict the results of the purely radiative contributions, zonally-averaged over the ocean-atmosphere system for this study, Figs. 18(a, b) and 19(a, b) are presented. These figures present respectively the zonally-averaged radiative cross-sections for both the 2/3-CL and the full-CL cloud amounts. These cross-sections show the results after zonal-averaging over the four meridians considered in this study. The results are then displayed in the format of Fig. 17, which gives the key to the line items of the cross-sections. Note that Fig. 17 simply combines the radiative-transfers Q68, Q810, and also F68 with F810 of Fig. 12 to arrive at layer-average radiational warming rates in the combined layer (6, 10). Also in the results of this section, turbulent-transfer heating rates into the atmosphere (and corresponding cooling in the underlying ocean) have merely been omitted from the results of Figs. 13,...,16, in passing to the radiative composites presented here.

In obtaining a simple zonally-averaged set of radiative heating-rates at each latitude ϕ, all values of each parameter listed in Fig. 17 at latitude ϕ in the range 20S,...,65N (by 5° steps) were simply averaged over the meridians providing the averaged value at ϕ. It should be noted that at ϕ = 65N, there was only one contribution to the average. In the Southern Hemisphere region 20S,...,10S, only two values (from 125W and

k	LAT		latitude of the gridpoints in 5° increments
	a)	QAVE	24-hour averaged mean insolation at level k=2
	b)	QREF	mean reflected average insolation at level k=2
	c)	F_2*	mean net outgoing long-wave flux at level k=2
2	d)	BALT	mean averaged earth tropospheric gain rate (a-b-c)
	e)	Q26	mean averaged solar insolation absorbed by layer (2,6)
	f)	F26	mean IR flux loss by layer (2,6)
	g)	BAL26	mean averaged radiative cooling rate, layer (2,6) (e-f)
		(CL_1)	upper layer (4,6) cloud amount)
		(CL_2)	lower layer (8,9) cloud amount)
6			
	h)	Q610	mean averaged solar insolation absorbed by layer (6,10)
	i)	F610	mean IR flux loss by layer (6,10)
	j)	BAL610	mean averaged radiative cooling rate, layer (6,10) (h-i)
10			
	k)	QABG	mean averaged solar insolation absorbed by surface
	l)	F_{10}*	mean net long-wave flux at earth's surface
	m)	BAL10	mean averaged radiational warming (cooling) rate at earth's surface (k-l)

Figure 17. Key to zonally-averaged radiational cross-section for Figs. 18(a,b) and 19(a,b). All radiational values have been averaged over a 24-hour day and are expressed in ly min^{-1} for the levels or layers considered. The zonal averages have been taken over the meridians (125°W, 170°W, 145°E, and 35°W) used in this study. The cloud-amounts (in parentheses) are by the 2/3-cloud model in Fig. 18 and by the full-CL model in Fig. 19.

LAT	20.0S	15.0S	10.0S	5.0S	0.0	5.0N	10.0N	15.0N	20.0N	25.0N
k	.6812	.6646	.6437	.6139	.5850	.5563	.5197	.4799	.4372	.3920
	.3036	.2882	.2484	.2108	.2034	.1870	.1486	.1390	.1254	.1235
	.3094	.3214	.3465	.3556	.3633	.3742	.3852	.3898	.3931	.3623
2	.0680	.0550	.0488	.0475	.0183	.0050	-.0141	-.0489	-0.0813	-.0938
	.0636	.0596	.0524	.0505	.0464	.0420	.0373	.0326	.0284	.0296
	.1214	.1200	.1118	.1152	.1142	.1128	.1102	.1091	.1082	.1143
	-.0578	-.0604	-.0594	-.0647	-.0678	-.0708	-.0728	-.0765	-.0798	-.0847
	(.377)	(.320)	(.196)	(.170)	(.133)	(.087)	(.052)	(.025)	(.002)	(.113)
	(.624)	(.625)	(.551)	(.442)	(.481)	(.472)	(.331)	(.320)	(.282)	(.231)
6										
	.0733	.0755	.0797	.0777	.0728	.0716	.0622	.0563	.0513	.0382
	.1097	.1223	.1472	.1503	.1670	.1755	.1678	.1660	.1652	.1280
	-.0364	-.0468	-.0675	-.0726	-.0942	-.1039	-.1056	-.1097	-.1138	-.0898
10										
	.2405	.2414	.2632	.2803	.2624	.2557	.2717	.2520	.2321	.2006
	.0782	.0789	.0852	.0901	.0822	.0825	.1072	.1147	.1198	.1199
	.1622	.1625	.1780	.1902	.1802	.1732	.1645	.1373	.1124	.0807

Figure 18(a). Zonally-averaged radiational cross-section for tropical latitudes with 2/3-CL model. Refer to Fig. 17 for key. All values listed are daily averages in ly min^{-1} and are computed from data for 16 January 1974.

LAT	30.0N	35.0N	40.0N	45.0N	50.0N	55.0N	60.0N	65.0N
k	.3446	.2957	.2459	.1958	.1462	.0984	.0542	.0170
	.1264	.1095	.1051	.1008	.0758	.0598	.0262	.0074
	.3180	.3359	.3097	.2745	.2766	.2394	.2212	.2355
2	-.0998	-.1497	-.1689	-.1795	-.2062	-.2008	-.1932	-.2258
	.0306	.0215	.0178	.0154	.0121	.0118	.0053	.0011
	.1142	.1018	.0959	.1047	.0975	.1090	.0728	.0628
	-.0836	-.0804	-.0781	-.0893	-.0854	-.0972	-.0674	-.0618
	(.260)	(.156)	(.237)	(.344)	(.318)	(.512)	(.414)	(.265)
	(.233)	(.285)	(.366)	(.680)	(.647)	(.432)	(.170)	(.341)
6								
	.0286	.0272	.0242	.0217	.0170	.0078	.0036	.0008
	.0922	.1118	.1058	.1116	.1124	.0496	.0427	.0792
	-.0636	-.0846	-.0816	-.0898	-.0954	-.0418	-.0391	-.0684
10								
	.1591	.1374	.0988	.0578	.0413	.0274	.0190	.0078
	.1116	.1222	.1079	.0672	.0688	.0683	.1058	.0934
	.0475	.0152	-.0091	-.0094	-.0275	-.0409	-.0868	-.0856

Figure 18(b). Zonally-averaged radiational cross-section for mid to high latitudes with 2/3 CL model. Refer to Fig. 17 for key. All values listed are daily averages in ly min^{-1} and are from data for 16 January 1974.

LAT	20.0S	15.0S	10.0S	5.0S	0.0	5.0N	10.0N	15.0N	20.0N	25.0N
k	.6812	.6646	.6437	.6139	.5850	.5563	.5197	.4799	.4372	.3920
	.3720	.3576	.3155	.2662	.2601	.2386	.1836	.1688	.1482	.1436
	.2878	.3018	.3320	.3431	.3526	.3654	.3790	.3847	.3900	.3541
2	.0214	.0052	-.0038	.0046	-.0277	-.0477	-.0429	-.0736	-.1010	-.1057
	.0694	.0642	.0552	.0529	.0482	.0432	.0380	.0330	.0285	.0306
	.1412	.1373	.1246	.1241	.1211	.1174	.1126	.1104	.1082	.1194
	-.0718	-.0731	-.0694	-.0712	-.0729	-.0742	-.0746	-.0774	-.0797	-.0888
	(.566)	(.478)	(.294)	(.255)	(.200)	(.131)	(.078)	(.038)	(.002)	(.170)
	(.872)	(.894)	(.827)	(.663)	(.722)	(.708)	(.502)	(.480)	(.423)	(.284)
6										
	.0736	.0784	.0870	.0780	.0817	.0762	.0680	.0617	.0561	.0404
	.0925	.1126	.1527	.1559	.1793	.1918	.1816	.1806	.1794	.1312
	-.0189	-.0342	-.0657	-.0779	-.0976	-.1156	-.1136	-.1189	-.1233	-.0908
10										
	.1663	.1644	.1858	.2168	.1966	.1948	.2301	.2164	.2045	.1774
	.0540	.0523	.0366	.0631	.0523	.0562	.0847	.0937	.1023	.1036
	.1123	.1121	.1492	.1537	.1443	.1386	.1454	.1227	.1022	.0738

Figure 19(a). Similar to Fig. 18(a) except full-CL model (after Smagorinsky, Eq. 2-14) is used in all radiative calculations.

LAT	30.0N	35.0N	40.0N	45.0N	50.0N	55.0N	60.0N	65.0N
k	.3446	.2957	.2459	.1958	.1462	.0984	.0542	.0170
	.1453	.1226	.1130	.1088	.0831	.0562	.0281	.0073
	.3035	.3283	.3035	.2705	.2600	.2092	.2020	.2364
2	-.1042	-.1552	-.1706	-.1835	-.1969	-.1670	-.1759	-.2265
	.0325	.0221	.0182	.0165	.0129	.0125	.0058	.0010
	.1254	.1065	.0996	.1137	.1091	.1234	.0850	.0623
	-.0929	-.0844	-.0814	-.0972	-.0962	-.1109	-.0792	-.0613
	(.392)	(.207)	(.273)	(.474)	(.478)	(.685)	(.621)	(0.0)
	(.350)	(.422)	(.484)	(.814)	(.818)	(.663)	(.256)	(0.0)
6								
	.0288	.0294	.0257	.0210	.0198	.0079	.0034	.0008
	.0830	.1148	.1062	.1007	.0976	.0342	.0448	.0790
	-.0542	-.0854	-.0805	-.0797	-.0778	-.0263	-.0414	-.0782
10								
	.1381	.1216	.0890	.0494	.0334	.0218	.0166	.0081
	.0952	.1071	.0962	.0561	.0533	.0518	.0850	.0949
	.0429	.0145	-.0072	-.0067	-.0199	-.0300	-.0684	-.0868

Figure 19(b). Similar to Fig. 18(b) except full-CL model (after Smagorinsky, Ea. 2-14) is used in all radiative calculations.

and 35W) of each parameter contributed to the means listed here in Figs. 18 and 19. At all other latitudes, there were in general four values of each radiative parameter entering into the computed radiative mean cross-section. As a result, one may conclude that near the northern and southern boundaries of Figs. 18 and 19, the listed values of the zonally-averaged quantities may not be exact, but the general zonal trend is probably reliable. (Fig. 20 shows this to be a valid result.)

Figures 18, 19, and 20 are useful for the discussion of the earth-atmosphere system radiative balance, and in the discussion of the relative merits of the two-thirds cloud-model as compared with the full-CL model. The full-cloud model used by Warner [1974], is also used in comparative discussion of the heat budget of the earth-atmosphere system of Section VIII.

B. EARTH-ATMOSPHERE SYSTEM RADIATIONAL BALANCE RESULTS

Figure 20 depicts the zonally-averaged distribution of three parameters, R_s, R_a, and R for full cloud amounts and two-thirds cloud amounts, respectively. These parameters were defined (after Malkus, 1962) as (1) R_s, the mean radiative energy transfer rate across the top of the ocean-tropospheric system (referred to as $\overline{\mathrm{BALT}}$ at k = 2 in Fig. 17; (2) R_a, the mean radiative cooling rate in the troposphere, i.e., the sum of $\overline{\mathrm{BAL26}}$ and $\overline{\mathrm{BAL610}}$ in Fig. 17; and (3) R, the mean radiative warming (cooling) rate at the earth's surface, referred to as $\overline{\mathrm{BAL10}}$ in Fig. 17. The relationship between

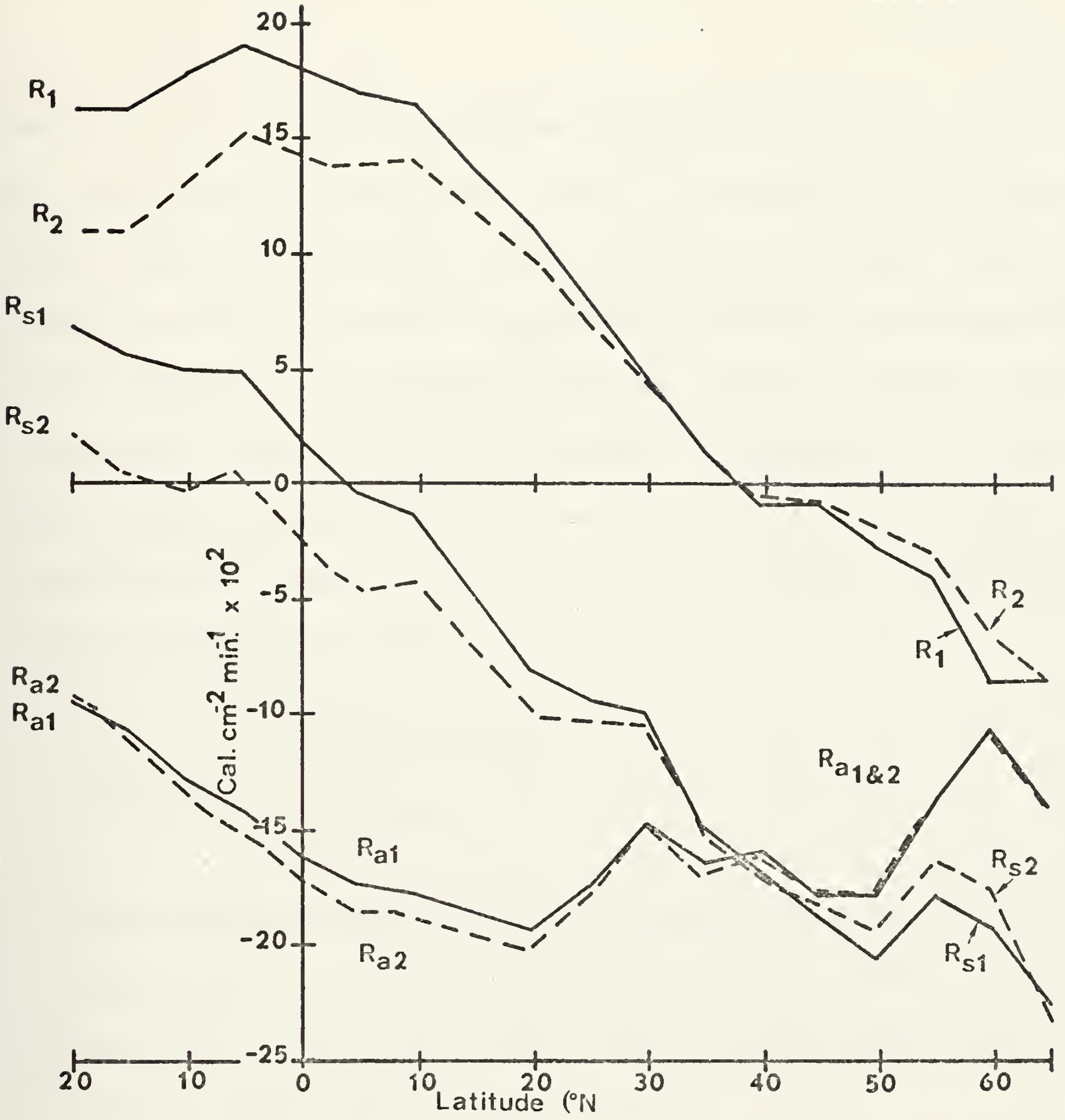

Figure 20. Radiational balance at the tropopause (R_s), at the ocean surface (R), and in the tropospheric column (R_a). Solid lines denote computations made with the 2/3-CL (subscripted "1") cloud model and dashed lines correspond to the full-CL model, (subscripted "2"). All computations are for 16 January 1974 on ly(min) × 10^2.

these three radiative parameters is as follows:

$$R_s = R + R_a. \tag{7-1}$$

Table V lists zonally-averaged comparisons of R_s, R_a, and R as a function of latitude ϕ for this study for 16 January 1974, both for the 2/3-CL and the full-CL cases. Also included is the R_{s4} values (signifying satellite climatology) after Raschke *et al.* [1973], and R_3 and R_{a3} values. The latter two symbols denote December climatological values after Berliand [1956] corresponding to R and R_a respectively. "Hemispheric" means of any Q-value are then by the following cosine-weighting scheme:

$$Q_{Wt.Avg.} = \frac{\sum_{i=0}^{65} Q_i \operatorname{Cos} \phi_i}{\sum_{i=0}^{65} \operatorname{Cos} \phi_i} . \tag{7-2}$$

The tabular values of R_s, R, and R_a as a function of latitude and for the two cases, 2/3-CL, and full-CL, have been plotted in Fig. 20, where some interesting results of the radiational model become evident.

It is evident from Fig. 20 that the R_s values obtained with the 2/3-CL cloud model exceed those based upon the full-CL model up to $\phi = 40N$. Poleward of this latitude the two R_s-curve cross with R_s(CL) becoming slightly larger (although negative) than R_s(2/3-CL). The same general results hold for both R_1 and R_2 and for R_{a1} relative to R_{a2}, up to latitudes 40-45N, where also cross-overs in the graphical depictions occur in both cases. These results are related to the zonally-averaged radiative budgetary cross-sections of Figs. 18 and 19 as is explained in Section VII (C).

	Earth-Troposphere Net Radiation, R_s (k=2)			Surface Net Net Radiation, R (k=10)			Atmospheric-Net Radiation Gain R_a		
Lat	R_{s_4}	R_{s_1}	R_{s_2}	R_1	R_2	R_3	R_{a_1}	R_{a_2}	R_{a_3}
20S	.1800	.0681	.0216	.1622	.1123		-.0942	-.0913	
15	.1700	.0552	.0052	.1624	.1125		-.1073	-.1075	
10	.1600	.0488	-.0039	.1780	.1310		-.1292	-.1347	
5	.1430	.0475	.0046	.1902	.1537		-.1426	-.1492	
0	.1150	.0182	-.0270	.1802	.1443	.1713	-.1621	-.1720	-.0833
5	.0825	-.0050	-.0478	.1697	.1387		-.1746	-.1864	
10	.0550	-.0140	-.0428	.1645	.1454	.1481	-.1787	-.1882	-.1157
15	.0150	-.0489	-.0736	.1374	.1226		-.1863	-.1962	
20	-.0125	-.0813	-.1010	.1123	.1022	.1088	-.1937	-.2031	-.1551
25	-.0256	-.0938	-.1058	.0807	.0738		-.1745	-.1796	
30	-.0400	-.0998	-.1041	.0475	.0429	.0463	-.1472	-.1471	-.1551
35	-.1050	-.1497	-.1551	.0152	.0145		-.1648	-.1696	
40	-.1375	-.1689	-.1706	-.0092	-.0072	-.0116	-.1597	-.1634	-.1597
45	-.1625	-.1884	-.1835	-.0094	-.0068		-.1791	-.1768	
50	-.1750	-.2062	-.1969	-.0275	-.0200	-.0417	-.1788	-.1769	-.1828
55	-.2025	-.1798	-.1671	-.0409	-.0300		-.1388	-.1371	
60	-.2300	-.1932	-.1759	-.0868	-.0683	-.0509	-.1065	-.1077	-.2037
65N	-.2400	-.2265	-.2265	-.0868	-.0868		-.1397	-.1397	
Wt. Avg (N. Hem)	-.0500	-.1000	-.1139	.0668	.0581	.0699	-.1668	-.1720	-.1437

Table V. Zonally-averaged components R, R_s, R_a of the earth-atmosphere system as a function of latitude. The averaged values as found in this study using subscript "1" for the 2/3-CL case and the subscript "2" for the full-CL case. Corresponding values of R_s reported by Raschke et al. (1973) are denoted by subscript "4" and those of R_a and R reported after Berliand (1956) for December climatology denoted by subscript "3". Weighted averages over the latitude range 0-65N are shown in the last line of the table. (All values in ly min^{-1}).

C. EXPLANATION OF THE MEAN ZONAL RADIATIVE-BUDGET DISTRIBUTIONS

It should be observed that in Table V, the R_s values obtained with the 2/3-CL model are greater than those resulting from the full-CL model throughout the tropics and up to latitude 40N (approximately). Poleward of latitude 40N, the values of R_s(2/3-CL) become smaller than those for full-CL. These comparisons are illustrated clearly in Fig. 20 by the zonal depictions of the R_s values calculated by the two cloud-model cases. Examination of Table V for comparative values of the radiative balances at the surface shows the same general effect at the ocean surface, with the cross-over between 2/3-CL and full-CL cases (R_1 and R_2 curves in Fig. 20) occurring near latitude 40N. Finally, the same general effect is evident in the comparative values of R_a(2/3-CL) compared to R_a(CL). That these three comparisons should follow each other systematically is perhaps to be expected in view of the connecting relationship

$$R_s = R + R_a .$$

Of the changes resulting from substituting (2/3-CL) for the full-CL cases, the largest gain in low and mid-latitudes occurs in the comparative R_s-curve for the (2/3-CL) case. The smallest gain occurs for the computed R_a-changes, and an intermediate gain is registered for the R(2/3-CL), the net radiative flux at the ocean surface.

The same results for R_s-changes may be seen by comparing Fig. 18 for the 2/3-CL case with Fig. 19 for the full-CL case. In such a comparison it is seen that the systematic reduction

of CL to 2/3-CL increases the net useful solar insolation at $k = 2$, (Figs. 17, 18, and 19) by reducing QREF. However, the reduction achieved in QREF(2/3-CL) is quite small at latitudes $\phi \geq 45N$. On the other hand with the 2/3-CL case, the $F_2{*}$ values (net terrestrial loss to space at $k = 2$) is increased by a small but consistent amount which at higher latitudes $\phi \geq 45N$, exceeds the very small net solar insolation gain ($k = 2$).

It therefore turns out that in the consideration of Figs. 18 and 19 of the atmospheric-layer radiative transactions (both solar and terrestrial) that the net radiation R penetrating to the surface is influenced primarily by QREF, at best in lower latitudes and up to $\phi = 40N$. Here $-\Delta$(QREF) exceeds $\Delta F_2{*}$ as a result of the change in cloud cover and thus accounts for greater R_s-values. The same effects account for R-changes at the surface, while at $\phi \geq 45N$ the cross-over effect holds both at $k = 2$, and also at $k = 10$.

The curves of R_a versus ϕ in Fig. 20, in effect measure the atmospheric participation in the radiative absorption and emission processes, follow the lead of $-\Delta$(QREF) in lower latitudes and of $F_2{*}$ in higher latitudes, which act as the forcing functions in the radiative balance of the system.

Recent satellite results especially of Von der Haar and Hanson [1969] as well as of Raschke *et al.* [1973], also draw attention to the reduced values of global albedo, compared to previous heat budget estimates (e.g., London, 1957) in tropical and subtropical latitudes. This also shows up in Table V in the comparative values of Raschke's distribution

of R_s with the "best" R_s distribution computed here for the 2/3-CL model. It should be noted from Table V that the use of the 2/3-CL model leads to R_{s1}-values which are in closer agreement with R_{s4} up to latitude 40N, than that generated by the full-CL model. At high latitudes in Table V the comparisons between the results of these two cloud models are inconclusive in their relationship to Raschke's results. However, his results in some of these areas are over ice, which enhances his effective QREF as compared with either model used here.

Finally note that comparative values after Berliand [1956] are also included in Table V for R and R_a at 10° latitude intervals based on December global climatology. The most noteworthy comparisons to be made here is the transition from positive to negative surface net flux R_3 which occurs between 35-40N, in reasonable agreement with the results interpolated either from the R_1-, R_2-distribution of Table V. In general, the global results of Berliand reflect a greater continental trend with latitude than is found in the January 1974 study over the oceans.

VIII. ZONALLY-AVERAGED TROPOSPHERIC AND OCEANIC HEAT BUDGETS FOR 16 JANUARY 1974

A. THE TROPOSPHERIC HEAT BUDGET OVER ICE-FREE OCEANS

By averaging over the tropospheric column for the four meridians displayed in Figs. 13,...,16, latitude by latitude, the zonally-averaged tropospheric balance results (Table VI and Fig. 21). Values presented in Table VI and Fig. 21 are R_a, the tropospheric radiative net cooling defined in Section VIII.B., and $E + H_\Gamma$ as formulated in Equations 5-2, 5-7. The latter parameter represents the combined turbulent heat-transfer $H_\Gamma + E$ across the ocean-air interface (see for example, Figs. 13,...,16). The heat-budget equation for the atmosphere column at latitude ϕ then becomes, with the notation of Malkus [1962]:

$$Q_{va} + S_a = R_a + (E + H_\Gamma). \qquad (8-1)$$

Here S_a is the *in-situ* storage-heating rate of the column, and Q_{va} is the required flux-divergence of heat necessary to bring about the "balance" in the column, for the observed values of R_a $E + H_\Gamma$ and S_a.

Table VI lists the zonally-averaged values of R_a, $E + H_\Gamma$ and the resulting values of $Q_{va} + S_a$, which are computed from (8-1). As before the subscript notation "1" and "2" denote the 2/3-CL and full-CL computations respectively. Figure 21 depicts each function R_a, $E + H_\Gamma$ and $Q_{va} + S_a$, computed by the two cloud-models.

As noted before in Section VII.C., R_{a1} tends to exceed R_{a2} over most of the tropical Southern Hemisphere and in the

	Tropospheric Radiative heating rate R_a			Turbulent transport heating rate in troposphere			Tropospheric Balance requirements $Q_{va}+S_a$		
Lat	R_{a_1}	R_{a_2}	R_{a_3}	$(E+H_\Gamma)_1$	$(E+H_\Gamma)_2$	$(E+H_\Gamma)_3$	$(Q_{va}+S_a)_1$	$(Q_{va}+S_a)_2$	$(Q_{va}+S_a)_3$
20S	-.0942	-.0913		.1402	.1402		.0461	.0490	
15	-.1073	-.1075		.1718	.1718		.0644	.0642	
10	-.1292	-.1347		.1689	.1689		.0397	.0342	
5	-.1426	0.1492		.1197	.1197		-.0229	-.0294	
0	-.1621	-.1720	-.0833	.0839	.0839	.0764	-.0782	-.0882	-.0069
5	-.1746	-.1864		.0791	.0791		-.0956	-.1073	
10	-.1787	-.1882	-.1157	.1374	.1374	.1018	-.0413	-.0508	-.0139
15	-.1863	-.1962		.1611	.1611		-.0252	-.0351	
20	-.1937	-.2031	-.1551	.1430	.1430	.1342	-.0507	-.0601	-.0209
25	-.1745	-.1796		.1257	.1257		-.0488	-.0538	
30	-.1472	-.1471	-.1551	.1998	.1998	.1250	.0526	.0528	-.0301
35	-.1648	-.1696		.2341	.2341		.0692	.0644	
40	-.1597	-.1634	-.1597	.2971	.2971	.1134	.1374	.1337	-.0463
45	-.1791	-.1768		.2172	.2172		.0382	.0404	
50	-.1788	-.1769	-.1828	.1901	.1901	.1458	.0113	.0132	-.0370
55	-.1388	-.1371		.1301	.1301		-.0087	-.0070	
60	-.1065	-.1077	-.2037	.1156	.1253	.1944	.0091	.0172	-.0093
65N	-.1397	-.1397		-.0721	-.0721		-.2118	-.2118	
Wt. Avg (N. Hem)	-.1668	-.1720	-.1437	.1508	.1512	.1208	-.0160	-.0208	-.0229

Table VI. Zonally-averaged components R_a, $(E+H_\Gamma)$ and $(Q_{va}+S_a)$ of the tropospheric heat budget. The averaged values as found in this study using subscript "1" for the 2/3-CL case and the subscript "2" for the full-CL case. Corresponding values reported after Berliand (1956) for December climatology denoted by subscript "3". Weighted averages over the latitude range 0-65N are shown in the last line of the table. (All values are in ly min^{-1}).

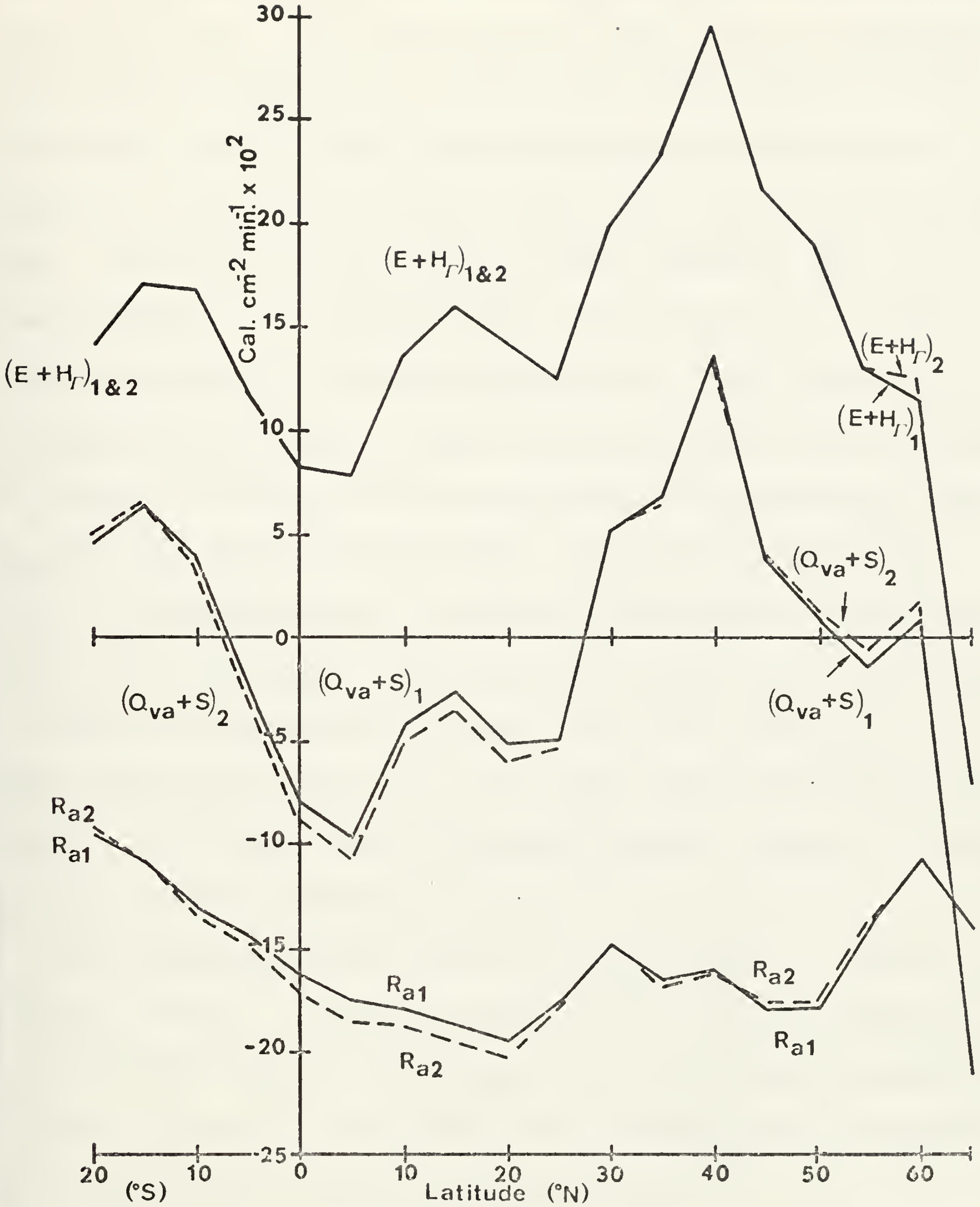

Figure 21. Distribution of R_a, $E+H_\Gamma$ and of $Q_{va}+S_a$ as a function of latitude for the two cloud-model cases. (solid curves -- 2/3-CL case; dashed curves -- full-CL case)

Northern Hemisphere to close to 40N, although these differences are quite small. The distribution of $E + H_\Gamma$ as a function of latitude is independent of the cloud-model except at high latitudes over a frozen sea-surface which occurs near $\phi \geq 60N$. Figure 21 shows the identical sets of $E + H_\Gamma$ up to latitudes 55N. The curves of $Q_{va} + S_a$ are also shown in Fig. 21, as the residual of the right sides of Equation 8-1 for both the 2/3-CL and full-CL cases, respectively. Note that $(Q_{va} + S_a)_1$ slightly exceeds $(Q_{va} + S_a)_2$ over most of the latitude range to 25N as a result of the corresponding of excess R_{a1} over R_{a2} for the same latitude range. Note also that both $Q_{va} + S_a$ distributions reach peak values at $\phi \doteq 40N$, and that the values $Q_{va} + S_a$ are generally positive over 30-50N.

This latter feature follows from (8-1), since $Q_{va} + S_a$ must follow the trend of $E + H_\Gamma$ where the latitudinal variation of the latter function peaks sharply, relative to more or less uniform behavior of $R_a(\phi)$.

The hemispheric mean value of $\overline{(Q_{va} + S_a)} = -.0160$ ℓy min^{-1} per cm^2 column. In this study, $\overline{Q_{va}}$ has not been computed, but if the $\overline{(Q_{va} + S_a)}$ is attributed to mean storage-cooling $\overline{S_a}$ of the troposphere alone, the daily storage rate corresponds to a temperature-change rate given by

$$\left(\overline{\frac{\partial T}{\partial t}} \right)_a = 4.1 \, \frac{(\overline{R_a} + \overline{E + H_\Gamma})}{\Delta P \text{ mb}} \times 1440 \text{ min/day} \qquad (8\text{-}2)$$

with ΔP mb $\doteq$ 800 mb in the troposphere. This resultant mean *in-situ* hemisphere cooling rate (8-2) over the tropospheric depth of 800 mb is then

$$\left.\frac{\overline{\partial T}}{\partial t}\right)_a = -.12°C(\text{day})^{-1}$$

averaged over the cm² tropospheric column. This seems to be a reasonable midwinter global value.

The variation in the computation of $E + H_\Gamma$ in the 2/3-CL and the full-CL cases which occurs poleward of latitude 55N is explained in Section VIII.C.

B. THE ZONALLY-AVERAGED HEAT BUDGET OF THE ICE-FREE OCEAN

For the present, neglect the minor variations attributed to water-to-ice conduction rates which occur in latitudes poleward of 55N (see for example H_{ice} of Equation 5-10). Neglecting this ice-conduction term, the zonally-averaged heat-budget of the ocean water-mass obeys the thermodynamic relationship

$$Q_{vo} + S = R + [-(E + H_\Gamma)] \tag{8-3}$$

for both the 2/3-CL and full-CL cases. Note that Equation 8-3 is the analog of (8-1) for the atmosphere, with $-(E+H_\Gamma)$ representing generally the cooling rate for the water mass.

The terms of the right side of (8-3) have been computed for each meridian and averaged by latitude, with the results shown in Table VII. Then $Q_{vo} + S$ is computed as the residual of the sum of the two functions on the right side of (8-3), and shown also in columns 1 and 2 of Table VII. The graphical distribution of the results listed in this table are shown in Fig. 22 both for the 2/3-CL (subscript "1") and the full-CL (subscript "2") cases.

As before the primary ocean-mass heating-function is R, the radiative heating rate at the ocean-air interface. For

	Surface Net Radiation, R (k=10)			Turbulent transport heating rate loss			Surface Balance Requirements		
Lat	R_1	R_2	R_3	$-(E+H_\Gamma)_1$	$-(E+H_\Gamma)_2$	$-(E+H_\Gamma)_3$	$(Q_{vo}+S)_1$	$(Q_{vo}+S)_2$	$(Q_{vo}+S)_3$
20S	.1622	.1123		-.1402	-.1402		.0220	-.0280	
15	.1624	.1125		-.1718	-.1718		-.0094	-.0592	
10	.1780	.1310		-.1689	-.1689		.0091	-.0379	
5	.1902	.1537		-.1197	-.1197		.0705	.0340	
0	.1802	.1443	.1713	-.0839	-.0839	-.0764	.0964	.0604	.0949
5	.1697	.1387		-.0791	-.0791		.0906	.0596	
10	.1645	.1454	.1481	-.1374	-.1374	-.1018	.0271	.0080	.0463
15	.1374	.1226		-.1611	-.1611		-.0238	-.0385	
20	.1123	.1022	.1088	-.1430	-.1430	-.1342	-.0306	-.0408	-.0254
25	.0807	.0738		-.1257	-.1257		-.0450	-.0520	
30	.0475	.0429	.0463	-.1998	-.1998	-.1250	-.1524	-.1570	-.0787
35	.0152	.0145		-.2341	-.2341		-.2188	-.2195	
40	-.0092	-.0072	-.0116	-.2971	-.2971	-.1134	-.3063	-.3043	-.1250
45	-.0094	-.0068		-.2172	-.2172		-.2266	-.2240	
50	-.0275	-.0200	-.0417	-.1901	-.1901	-.1458	-.2176	-.2101	-.1875
55	-.0409	-.0300		-.1301	-.1301		-.1710	-.1601	
60	-.0868	-.0683	-.0509	-.1156	-.1253	-.1944	-.2024	-.1933	-.2453
65N	-.0868	-.0868		.0721	.0721		-.0147	-.0147	
Wt. Avg (N. Hem)	.0668	.0581	.0699	-.1508	-.1512	-.1208	-.0840	-.0931	-.0509

Table VII. Zonally-averaged components R, $-(E+H_\Gamma)$ and $(Q_{vo}+S)$ of the surface heat budget. The averaged values as found in this study using subscript "1" for the 2/3-CL case and the subscript "2" for the full-CL case. Corresponding climatology values for the month of December reported after Berliand (1956) are denoted by subscript "3". Weighted averages are listed in the final line for the latitude range available in the N. Hemisphere. (All values in ly min^{-1}.)

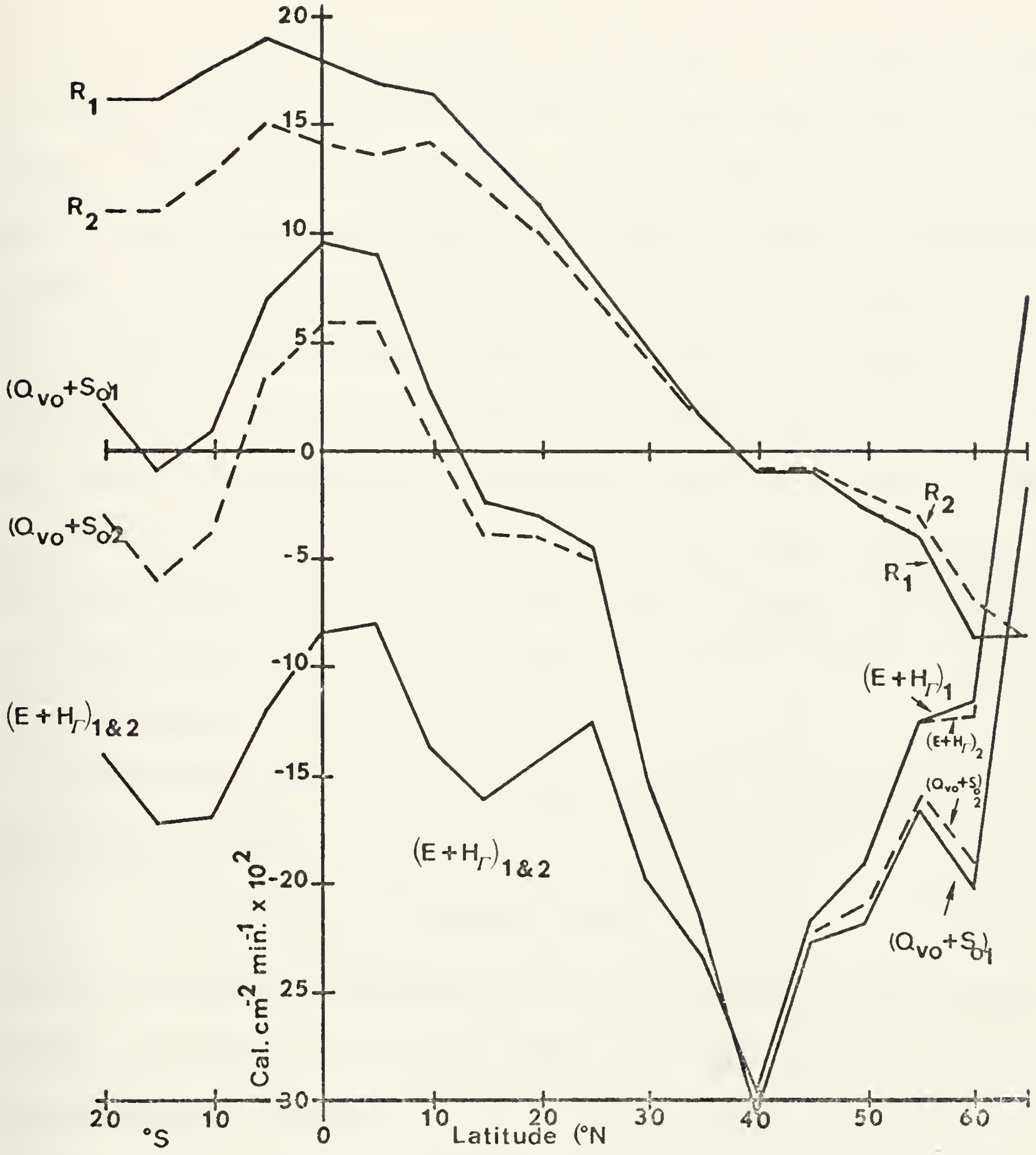

Figure 22. Distribution of R, - $(E+H_\Gamma)$ and of $(Q_{vo}+S_o)$ as a function of latitude for the two cloud-model cases. (solid curves -- 2/3-CL case; dashed curves -- full-CL case)

the 2/3-CL case, the corresponding R_1 is considerably larger in low- and mid-latitudes than R_2, for the full-CL case. There is virtually no change in the $-(E + H\ )$ profiles over latitude (except poleward of 60N). This means that the internal heating rate of the ocean-mass, which is given by the sum of the two terms on the right side of (8-3), is generally greater in the 2/3-CL case than in the full-CL case. Here Q_{vo} is the required mean oceanic heat-flux divergence at latitude ϕ. Figure 22 supports the conclusions of Von der Haar and Oort [1973] which requires increased lateral transport-divergences Q_{vo} in the oceans, based upon the recently observed satellite-values of the global albedo. The values ascribed here to $(Q_{vo} + S_o)_1$ seem to corroborate the satellite findings.

The "hemispheric" mean value of $\overline{(Q_{vo} + S_o)_1}$ computed between 0 - 65N is

$$(\overline{Q_{vo} + S})_1 = -.0839 \ \ell y \ \text{min}^{-1}$$

which corresponds to negligible cooling rate in the water-mass column, although it is five times as great as the corresponding atmospheric effect.

C. OCEAN-TROPOSPHERIC HEAT-BUDGETS FOR ICE-COVERED OCEANS

1. Computation of $(E + H_\Gamma)$ Over Ice-Covered Oceans

The determination of $E + H_\Gamma$ over ice-covered ocean was computed (following Equation A-36 of Kaitala, 1974)) with the following interface conditions used in Section V:

$$E + H_\Gamma = R + H_{ice} \qquad (5\text{-}11)$$

$$H_{ice} = BBB(T_o - T_g). \qquad (5\text{-}10)$$

In latitudes where ice-covered oceans occur, R is negative in January, and H_{ice} is usually positive but of an order of magnitude smaller than the magnitude of R. Hence the $(E + H_\Gamma)$ values computed at both $\phi = 60N$ and $\phi = 65N$ from the 170W meridian are both negative (here the Bering Sea is frozen on January 16, 1974).

Solution for H_{ice} and $H_\Gamma + E$ at $\phi = 60$ and 65 N then gave the following results

TABLE VIII. Surface heat-transports over ice at 170W

Lat	H_{ice} ℓy $\min^{-1}$		$E + H_\Gamma$ ℓy $\min^{-1}$	
	2/3-CL	FULL-CL	2/3-CL	FULL-CL
$\phi = 65N$	.0147	.0147	-.0721	-.0721
$\phi = 60N$	.0041	.0070	-.0683	-.0513

The values of $E + H_\Gamma$ of the foregoing display are used in the computation of zonally-averaged heat balance, both in the troposphere, and the ocean as reproduced in Tables VI and VII, respectively.

The reason for the difference in computed values of $E + H_\Gamma$ associated with the 2/3-CL and full-CL cases at latitudes $\phi \geq 60N$ is associated primarily with Equation 5-11 and the presence of ice. At $\phi \geq 60N$, the surface radiative quantities satisfy the inequality

$$|R_2| < |R_1|, \text{ when } CL > 0$$

although both are negative. Furthermore, H_{ice} in either case is an order of magnitude smaller than R_2 or R_1, respectively. Hence, when $CL > 0$

$$|E + H_\Gamma|_2 < |E + H_\Gamma|_1$$

and there must be a smaller turbulent flux from air to ice in the full-CL case. The results of Table VIII at latitude 60N exemplify this feature.

2. Budgetary Equations in Both Media with Ice-Covered Ocean

Finally, H_{ice} represents the result of a molecular conduction transfer rate, which leaves the ocean and enters the atmosphere over the ice by a process not included in the turbulent exchange rate $E + H_\Gamma$. Hence at ice-covered grid-points the heat budget equations of the troposphere and water-body become:

Air-mass over ice:

$$Q_{va} + S_a = R_a + (E + H_\Gamma) + H_{ice} \qquad (8\text{-}4)$$

Water-body under ice:

$$Q_{vo} + S_o = R - (E + H_\Gamma) - H_{ice}. \qquad (8\text{-}5)$$

The additive terms on the right side of 8-4, 8-5 did not modify the weighted-mean heating rates of the air-column or the water body significantly over the values resulting from Figs. 21 and 22.

IX. CONCLUSIONS

The present work has been primarily involved with the development of the radiational two-layer cloud model adapted from Warner's earlier thesis [1974]. The data employed was oceanic data from the FNWC gridpoint analyses for 16 January 1974. Here, it was found that the net radiative flux available for the earth-troposphere system was best verified against January satellite climatology (Raschke *et al.*, 1973) when the Smagorinsky cloud-amounts were arbitrarily reduced by a factor of one-third. It is recognized that there were some minor differences in the comparisons which could be attributed to the one day space-time average as opposed to the average of several weeks for satellite data, and years insofar as surface climatological data was concerned.

Reduction of Smagorinsky cloud amounts by one third was found to provide more realistic global albedo estimates than resulted using unreduced cloud-amounts. In the comparison with satellite data, the radiative model with a reduced CL gave slightly higher albedo estimates in the tropics and mid-latitudes and slightly lower albedo in the high-latitudes. The radiative model still lacks an effective surface albedo model over ice.

With the reduced cloud amounts greater surface net heating rates in the low to mid latitudes were computed than when using the original Smagorinsky cloud amounts. This latter finding is in accord with recent heat balance studies using satellite data which have found an increase in surface

heating particularly in the tropics. It is felt that further investigation of the tropical radiative balances are necessary. Thought should also be directed towards the geometry of solar radiation reflection problem among cumulus subgrid cells in the tropics as contrasted with the larger-scale two-cloud layer model used in this study, which proved fairly reliable in middle and high latitudes. Moreover, specification of the primarily cumuliform cloud distributions in the tropics is evidently closely related to the subgrid scale convection model rather than to the large-scale distribution of relative humidity (of Smagorinsky). It is recommended that further testing of the radiative model for the different seasons of the year continue, particularly with the one-third or similar reduction in the Smagorinsky cloud-amounts.

Further differences from climatological data might be attributed to the treatment of cloud reflectivity and absorptivity for solar wavelengths, as well as the parameterization of the sea-air exchanges of sensible and latent heat. In the latter case a new interpretation of the simple bulk formulas and of a redefined distribution of the turbulent sensible and latent fluxes in the planetary boundary layer parameterization model seemed to give a new, conceptually satisfying view of the planetary boundary layer model. Additional testing with the redefined planetary boundary layer or any new interpretation of such, might also prove productive in providing better comparisons with recent investigations such as the GATE and BOMEX experiments involving surface heat budget calculations.

APPENDIX A: EMISSIVITY ε_{wc} FORMULAS AS A FUNCTION OF WATER VAPOR AND CO_2 ABSORBER MASSES ALONG PATH OF INTEGRATION.

The general form of the calculation required for computing net IR flux is:

$$F_{10}{}^{*} = B_{10} - \int_{B=0}^{B_{10}} \varepsilon_{wc}(U,C,T)\ dB \qquad \text{(A-1)}$$

where B_{10} = Stephen-Boltzman blackbody flux at T_{10} and ε_{wc} is the emissivity of the atmosphere as a function of both water vapor and CO_2 absorber masses along the path of integration. The hatched areas in Section III figures are represented by $\int_{B=0}^{B_{10}} \varepsilon_{wc}\ dB$ which is the key integral to be computed. In order to perform this calculation, Sasamori [1968] proposed emissivity formulas of the following form:

$$\begin{aligned}\varepsilon_{wc}(6,8) = \{&.240 \log_{10}[U(6,8)] + .622\} \\ &+ .07262\{(1. - .62556[U(6,8) + .0286]^{.26}) \\ &* [\log_{10} C(6,8) + 1.064]\} \qquad \text{(A-2)}\end{aligned}$$

for the layer 6-8 relative to the level 6 as reference level for temperatures $T \geq 210$ deg k where ε_{wc} is very nearly temperature independent. Also note that U is the water vapor absorber mass given by (2-7) measured from the reference level 10, 6, or 2 and C is the correspondingly

carbon dioxide absorber mass. Water vapor emissivity alone, contribution is represented by the quantity within the brace of Eq. A-2. The second brace indicates the additional contribution made by the part of the CO_2 emissivity transmitted through the water vapor "overlap" near 15μm, i.e., the part not already counted in this spectral region by the water vapor integration.

Equation A-2 was used to compute atmospheric emissivities over all the layers (8, 10), (6, 10), (4, 10).....(1, 10) for which the running mass values U(8, 10), C(8, 10), etc. were ready to be implied from the radiative soundings. To complete the $F_{wc}\downarrow$ integration given by (A-1) from level $k = 1$ to the origin ($B = 0$, $\varepsilon_{wc} = 1.0$), on the Yamato Radiation Chart (Appendix Fig. A-1), $U(T_k)$, $C(T_k)$ soundings were adopted as isothermal from $T = T_1$ ($k = 1$) to $T = T_o$ ($k = 0$), and then extended from the last "sounding" point $(U[(0,10),T_1])$ along the last emissivity value for $T \leq T_1 \doteq 210$ deg k where the emissivity of the water vapor is known to be temperature-dependent. This value of emissivity is denoted $\tilde{\varepsilon}_{wc}$ and is written, after Sasamori [1968]

$$\begin{aligned}\tilde{\varepsilon}_{wc}[U(0,10),T_1] = 8.34\ T_1^{[.353\ \log_{10} U(0,10)\ -\ .44]} \\ * U(0,10)^{[-.03455\ \log_{10} U(0.10)\ -\ .705]} \\ * [8.0/(.353\ \log_{10} U(0,10) + 3.56)] \\ + .07262\{(1. - .62556[U(0,10) + .0286]^{.26}) \\ * [\log_{10} C(0,10) + 1.064]\} \qquad \text{(A-3)}\end{aligned}$$

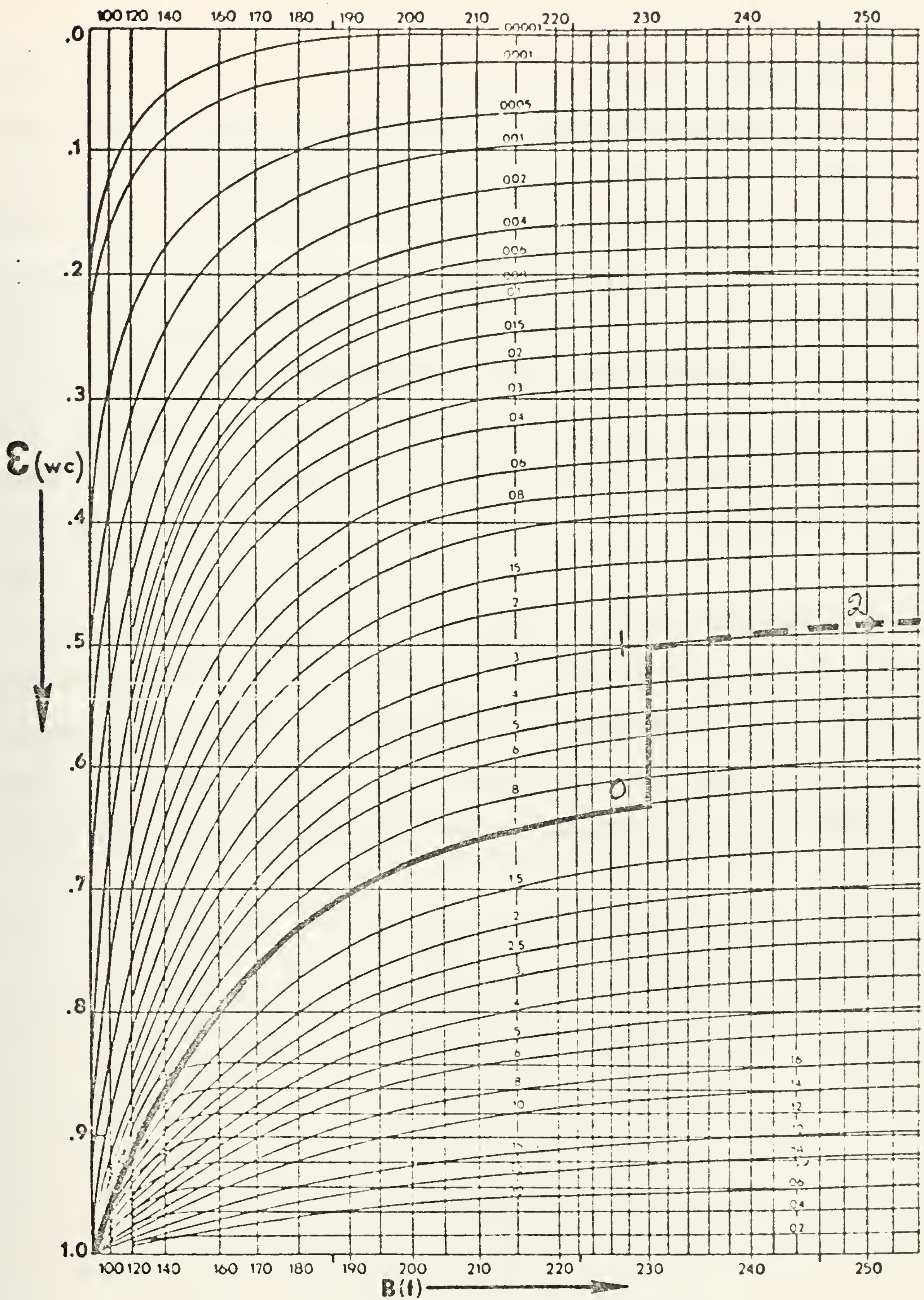

Figure A-1. Depiction of $\tilde{\varepsilon}_{wc}$ given by Eq. (A-3) on the Yamato Radiation Chart. Area above heavy dark curve represents $F_{wc}\downarrow$ above level k=1 from a radiative sounding.

Here the final term in the braces of Eq. A-3 is almost the same form of the CO_2 correction to the total emissivity is in Eq. A-2. In Eq. A-3, however, this term refers to the full layer (0, 10), the first term is temperature dependent as well as dependent upon the summed absorber masses relative to the reference level k = 10. It can be seen clearly that Eq. (A-3) is usable with proper final parameters U(0, k), C(0, k), and T_1 for the determination of the curvilinear portion of the downward flux contribution through level k for all of the reference level cases to be investigated below, that is k = 2, 6.

It should also be noted that $\tilde{\varepsilon}_{wc}$ has been integrated over the temperature $T \leq T_1$ for which the water vapor emissivity curves are temperature dependent (see Appendix Fig. A-1) so that the result of Eq. A-3 is really the average of the final curvilinear emissivity value multiplied by $B_1 = St\ T_1^4$.

APPENDIX B: FORMULAS USED IN DEPICTING THE DISPOSITION OF INCOMING SOLAR (F(A)) FROM LEVEL k = 2 TO THE EARTH'S SURFACE

These formulas are depicted by Figs. 7, 8, and 9 in Section IV. They are used in this study to calculate amounts of insolation absorbed by the atmospheric layers and the earth's surface. For further explanation and key to these formulas consult Section IV.C. Dashed separation lines are used to divide those equations involving absorptions in successive layers e.g., (2,4), (4,6), (6,8), etc.

1. Case (1,1) Overcast in Both High and Low Cloud Layers (see also Fig. 7)

$$\begin{aligned}
F4\downarrow &= F(A)(1-.271[U(2,4)\ \mathrm{Sec}\ Z]^{.303} \\
F4\uparrow &= F4\downarrow(RA(1)) \\
A24\downarrow &= F(A).271[U(2,4)\ \mathrm{Sec}\ Z]^{.303} \\
A24\uparrow &= F4\uparrow.271[U(2,4)\ \mathrm{Sec}\ Z]^{.303}
\end{aligned} \tag{B-1a}$$

- -

$$\begin{aligned}
F6 &= F4\downarrow(1-RA(1)-A(1)) \\
A46 &= F4\downarrow(A(1)) \\
A26 &= A24\downarrow + A24\uparrow + A46
\end{aligned} \tag{B-1b}$$

$$\begin{aligned}
TD68 &= 1-.271[U(6,8)5/3]^{.303} \\
TD910 &= 1-.271[U(9,10)5/3]^{.303}
\end{aligned} \tag{B-2}$$

where TD is a term to denote the Manabe-Möller transmissivities for insolation beneath a cloud layer. In this event, Sec Z

is changed to the mean slant-path $\sec z \simeq 5/3$ [after Katayama, 1966].

$$\begin{aligned}
F8\downarrow &= F6\downarrow(TD68)\\
F8\uparrow &= F8\downarrow(RA(2))\\
F6\uparrow &= F8\uparrow(TD68)\\
F6\downarrow\downarrow &= F6\uparrow(RA(1))\\
F8\downarrow\downarrow &= F6\downarrow\downarrow(TD68)\\
A68\downarrow &= F6\downarrow - F8\downarrow\\
A68\uparrow &= F8\uparrow - F6\uparrow\\
A68\downarrow\downarrow &= F6\downarrow\downarrow - F8\downarrow\downarrow\\
A68 &= A68\downarrow + A68\uparrow + A68\downarrow\downarrow
\end{aligned}\tag{B-3a}$$

- -

$$\begin{aligned}
F9\downarrow &= F8\downarrow(1-RA(2) - A(2)) + F8\downarrow\downarrow(1-A(2))\\
A89 &= F8\downarrow(A(2)) + F8\downarrow\downarrow(A(2))
\end{aligned}\tag{B-3b}$$

- -

$$\begin{aligned}
F10\downarrow &= F9\downarrow(TD910)\\
F10\uparrow &= F10\downarrow(\alpha(G))\\
F9\uparrow &= F10\uparrow(TD910)\\
F9\downarrow\downarrow &= F9\uparrow(RA(2))\\
F10\downarrow\downarrow &= F9\downarrow\downarrow(TD910)\\
A910\downarrow &= F9\downarrow - F10\downarrow\\
A910\uparrow &= F10\uparrow - F9\uparrow\\
A910\downarrow\downarrow &= F9\downarrow\downarrow - F10\downarrow\downarrow\\
A910 &= A910\downarrow + A910\uparrow + A910\downarrow\downarrow\\
A810 &= A89 + A910
\end{aligned}\tag{B-3c}$$

2. Case (1,0) Upper Overcast Only (see also Fig. 8)

$$A24\downarrow = F(A).271[U(2,4) \text{ Sec } Z]^{.303}$$

$$\begin{aligned} A24\uparrow &= F(A)\{1-.271[U(2,4) \text{ Sec } Z]^{.303}\}RA(1) \\ &\times\{.271[U(2,4) \text{ Sec } Z]^{.303}\} \end{aligned} \qquad \text{(B-4a)}$$

$$A24 = A24\uparrow + A24\uparrow$$

- -

$$F6\downarrow = F(A)\{1-.271[U(2,4) \text{ Sec } Z]^{.303}\}[1-RA(1)-A(1)]$$

$$A46 = F(A)\{1-.271[U(2,4) \text{ Sec } Z]^{.303}\}A(1) \qquad \text{(B-4b)}$$

$$A26 = A24 + A46$$

- -

$$F10\downarrow = F6\downarrow(TD610)$$

$$F10\uparrow = F10\downarrow(\alpha(G))$$

$$F6\uparrow = F10\uparrow(TD610)$$

$$F6\downarrow\downarrow = F6\uparrow(RA(1)) \qquad \text{(B-4c)}$$

$$F10\downarrow\downarrow = F6\downarrow\downarrow(TD610)$$

$$A610\downarrow = F6\downarrow - F10\downarrow$$

$$A610\uparrow = F10\uparrow - F6\uparrow$$

$$A610\downarrow\downarrow = F6\downarrow\downarrow - F10\downarrow\downarrow$$

$$A610 = A610\uparrow + A610\downarrow + A610\downarrow\downarrow$$

3. Case (0,1) Low Overcast Only (see also Fig. 9)

$$A26\downarrow = F(A).271[U(2,6)\ \mathrm{Sec}\ Z]^{.303}$$

$$A68\downarrow = F(A).271\{[U(2,8)\ \mathrm{Sec}\ Z]^{.303} - [U(2,6)\ \mathrm{Sec}\ Z]^{.303}\}$$

$$F8\downarrow = F(A)\{1-.271[U(2,8)\ \mathrm{Sec}\ Z]^{.303}\}$$

$$F8\uparrow = F8\downarrow[RA(2)]$$

$$F6\uparrow = F8\uparrow\{1-.271[U(6,8)\ \mathrm{Sec}\ Z]^{.303}\} \tag{B-5a}$$

$$F2\uparrow = F8\uparrow\{1-.271[U(2,8)\ \mathrm{Sec}\ Z]^{.303}\}$$

$$A68\uparrow = F8\uparrow - F6\uparrow$$

$$A26\uparrow = F6\uparrow - F2\uparrow$$

$$A26 = A26\downarrow + A26\uparrow$$

- -

$$F9 = F8\downarrow[1-RA(2) - A(2)] \tag{B-5b}$$

$$A89 = F8\downarrow[A(2)]$$

- -

$$F10\downarrow = F9\downarrow(TD910)$$

$$F10\uparrow = F10\downarrow(\alpha(G))$$

$$F9\uparrow = F10\uparrow(TD910)$$

$$F9\downarrow\downarrow = F9\uparrow(RA(2)) \tag{B-5c}$$

$$F10\downarrow\downarrow = F9\downarrow\downarrow(TD910)$$

$$A910\downarrow = F9\downarrow - F10\downarrow$$

$$A910\uparrow = F10\uparrow - F9\uparrow$$

$$A910\downarrow\downarrow = F9\downarrow\downarrow - F10\downarrow\downarrow$$

$$A910 = A910\downarrow + A910\uparrow + A910\downarrow\downarrow$$

$$A610 = A68\downarrow + A68\uparrow + A89 + A910$$

SUBROUTINE FOR COMPUTATION OF SURFACE WINDS FROM SECTION II.C.

```
      SUBROUTINE WINDS(SINT,ALAT,VG,VSFC,ISOJN)
      IF((ALAT.LT.5.0).AND.(ALAT.GT.-5.0))GO TO 20
      READ (5,100)X2;X1,Y2,Y1
  100 FORMAT(5X,4(F7.1))
      G=9.80665
      D=381.E+03
      DELTX=X2-X1
      DELTY=Y2-Y1
      DELTZ=SQRT((DELTX*DELTX)+(DELTY*DELTY))
      F=((4.*3.145926)/8.64E+04)*SINT
      IF(ABS(F).LT.2.5E-05) F=2.5E-05
      BM=1.86603/(1.+SINT)
      IF (ISOUN.EQ.1.OR.ISOUN.EQ.68) GO TO 17
      VG=ABS((G/F)*(DELTZ/(2.*(D/BM))))
      GO TO 30
   17 VG=ABS((G/F)*(DELTZ/(D/BM)))
      GO TO 30
   20 READ(5,150)V1
  150 FORMAT(40X,F6.1)
      VG=V1*5.1479166E-01
   30 VSFC=(.8*VG)+2.2
      RETURN
      END
```

A. SUBROUTINE FOR COMPUTING TEMPERATURE AT LEVEL 'X' FROM EQ. 5-5

```
      SUBROUTINE TXA(VSFC,DA          ,AN        ,DAT        ,ISOUN,TX,PT2,DZ91
     10,CD)
      CLR=3.E-05
      CD=1.4E-03
      AK=1.E 05
      AA=5.E 04
      T9=(AN        +273.16)*((10./9.)**(2./7.))
      TG=(DA         +273.16)*((1000./DAT        )**(2./7.))
      T9G=T9-TG
      DZ910=(28704./9.80665)*((AN        +DA         +2.*273.16)/2.)*ALOG(DA
     1T       /900.)
      PT2D=1.+AA*((T9-TG)/DZ910)
      IF(PT2D.LT.0.750)PT2D=0.750
      PT2=AK/PT2D
      A=CD*VSFC*DA*1.E02
      B=(2.*PT2*(T9-273.16))/DZ910
      C=2.*PT2*CLR
      D=(2.*PT2)/DZ910
      E=CD*VSFC*1.E02
      TX=(A+B-C)/(D+E)
      RETURN
      END
```

B. SUBROUTINE FOR COMPUTING THE MIXING RATIO AT LEVEL 'X' FROM EQ. 5-9

```
      SUBROUTINE QXA(VSFC,TG,DZ910,SFP,QN,TILK,QX,ES,QS,CD)
      ES=EXP(21.656-5418./(TG+273.16))
      QS=(.62197*ES)/(SFP-ES)
      Q9=QN/1000.
      A=CD*VSFC*QS*1.E02
      B=2.*Q9*(TILK/DZ910)
      C=CD*VSFC*1.E02
      D=(2.*TILK)/DZ910
      QX=(A+b)/(C+D)
      RETURN
      END
```

SUBROUTINE FOR COMPUTING LATENT HEAT FLUX IN THIS STUDY FROM EQ. 5-7

```
      SUBROUTINE EVAP (VSFC,TG,EX,ES,SFP,CLOG,EVAPO,TX,QX,QS,D,CD,PT2)
      W=596.73-.601*(TG)
      D=(SFP*1000.)/((.28704*10**7)*(TG+273.16))
      ES=EXP(21.656-5418./(TG+273.16))
   30 QS=(.62197*ES)/(SFP-ES)
      PT1=W*D
      PT2=QS-QX
      EVAPO=PT1*VSFC*CD*PT2*60.*1.E02
  100 FORMAT(//,T3,'LATENT',T14,'DENSITY',T25,'LATENT*DENS',T36,' EX ',T
     147,'QX',T58,'ES',T69,'QS    ',T80,'QS-QX      ',T91,'DRAG       ',T
     2101,'WINDS',T114,'EVAPORATION'//,T3,11(E10.4,1X))
      RETURN
      END
```

SUBROUTINE FOR COMPUTING SENSIBLE HEAT FLUX IN THIS STUDY FROM EQ. 5-2

```
      SUBROUTINE SENS (D,CD,VSFC,TG,TX,SENSI,EVAP,BOW,PT2)
      CP=.239
      PT1=D*CP
      PT2=TG-TX
      SENSI=PT1*CD*VSFC*PT2*60.*1.E02
      TOT=SENSI+EVAP
  200 FORMAT(3(E10.4,1X))
      BOW=SENSI/EVAP
  150 FORMAT (//,T3,'DENSITY',T14,'DENSITY*CP',T25,'DRAG',T36,'WINDS',T4
     17,'TG',T58,'TX',T69,'TG-TX',T80,'SENSIBLE',T91,'BOWEN'//,T3,9(E10.
     24,1X))
      RETURN
      END
```

SUBROUTINE FOR COMPUTATION OF HEAT CONDUCTION INTO ICE AND SENSIBLE AND LATENT HEAT FLUXES OVER ICE FROM SECTION V.D.

```
      SUBROUTINE HEICE(TG,SINT,EVAP,HAIR)
      READ (5,700)QABG,E10
  700 FORMAT(2(F7.4,1X))
      HIC=697.83*(271.3-(TG+273.16))
      HIC=(HIC/4.186E 07)*60.
      HAIRE=HIC+QABG-E10
      XX=(9.6*SINT*SINT)-(7.93*ABS(SINT))+2.
      IF(XX.LT.1.3333) XX=1.3333
      HAIR=(XX/(XX+1.))*HAIRE
      EVAP=HAIR/XX
      TOT=EVAP+HAIRE
  800 FORMAT(/,T2,'EVAPORATION=',E10.4,'   SENSI = ',E10.4,'   BOWEN=',E
     110.4,'  QABG=',E10.4,'  E10=',E10.4,  '  HIC=',E10.4,' HAIRE=',E10
     2.4)
      RETURN
      END
```

LIST OF REFERENCES

1. Arakawa, A., 1972: Design of the UCLA General Circulation Model, Numerical Simulation of Weather and Climate Tech. Rpt. NO. 7, Department of Meteorology, University of California.

2. Atkinson, 1970: Mean-Cloudiness and Gradient-Level-Wind Charts Over the Tropics, Air Weather Service (MAC), United States Air Force.

3. Berliand, T. G., 1956: "Heat Balance of the Atmosphere of the Northern Hemisphere," article from A.I. Voeikov and Problems in Climatology, M. I. Budyko, General editor, Leningrad, pp. 57-84 (Translated by the Israel Program for Scientific Translations, Jerusalem, 1963; distributed by the National Science Foundation, Washington, D.C.)

4. Budyko, M. I., 1956: The Heat Balance of the Earth's Surface, Leningrad, pp. 255 (Translated by N. A. Slepanova; translation distributed by U.S. Weather Bureau, Washington, D.C.)

5. Crow, E. L., Davis, F. A., and Maxfield, M. W., 1955: Statistics Manual, pp. 288, NAVORD Report 3369.

6. Coulson, K. L., 1959: Radiative Flux from the Top of Rayleigh Atmosphere, Ph.D. Dissertation, Department of Meteorology, University of California, pp. 60.

7. Dixon, W. J., 1973: Biomedical Computer Programs, University of California Press, pp. 773.

8. Fleagle, R. G., Businger, J. A., 1963: An Introduction to Atmospheric Physics, Academic Press, New York, pp. 346.

9. Gates, W. L., Batten, E. S., Kahle, A. B., and Nelson, A. B., 1971: A Documentation of the Mintz-Arakawa Two-Level Atmospheric Circulation Model, Advance Research Projects Agency Report No. R-877-ARPA, Rand Corporation Santa Monica, California, pp. 408.

10. Haney, R. L., 1971: "Surface Thermal Boundary Condition for Ocean Circulation Models," Journal of Physical Oceanography, Vol. 1, No. 4, pp. 241-248.

11. Hanson, K. J., 1971: Studies of Cloud and Satellite Parameterization of Solar Irradiance at the Earth's Surface, paper presented at the Miami Workshop on Remote Sensing, Miami, Florida, 29-31 March 1971.

12. Jenks, F. W., 1974: Radiative Parameterization for the FNWC Global Primitive Equation Model, M.S. Thesis, Department of Meteorology, Naval Postgraduate School, Monterey, California, pp. 89.

13. Joseph, J. H., 1971: "On the Calculation of Solar Radiation Fluxes in the Troposphere," Solar Energy, Vol. 13, Pergamon Press, London, pp. 251-261.

14. Kaitala, J. E., 1974: Heating Functions and Moisture Source Terms in the FNWC Primitive Equation Models, paper presented at the Continuing Education Program for Meteorological Specialists, Naval Postgraduate School, Monterey, California, 29 April 1974.

15. Katayama, A., 1966: "On the Radiation Budget of the Troposphere over the Northern Hemisphere (I)," Journal of the Meteorological Society of Japan, Vol. 44, No. 6, pp. 381-401.

16. Kesel, P. G., Winninghoff, F. J., 1972: "The Fleet Numerical Weather Central Operational Primitive-Equation Model," Monthly Weather Review, Vol. 100, No. 5, pp. 360-373.

17. Langlois, W. E., Kwok, H. C. W., 1969: Description of the Mintz-Arakawa numerical general circulation model. Numerical Simulation of Weather and Climate Tech. Rpt. No. 3, Department of Meteorology, University of California.

18. List, R. J., 1958: Smithsonian Meteorological Tables, Smithsonian Institute, Washington, pp. 527.

19. Malkus, J. S., 1962: "Large Scale Interactions," The Sea, Vol. 1, Interscience Publishers.

20. Martin, F. L., 1972: Description of a Radiation Package for the Naval Postgraduate School General Circulation Model, Department of Meteorology, Naval Postgraduate School, Monterey, California.

21. Martin, F. L., 1974: Unpublished manuscript, Department of Meteorology, Naval Postgraduate School, Monterey, California.

22. Plante, R. J., 1973: Tests of a Radiative Transfer Model for Numerical Prediction of the Atmospheric General Circulation, M.S. Thesis, Department of Meteorology, Naval Postgraduate School, Monterey, California, pp. 115.

23. Quinn, W. H., 1971: Studies of Parameterization of Solar Irradiance at the Earth's Surface, paper presented at the Miami Workshop on Remote Sensing, Miami, Florida, 29-31 March 1971.

24. Raschke, E., Vonder Haar, T., Bandeen, W., Pasternak, M., 1973: "The Annual Radiation Balance of the Earth-Atmosphere System during 1969-1970 from NIMBUS III Measurements," Journal of the Atmospheric Sciences, Vol. 30, No. 3, pp. 341-364.

25. Rodgers, C. D., 1967: "The Radiative Heat Budget of the Troposphere and Lower Stratosphere," Planetary Circulation Project Report N. A2, Department of Meteorology, Massachusetts Institute of Technology, pp. 99.

26. Sasamori, T., 1968: "The Radiative Cooling Calculation for Application to General Circulation Experiments," Journal of Applied Meteorology, Vol. 7, No. 5, pp. 721-729.

27. Sellers, W. D., 1965: Physical Climatology, University of Chicago Press, pp. 272.

28. Smagorinsky, J., 1960: "On the Dynamical Prediction of Large Scale Condensation by Numerical Methods," Geophysical Monograph, No. 5, American Geophysical Union, Washington, D.C., pp. 71-78.

29. Sverdrup, H. U., Johnson, M. W., Fleming, R. H., 1942: The Oceans: Their Physics, Chemistry and General Biology, Prentice-Hall, New York, pp. 1097.

30. Swinbank, W. C., 1963: "Long-wave Radiation from Clear Skies," Quarterly Journal of Royal Meteorology Society, Vol. 4, pp. 339-348.

31. Vonder Haar, T. H., Hanson, K. J., 1969: "Absorption of Solar Radiation in Tropical Regions," Journal of the Atmospheric Sciences, Vol. 26, No. 4, pp. 652-655.

32. Vonder Haar, T. H., Oort, A. H., 1973: "New Estimate of Annual Poleward Energy Transport by Northern Hemisphere Oceans," Journal of Physical Oceanography, Vol. 3, No. 2, pp. 169-172.

33. Vowinckel, E., Taylor, B., 1964: Evaporation and Sensible Heat Flux over the Arctic Ocean, Scientific Report No. 10 under Contract No. AF 19(604)-7415, Project No. 8623, Task No. 862303, Air Force Cambridge Research Laboratories, Office of Aerospace Research, United States Air Force, Bedford, Massachusetts.

34. Weiler, H., Burling, R. W., 1967: "Direct Measurements of Stress and Spectra of Turbulence in the Boundary Layer Over the Sea," Journal of the Atmospheric Sciences, Vol. 24, pp. 653-664.

35. Yamamoto, G., 1952: "On a Radiation Chart," Science Repts. of the Tohoku University, Series No. 5, pp. 9-23.

INITIAL DISTRIBUTION LIST

		No. Copies
1.	Defense Documentation Center Cameron Station Alexandria, Virginia 22314	2
2.	Library, Code 0212 Naval Postgraduate School Monterey, California 93940	2
3.	Professor F. L. Martin, Code 51Mr Department of Meteorology Naval Postgraduate School Monterey, California 93940	6
4.	LT Warren T. Spaeth, Jr. USN 1607 Fairhill Place Clementon, New Jersey 08021	2
5.	Department Chairman, Code 51 Department of Meteorology Naval Postgraduate School Monterey, California 93940	1
6.	Asst. Professor R. L. Haney, Code 51Hy Department of Meteorology Naval Postgraduate School Monterey, California 93940	1
7.	Naval Weather Service Command Naval Weather Service Headquarters Washington Naval Yard Washington, D.C. 20390	1
8.	Fleet Numerical Weather Central Attn: Mr. Leo Clarke Monterey, California 93940	2
9.	Commanding Officer Environmental Prediction Research Facility Monterey, California 93940	1

23 MAR 78 24877

Thesis 160063
S66628
c.1

Spaeth

Heat budget parameterization for the FNWC primitive equation model using data for 16 January 1974.

23 MAR 78 24877

Thesis 160063
S66628 Spaeth
c.1
Heat budget parameterization for the FNWC primitive equation model using data for 16 January 1974.

thesS66628
Heat budget parameterization for the FNW
3 2768 002 01719 6
DUDLEY KNOX LIBRARY